

Interner Bericht

DLR-IB-SY-SD-2025-208

**On the consolidation quality of
high-speed tape-wound CFRP
preforms using resistive
heating**

Masterarbeit

Mihai Fetecau

Deutsches Zentrum für Luft- und Raumfahrt

Institut für Systemleichtbau




DLR

**Deutsches Zentrum
für Luft- und Raumfahrt**

Dokumenteigenschaften

Titel	<u>On the consolidation quality of high-speed tape-wound CFRP preforms using resistive heating</u>
Betreff	<u>Masterarbeit</u>
Institut	<u>Systemleichtbau</u>
Erstellt von	<u>Mihai Fetecau</u>
Beteiligte	<u>Jonas von Heusinger</u>
Geprüft von	<u>Prof. Dr. Clemens Dransfeld</u>
Freigabe von	<u>Dr.-Ing. Daniel Stefaniak</u>
Zugänglichkeit	<u><input checked="" type="checkbox"/> Stufe 1: Allgemein zugänglich (in elib ohne Zugangsbeschränkung)</u>
	<u><input type="checkbox"/> Stufe 2: DLR intern zugänglich (in elib mit Beschränkung „nur DLR-intern zugänglich“)</u>
Datum	<u>20.08.2025</u>
Version	<u>1.0</u>
Datei Info	<u>IB_2025_208_MA_Fetecau.pdf</u>



MASTER OF SCIENCE THESIS

On the consolidation quality of high-speed tape-wound CFRP preforms using resistive heating

An experimental study on the influence of consolidation parameters on preform quality of CF-LMPAEK wound pipes using CoRe Heat

Mihai Fetecau

Faculty of Aerospace Engineering

Delft University of Technology

On the consolidation quality of high-speed tape-wound CFRP preforms using resistive heating

**An experimental study on the influence of consolidation
parameters on preform quality of CF-LMPAEK wound pipes
using CoRe HeaT**

MASTER OF SCIENCE THESIS

For obtaining the degree of Master of Science in Aerospace
Engineering at Delft University of Technology

Mihai Fetecau

20 August 2025

The work in this thesis was in collaboration with the Center for Lightweight Production Technology, German Aerospace Center (DLR), Stade. Their cooperation is gratefully acknowledged.

DELFT UNIVERSITY OF TECHNOLOGY
FACULTY OF AEROSPACE ENGINEERING
DEPARTMENT OF AEROSPACE STRUCTURES AND MATERIALS

GRADUATION COMMITTEE & SUPERVISORS

Dated: 20 August 2025

Chair holder:

Asst. Prof. Dr.Ir.Daniel M.J. Peeters

Supervisor:

Prof. Dr.Ir. Clemens A. Dransfeld

Independent committee member:

Asst. Prof. Dr. Ir. Yinglu Tang

External supervisor:

Ir. Jonas L. v.Heusinger

Abstract

Fiber-reinforced thermoplastic polymers are being considered as alternatives to thermoset composites because they are recyclable, easier to repair, less hazardous to produce, and offer better impact resistance. However, high material costs and processing challenges hinder their widespread adoption in high-performance applications. Continuous Resistance Heating Technology (CoRe HeaT) is an innovative method for the rapid processing of continuous fiber prepreg tapes, aiming to accelerate manufacturing and reduce costs. This study examines how process parameters such as moisture, maximum temperature, heating rate, and tape tension affect CoRe HeaT deconsolidated carbon fiber low-melt polyaryletherketone (CF-LMPAEK) pre-preg tapes. It also investigates how consolidation parameters, such as average compaction pressure, compaction duration, tape tension, and tooling temperature, influence the quality of CF-LMPAEK pipe preforms produced using high-speed (500 mm/s) CoRe HeaT tape winding. Image processing of cross-sectional micrographs are used to quantitatively evaluate both deconsolidated tapes and wound preforms. Void content, root mean square surface roughness and waviness, and pore distribution are used as indicators for tape and laminate quality, since they can have significant impacts on mechanical performance, durability, and further stages in product manufacturing.

The deconsolidation of tape is performed by heating a 70 cm long, pre-tensioned CF-LMPAEK tape clamped between two double-plate electrodes using one electrical pulse. The oven-dried tape had a 40% lower porosity as compared to the tape kept at ambient conditions. A tenfold increase in tension could also be seen to decrease porosity by 25%. Temperature and heating rate were linked in pore proliferation, while temperature alone was seen to be critical to roughness increases. A lack of tow tension was seen to cause global wrinkling of the tape, increasing waviness by 62%, while excessive tensioning was correlated with a decrease in tape width by 6.4%. The preform winding is performed using a purpose-built tape winding machine and consolidated using custom-built pressure elements, spanning rigid and conformable rollers and area compactors. The rate of porosity increase with an increase in compaction duration was seen to be negatively correlated with the applied compaction pressure. The lowest level of volumetric void content of 0.75% was achieved with the use of a silicone area compactor at 1.22 MPa within the preform tubes wound at 500 mm/s. The lowest levels of roughness and waviness, of 2.27 μm and 9.5 μm , respectively, were obtained using a copper roller delivering 4.56 MPa at 500 mm/s winding speed. Compaction pressure was linked to a power fitting decrease in porosity. Increasing

tension was also connected to a decrease in porosity, yet excessive tensioning led to gap widening, ineffective gap filling, and layer crumbling, which negatively impacted laminate quality. A marginal improvement in outer surface quality could be linked to heating the tooling above the glass transition temperature (T_g) of LMPAEK. The impact of increasing tooling temperature on porosity and pore distribution was negligible. It was concluded that further optimization of conformable area compactors may bring significant improvements in laminate quality for winding speeds exceeding 500 mm/s, and should be further studied. Furthermore, additional studies on the impact of tape temperature at the nip-point are expected once sufficient temperature monitoring and control capabilities are achieved.

Acknowledgments

I would firstly like to show my gratitude to my supervisor from DLR, Jonas von Heusinger, for being by my side for every step of this thesis and even beyond that, ever since I started as an intern at the ZLP in Stade. He has been so open to my questions, so willing to share his feedback and thoughts, and so generous with his help. From the almost daily discussions at the start of this project to the long evenings on the shopfloor spent under the looming deadline of the greenlight review, he has always pushed me to achieve my goals, made sure I had all the resources I needed, and rooted for my success. I would also like to thank Yannis Grohmann for his eagerness to share his knowledge and experience, his candid and constructive input, and his efforts to make sure everything was in place for me to put my ideas into practice, even in his final stages of his doctoral research. I am immensely grateful to both of them for welcoming me into the CoRe HeaT research team.

I would also like to thank my supervisor from TUDelft, Prof Clemens Dransfeld, for joining me on this academic path, for overseeing my progress with care, and being there when it mattered, even if from a distance. I am also grateful to Daniel Stefaniak for giving me the opportunity to join this institute and start my professional journey at such a cutting-edge institution.

Many thanks to my fellow students and colleagues here at DLR. My appreciation goes out to Sahil Khan, from whom I learned so much during my internship when he was finishing his Master Thesis production, who counseled me during all my research, and who helped me with proofreading this document until the very end. I would also like to thank Jonas Naumann for giving me permission to use his research work in laminate feature labeling and helping me fit the tool which played a major part in my thesis to my desires, Stefan Junker for always assisting me in preparing my microscopy samples, Lukas Fietz and Tai Nguyen for helping me with doing microscopy when I was overwhelmed with writing the first draft of this paper, and to Marvin Petersen for helping with proofreading.

I would also like to thank Daniel Peeters and Yinglu Tang from TUDelft for taking the time to read and review my first individual research thesis and being a part of my graduation committee.

Lastly, a huge thank you to my friends, who are always able to help me decompress through stressful times, and especially to my family, for their unconditional love and unfaltering support towards me reaching my goals and dreams, come what may.

Mihai Fetecau
06 August 2025

”The future is already here – it’s just not evenly distributed.”

— *William Gibson*

Contents

Acknowledgments	viii
List of Symbols	xiii
List of Tables	xiv
List of Figures	xv
1 Introduction	1
2 State of the Art	3
2.1 Search strategy	3
2.2 Reinforced thermoplastic manufacturing	4
2.3 Filament winding	5
2.4 Tape winding	6
2.4.1 Unloading zone	7
2.4.2 Heating zone	8
2.4.3 Nip point	10
2.4.4 Deposition zone	17
2.5 CoRe HeaT method	19
3 Research complex	21
3.1 Knowledge gap	21
3.1.1 CoRe HeaT deconsolidation	21
3.1.2 Consolidation elements influence.	22
3.1.3 Tooling temperature	22
3.2 Research objective	22
3.3 Research questions	23
3.4 Hypotheses	23

4	Methodology	25
4.1	Static deconsolidation	25
4.1.1	Experimental Setup.	25
4.1.2	Design of experiments	26
4.1.3	Evaluation.	27
4.2	Static compaction.	33
4.2.1	Experimental Setup.	33
4.2.2	Design of experiments	34
4.2.3	Evaluation.	37
4.3	Preform winding	37
4.3.1	Experimental Setup.	38
4.3.2	Design of experiments	41
4.3.3	Evaluation.	43
5	Results	45
5.1	Static deconsolidation	45
5.2	Static compaction.	51
5.3	Preform winding	52
6	Discussion	63
6.1	Tape deconsolidation	63
6.2	Compaction elements.	67
6.3	Preform winding	70
6.3.1	Void analysis	71
6.3.2	Slider performance	74
6.4	Hypotheses evaluation	78
7	Conclusion	80
8	Recommendations	86
	Bibliography	88
A	Appendix A	93

List of Symbols

(C)FRP/C	(Carbon) Fiber Reinforced Polymer/Composite	
(LM)PAEK	(Low-Melt) Polyaryletherketone	
AFP	Automated Fiber Placement	
CF	Carbon Fiber	
CNC	Computer Numerical Control	
CoRe HeaT	Continuous Resistance Heating Technology	
DiNAT	Dilated Neighborhood Attention Transformer	
DLR	German Aerospac Center (Ger.)	
DoE	Design of Experiments	
FFT	Fast Fourier Transform	
ILSS	Interlaminar Shear Strength	
IQR	Inter-Quartile Range	
MFFD	Multi-Functional Fuselage Demonstrator	
OEM	Original Equipment Manufacturer	
PA12	Polyamide 12	
PAHT	High Temperature Polyamide	
PAN	Polyacrylonite	
PEEK	Polyetheretherketone	
PEKK	Polyetherketoneketone	
PETG	Polethylene Terephthalate Glycol	
PLA	Polylactic Acid	
PPS	Polyphenylene Sulfide	
PTFE	Polytetrafluoroethylene	
RMS	Root Mean Square	
S/N	Signal to Noise ratio	
TAPAS	Thermoplastic Affordable Primary Aircraft Structure consortium	
TPC	Thermoplastic Polymer Composite	
UD	Uni-Directional	
ZLP	Center for Lightweight Production Technology (Ger.)	
λ_c	Central cut-off frequency	$1/\mu\text{m}$
λ_f	Upper cut-off frequency	$1/\mu\text{m}$
λ_s	Lower cut-off frequency	$1/\mu\text{m}$
μ_{mf}	Equivalent viscosity of matrix-fiber phase	Pa s
ω	Wavelength	m
ζ	Asperity height	μm
ζ_0	Tape thickness	μm
ζ_i	Initial tape asperity	μm
K	Permeation tensor	m^2
u	Velocity vector	m/s
a_0	Initial asperity height	μm
b_0	Initial asperity width	μm
D_{IC}	Degree of Intimate Contact	$\%$

l_s	Sampled length	μm
P_{app}	Applied pressure	Pa
R_q	Root mean square roughness	μm
$S_{(\omega)}$	Wavelength power spectrum	W/m
T_g	Glass transition temperature	$^{\circ}\text{C}$
T_m	Melting temperature	$^{\circ}\text{C}$
T_m^{∞}	Melting temperature of an infinite perfect crystal	$^{\circ}\text{C}$
T_p	Processing temperature	$^{\circ}\text{C}$
t_{IC}	Time to complete intimate contact	s
V_f	Fiber volume content	$\%$
w	Tape width	mm
w_0	Initial asperity gap width	m
W_q	Root mean square waviness	μm
$Z_{(x)}$	Deviation from surface profile mean	μm
CTE	Coefficient of Thermal Expansion	m/mK

List of Tables

4.1	Characteristics provided by OEM of all deconsolidated tapes	25
4.2	Static deconsolidation test matrix	27
4.3	General description of compaction behavior of considered compression elements . .	35
4.4	Parameters and their respective levels used to characterize the compaction behaviour of compression elements	37
4.5	Preform tape winding parameter set	42
5.1	Static deconsolidation parameter set and results, with averaged values and standard deviations given	45
5.2	Static compaction results	51
5.3	Tape winding final parameter set and results, with averaged values and standard deviations given	54
6.1	Signal-to-noise analysis of the void content of deconsolidated tapes	64
6.2	Signal-to-noise analysis of the surface roughness of deconsolidated tapes	65
6.3	Signal-to-noise analysis of the surface waviness of deconsolidated tapes	66
6.4	Signal-to-noise analysis of the width of deconsolidated tapes	67

List of Figures

2.1	Schematics related to winding processes	6
2.2	Schematic of the tape winding process, with specific process zones	7
2.3	Thermoplastic tape line and slitler designed by Cygnet Texkimp, showing material creels, heat shielded impregnation unit, calender rolls, and the final accumulation spool, reproduced	8
2.4	Void development mechanisms taking place in the presence of high temperatures .	9
2.5	Schematic of the bonding mechanism of thermoplastic reinforced tape, reproduced	10
2.6	Surface models schematic representations, reproduced	11
2.7	a) SEM scan of tape cross-section, b) isolated and segmented image with maximum width range marked by vertical lines, c) zoomed tape section illustrating fibers, matrix, and embedding resin, d) definition of local asperity height ζ , taken as the difference between the maximum width limit, and the tape width ζ_0 , reproduced .	12
2.8	SEM micrographs of CF-PPS laminates consolidated at various levels of compaction force, namely a) 500 N, b) 1000 N, c) 1500 N, and d) 2000 N, reproduced	14
2.9	Accudyne surface compactor used with AFP manufacturing, with temperature-controlled hot and cold zones, reproduced	16
2.10	Behaviour of tape width change due to transversal squeeze flow phenomena	17
2.11	Example of visible gaps in AFP-manufactured laminates and the schematics of gap and overlap influence on ply morphology prior to and following consolidation, reproduced	17
2.12	Simulated compaction and heating cycles during laser-assisted in-situ AFP, reproduced	18
2.13	Schematic of the CoRe HeaT technique utilised in AFP manufacturing of flat panels, reproduced	19
4.1	The deconsolidation setup, showing in the foreground the fixed tape, the pneumatic actuated electrodes, the thermal camera used for temperature readings, and in the background the weight used to tension the tape.	26

4.2	Visual of the deconsolidated tape using the FLIR thermal camera, as the maximum temperature is reached. The white rectangle represents the area used to estimate average tape temperature, while the green lines represent the delimitation location for the five microscopy samples.	28
4.3	Single tape embedding setup (left) and a polished micrograph-ready disc (right) . .	28
4.4	Micrograph of sample 2 of Run 2, taken at x500 magnification, with resolution of 0.44 μm per pixel	29
4.5	Entire tape cross-section being selected using the ImageJ wand tracing tool	29
4.6	Isolated tape cross-section	29
4.7	Method used for separating roughness from waviness	30
4.8	Roughness profile (down), waviness profile (middle), and the comparison between the original surface and the waviness profile (up)	31
4.9	Detailed view of sample 2 of Run 2 after segmentation	31
4.10	Whisker box plot used for data visualisation, with annotated important characteristics	32
4.11	Setup for the static compaction trials, showing a slider lying above the Prescale films placed on the mandrel	34
4.12	All considered compaction elements, grouped after geometry	35
4.13	Layers of a compaction roller, from interior to exterior: aluminum tube, cyanoacrylate adhesive, 3D printed PLA tube, 1K silicone adhesive, and 2K silicone	36
4.14	Render of the mandrel supports and frame	38
4.15	Deposition assembly in position to the side of the mandrel.	39
4.16	Deposition head, with a roller compaction element installed	40
4.17	CNC-controlled cutting machine	43
5.1	Representative specimens for all runs used in the deconsolidation study	46
5.2	Effects of moisture content on deconsolidated tape porosity, compared to pristine tape	47
5.3	Effects of moisture content on deconsolidated tape surface quality.	47
5.4	Effects of tape tension on deconsolidated tape porosity at low heating rate and above melt temperature, compared to pristine tape	48
5.5	Effects of tape tension on deconsolidated tape surface quality.	48
5.6	Effects of tape tension on deconsolidated tape width.	49
5.7	Effects of heating rate on deconsolidated tape void content at 100 N tape tension and far above melt temperature, compared to pristine tape	49
5.8	Effects of heating rate on deconsolidated tape surface quality.	50
5.9	Effects of maximum temperature on deconsolidated tape porosity at 100 N tape tension and high heating rate, compared to pristine tape	50
5.10	Effects of maximum temperature on deconsolidated tape surface quality.	51
5.11	Average compaction length as a function of theoretical compaction load for each compaction element, fitting curves	52

5.12	Average compaction pressure as a function of theoretical compaction load for each compaction element	52
5.13	Laminate thicknesses of all pipes, with the ideal laminate thickness provided at 1120 μm	55
5.15	Void content spread for each pressure element at increasing winding speeds	55
5.14	Representative specimens for winding runs 1 through 6	56
5.16	Effects of different pressure elements used at increasing winding speeds on laminate surface quality.	57
5.17	Representative specimens for winding runs 7 through 9	58
5.18	Effects of compaction pressure on porosity of preform wound laminates, using a hard silicone slider, with power law fitting curve provided	58
5.19	Effects of increasing average compaction pressures, using a hard silicone slider, on laminate surface quality.	59
5.20	Representative specimens for winding runs 7, 10, 11	59
5.21	Effects of tension on porosity of preform wound laminates, using a hard silicone slider	60
5.22	Effects of increasing tape tension, using a hard silicone slider, on laminate surface quality.	60
5.23	Representative specimens for winding runs 4 and 12	61
5.24	Effects of increasing mandrel temperature on porosity of preform wound laminates, using a hard silicone roller	61
5.25	Effects of increasing mandrel temperature, using a hard silicone roller, on laminate surface quality.	62
6.1	Sample of deconsolidated tape with high moisture content, displaying a large-size pore	63
6.2	Examples of large, well-rounded pores, within tapes heated far above melting temperature	65
6.3	Comparison between the impact of lack of tension (a), and of severe deconsolidation due to heating method (b) on surface waviness.	66
6.4	Critically damaged soft silicone roller	67
6.5	Contact theory of two aligned cylinders: a) internal stress distribution taken along the symmetry line, b) contour plot of principal shear stresses, reproduced	67
6.6	Upper surface profile analysis of a specimen belonging to Run 1, with a repeating pattern of roughness imparted by the silicone roller	68
6.7	Damaged sliders loaded under high compaction loading	69
6.8	Imprints of the copper roller at various actuator pressures, showing the impact of roller misalignment with the mandrel	69
6.9	Run 4, specimen 3, preform laminate showing step-wise indentation in the upper surface, consolidated using a copper roller	70
6.10	Voltage readings during the winding process, normalized to the target voltage, along with the layer count	71
6.11	Normalized cumulative distribution of voids throughout the thickness of specimens	72

6.12	Influence of various process parameters on the distribution of voids through laminate thickness, excluding large delaminations	72
6.13	Porous zones developed by partial filling of gaps and layer crumbling as caused by the forced filling of gaps	73
6.14	Laminate porosity plotted against the consolidation duration for Runs 1 through 6, with increasing average compaction pressure (up), and the slopes of the linear fitting laws, as plotted against their respective average compaction pressures. . . .	74
6.15	Comparison between the expected performance of a slider at 1.22 MPa average compaction pressure to that of the copier roller at 4.56 MPa for various winding speeds, given a simplified linear behaviour	75
6.16	Comparison between the expected performance of a slider at 2.4 MPa average compaction pressure and with an increased arclength of 70 mm to that of the copier roller at 4.56 MPa for various winding speeds, given a simplified linear behaviour	77

Chapter 1

Introduction

Over the past few decades, Thermoplastic Polymer Composites (TPC), and especially Carbon Fiber Reinforced Polymers (CFRPs) using thermoplastic matrices have been garnering increased interest in the aerospace industry. Original equipment manufacturers and aviation companies have taken a keen interest in these novel materials for several reasons. They offer significant weight reductions when compared to metals and alloys due to their high strength-to-weight ratios and can be used in high-performance applications, such as primary and secondary components. They allow for functional part integration and open new areas in the design space, which can lead to further weight savings. Unlike thermoset-based composites, they are weldable, and consequently more maintainable, and can be recycled, since they are able to soften when heated and reused for other, less strenuous applications. They are also less hazardous to handle, can be produced automatically with a fast throughput time, and the production feedstock does not have to be stored under special conditions, unlike thermoset materials.

Modern commercial aircraft utilize a plethora of parts made of composite materials, such as the Airbus A350 XWB sporting over 53% of composite material by weight [1]. Airbus and GKN Fokker paved the way for the use of thermoplastic components when they substituted a five-part honeycomb aluminum composite D-nose for a molded monolithic GF/PPS J-nose within the leading edge of the wing of the A340-600 back in 2002, leading to a 20% reduction in weight [2]. In 2019, the Thermoplastic Affordable Primary Aircraft Structure (TAPAS) Consortium, which included the likes of Airbus, GKN Fokker, and later Gulfstream, developed a demonstrator for a large-scale CF-PEKK fuselage panel with integrated stiffening elements produced using a combination of Automated Fiber Placement (AFP), molding, and welding techniques [3]. These efforts culminated in the Multifunctional Fuselage Demonstrator (MFD), the world's first entirely thermoplastic fuselage barrel, in 2024. The project was part of the European Union's Clean Sky 2 initiative, involved, amongst others, the German, Dutch, and French aerospace research centers, TU Delft, Airbus, and Fokker, and equated to a weight saving of 1 tonne, thus leading to a potential reduction of CO₂ emissions by 1-2% [4]. A market study performed by ReportLinker has shown that the thermoplastic composite industry is likely to exhibit a compounded annual growth rate of 8% from a market size of 38.49\$/FY2022 in 2023, to one of 76.94\$/FY2022 by 2032 [5].

The Continuous Resistance Heating Technology (CoRe HeaT), developed at the Center for Lightweight Production Technology (ZLP) of the German Aerospace Center (DLR) in Stade, Germany, was created in order to tackle the foreseen increase in thermoplastic composite demands. It leverages

the Joule effect, described by the increase in temperature of a conductor carrying electrical current, to heat continuous CF reinforced prepreg tapes at very rapid rates. This technology was implemented for the plastic tape winding processes in order to manufacture open-ended high-performance cylindrical thin-walled parts at fast winding speeds, which could later be used as lightweight hydrogen tanks, pipes, and supporting struts. The state-of-the-art method for CoRe HeaT tape winding comprises two parts: a winding stage, where the prepreg tape feedstock is melted and deposited on the tooling, and a post-consolidation stage, where the laminate is further post-processed under heat and pressure, in order to reach desirable porosity, interlaminar bonding, and crystallinity. This technology is still under research and development but shows great promise for high-speed tape laying and winding manufacturing processes. Multiple research projects are currently ongoing in order to increase the maturity of CoRe HeaT.

The aim of this study is twofold. Firstly, to investigate the deconsolidation behaviour of UD CF-reinforced thermoplastic tape using CoRe HeaT and relate it to the laminate preform quality. And secondly, to assess the influence of consolidation parameters, such as pressure element, applied pressure, consolidation duration, and tow tension, on quasi-90° preform laminate quality manufactured using CoRe Heat-based tape winding. It is believed that the insights developed by accomplishing these goals would bring significant improvements to the in-situ consolidation taking place during the winding stage, and consequently, curtailing post-processing, and increasing throughput time and energy efficiency.

The relevant research background for this study is presented in Chapter 2, which covers the employed method of literature research, a short introduction to reinforced thermoplastic manufacturing, and a detailed discussion on the functional elements and governing mechanics at play in filament and tape winding using CoRe HeaT. Chapter 3 describes the research complex of this study, including the knowledge gap to be filled, the objectives of this research, the research questions to be answered, and some initial hypotheses to be validated. The methodology used across this study is presented in Chapter 4, addressing three main experiments: static deconsolidation, static compaction, and preform winding. The results obtained following this methodology are described in Chapter 5, and are evaluated and discussed in Chapter 6, which also examines the validity of the hypotheses outlined prior. Based on this discussion, some main conclusions are highlighted in Chapter 7 in order to answer the previously established research questions. Recommendations for future work are presented in Chapter 8.

Chapter 2

State of the Art

This chapter contains relevant background knowledge, as well as some in-depth parametric studies and theoretical models, regarding the relevant fiber reinforced composite manufacturing methods and various material phenomena that influence these production methods. This information will be of great aid in establishing the research questions to be answered within this study, as well as the initial hypotheses that are to be verified. First, the search methodology that led to the selection of these sources is presented, after which a broad introduction into fiber reinforced thermoplastic production methods is given. The novel CoRe HeaT technology employed in this study is then described. Lastly, a collection of relevant literature, comprised of parametric experimental studies and validated theoretical models, is presented.

2.1. Search strategy

The literature used to support this chapter was searched, aggregated, and sorted using the following methodology:

Research: A relevant search query was assembled depending on the desired subject and scope of literature. The search query was separated into four distinct aspects: manufacturing process, reinforcement fiber type, resin type, and parameter of interest. These four aspects were to be established with enough specificity to yield relevant results but also broad enough to touch upon a large pool of titles. After compiling enough key terms, the search query was used in the "Web of Science" search engine. This search engine was selected based on the amount and relevance of results.

Refinement: Once a database was provided by the search engine, all publications in another language other than english were filtered out. Additionally, given the novelty and the rate of learning of the field of reinforced thermoplastics manufacturing, all results published prior to the year 2000 were eliminated. Furthermore all papers not being either a result of primary research, a review paper, or a conference proceeding were excluded.

Review: The relevancy of all titles within the sufficiently large database was verified by the means of the "ASReview Lab" tool [6]. Based on machine learning algorithms, this open-source tool is able to sort publications based on expected relevancy after it is provided with a small, around a few percent of the total number of papers, labeled set of relevant titles. This prior knowledge set is established based on manually reviewing the titles and abstracts

of some randomly selected papers and labeling them either relevant or irrelevant. Once the entire database is sorted, the abstract of the titles can be reviewed in order for a manual selection. Using a stopping rule, such as reaching 25 irrelevant publications since the last relevant one, can be then used to end the review phase. Additionally to this automated method, the resulting papers were further refined manually based on full content, yielding the final literature pool

To begin the literature review process described above, the following search query was used as a general starting point: (AFP OR automated fiber placement OR filament winding) AND (carbon fiber OR CFRP OR composite) AND thermoplastic AND (force OR tension OR pressure OR speed OR temperature OR crystallinity OR porosity). This search query, loaded in the "Web of Science", yielded 280 publications. After applying the aforementioned exclusion criteria, the database thinned to 233 results. These were loaded in ASReview, and using the aforementioned stopping rule, the relevant numbers of results was lowered to 52, out of 152 labeled results. After manual refinement, the relevant number of results was further lowered to 24. Yet, after manual inspection, an additional 8 papers were added to the database, based on the citations used by relevant papers.

2.2. Reinforced thermoplastic manufacturing

Advancements in the chemistry industry of the early to mid 20th century led to the creation and popularization of various functional polymers to be used in Fiber Reinforced Composites (FRC). These synthetic materials proved to be more resilient to environmental conditions and possessed more attractive mechanical properties per unit of weight than their conventional counterparts, such as aluminum alloys. Major strides in composite manufacturing were made in 1907, when the pattern for a new polycondensation phenolic resin called Bakelite was filled in the U.S. [7]. What followed was the implementation of this material, as both an adhesive and the matrix for fiber reinforced composites. During WWI Bakelite was used as a binder in the laminated canvas composite Bakelite-Micarta in bomber propellers [8]. During WWII the Horten brothers develop the first aircraft entirely made from composite materials, an experimental tail-less delta-wing made from paper reinforced phenolic resin [9]. During this period flax fibers are being introduced as reinforcements in phenolic resin composites and being used in Vickers Supermarine Spitfires [10].

By the end of the 1940s, Pierre Castan successfully applies for a patent for the production of epoxy resin, which, in one form or another, would dominate the civil aircraft composite industry to this day [11]. Glass fiber composites were also developed during the 1940s and 1950s, using fiberglass invented and produced by the Owens-Illinois company in the early 1930s, and were being used primary structures such as wings, fuselages, and empennages [12].

Another big leap in composite production was the development of Polyacrylonite (PAN) carbon fiber, first created by Akio Shinodo of the Government Industrial Research Institute in Osaka, Japan in 1961. Industrial scale production was realized by the Toray company in the early 1970s [13]. This proved to be a key step in the adoption of fiber reinforced composites by the civil aviation industry during the 1980s, with Airbus pioneering the practice of using carbon fiber reinforced polymers in primary structures with the vertical tail of the A310-300. Since then, Airbus has been gradually integrating fiber reinforced polymers into its aircraft, culminating in the launch of the A350 XWB in the mid-2010s. A wide body aircraft, it comprises of more than 53% composites by weight, with FRP being found all over the fuselage, internal and external wing structure, and in both vertical and horizontal tails[1].

Currently, the majority of the resin materials used in industrial composite manufacturing are of the thermoset variety, which come in the form of low-viscosity viscoelastic liquids comprised

of monomers and short-chain oligomers that require a chemical reaction to develop into a three-dimensional network of interlinked polymer chains forming an amorphous solid. This can be in part attributed to their material properties, such as high resilience against fatigue, resistance against corrosion, chemical degradation, and heat, and versatility regarding types, blends, and additives. From the perspective of manufacturing, the maturity of the textile industry, matching the high precision required by the aircraft industry, played a key role in the adoption of fiber reinforced thermosets, determining the now seen popularity of resin infusion processes using woven or non-woven fabrics and of autoclave processes using preinfused preforms. Yet, in order to face modern challenges, much effort is spent on the research and development of fiber-reinforced thermoplastics.

Thermoplastic materials are composed of individual polymeric chains held in place by intermolecular forces such as hydrogen bonds, weak Van der Waals forces, and strong aromatic interactions. These polymeric chains can become mobile and slide over each other under the application of heat, in a fully reversible manner. In the case of fully amorphous thermoplastics, these polymer chains are randomly oriented and entangled, making the initially brittle solid become rubbery once the glass transition temperature is exceeded. While, in the case of semi-crystalline polymers, certain regions of chains are neatly arranged in a crystalline matter, leading to stronger bonds and a higher transition temperature, known as the melting temperature. Further heating of both types of polymers would lead to a highly viscous liquid. For structural purposes, semicrystalline thermoplastics are favored, such as PEEK, PAEK, and PPS, for their improved relative strength and stiffness, high thermal stability, and improved impact resistance.

The characteristic of thermoplastic being reversibly deformable at high temperatures under conforming pressure opens numerous opportunities and brings various advantages in the aircraft industry. As opposed to thermoset preforms, thermoplastic prepregs can be stored in ambient conditions indefinitely prior to use. Thermoplastic parts can also be welded together to create seamless, airtight joints at no extra weight cost, improving part integration and facilitating maintenance. Thermoplastic structures can be more readily recycled at the end of life, decreasing waste in the industry. At the same time, the high viscosity during the melt phase becomes a hurdle to be overcome in the manufacturing process, especially in the production of large and complex structures. Consequences of partial resin penetration, such as porosities and delaminations, drastically reduce mechanical properties, while squeeze flow caused by the viscous resin displacing fibers along its movement causes variability in fiber content and fiber tortuosity, again contributing to inferior mechanical properties. Furthermore, given the complexity of manufacturing high quality thermoplastic impregnated tapes or fabrics, the price of thermoplastic prepregs is considerably higher than for thermoset prepregs.

Considering the technical and economic challenges associated with manufacturing high-performance fiber reinforced thermoplastics, the development of fast, efficient and effective production methods is of utmost importance towards fully commercializing this type of material at an industrial scale within the aviation industry.

2.3. Filament winding

Filament winding is a firmly established and widely used method to manufacture axis-symmetric fiber reinforced composite structures, such as struts, pipes, tanks, masts, shafts, etc. The process consists of the guided placement of continuous tensioned fiber yarns, powder-impregnated tapes, and UD prepreg tapes with the help of a laterally moving carriage on a rotating mandrel. Conventional filament winding processes, mostly using dry fiber, either as received or pulled through a resin bath or preimpregnated thermoset tapes, also require subsequent processing steps, such as resin infusion for dry deposition, and/or autoclave or vacuum bag only curing.

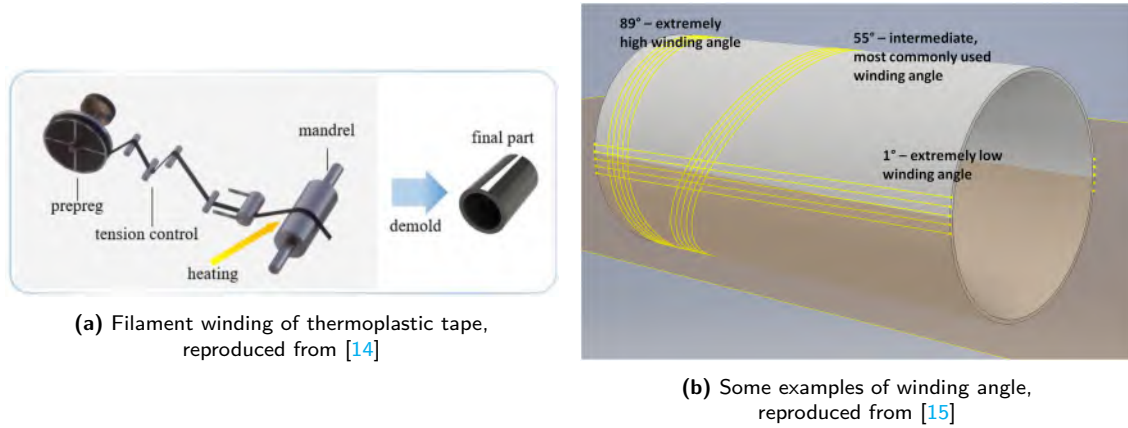


Figure 2.1: Schematics related to winding processes

The rotation rate of the mandrel is dictated by the translational speed of the cart and the desired layup, which is mainly described by the winding angle of incoming tape. By manipulating the ratio between the mandrel rotation and carriage translation, various winding patterns can be achieved, from circumferential winding, with a winding angle of 90° , to longitudinal winding, from pole to pole, with a winding angle of 0° , to helical winding, described by a winding angle in between the aforementioned values. Deposition accuracy is of high importance, especially in high-speed applications, which is why the tow is continuously maintained in tension, preventing tow sag and ensuring tight tow placement and promoting contact between the deposited tow and the laminate substrate. The variability of winding angle, and in turn the laminate layup, can lead to gaps and overlaps, which can locally influence wall thickness and porosity, yielding unsatisfactory mechanical properties. In turn, using automation such as robotic arms with multiple degrees of freedom and CNC-based control schemes that enable the mandrel and carriage to move independently are being used to open new possibilities in winding patterns, also known as deposition path, and part geometry, including non-axisymmetric designs. Sorrentino et al. used robotic filament winding in combination with forming techniques to manufacture a helicopter fork, the part upon which the rotor blade is attached, and which is non-axisymmetric and contains concave surfaces [16].

As previously mentioned, the use of thermoset resin baths and prepreg tapes requires additional manufacturing steps to promote resin curing, remove entrapped air in the form of bubbles, and increase interlayer contact and bonding. Although a necessity, these processes are time-consuming, include a large amount of auxiliary supplies that are single-use and thus end up as waste, and can be highly energy-intensive. It is thus in the general interest to further improve on these points while adapting the overall process to produce thermoplastic fiber reinforced composites.

2.4. Tape winding

Filament winding processes using thermoplastic prepreg UD tape, also referred to as tape winding, include a heating element prior to deposition in order to melt the polymer matrix, leading to autohesion with the substrate. Reaching the melt temperature of the polymer also greatly increases the surface tackiness of the tow, aiding the accuracy of tape placement. In-situ consolidation can be accommodated for tape winding processes in order to eliminate the need for subsequent autoclave or out-of-autoclave processes entirely. In-situ consolidation implies the use of consolidation pressure during tape deposition in order to promote intimate contact, force the diffusion of pores out of the laminate, and yield polymer autohesion. As shown in Figure 2.2, the tape winding process can be broken down into several regions of increased interest, namely :

Unloading zone: The region that contains the transition of the tow from the mother material

spool to the applicator head containing the equipment able to melt the tape, and represents the majority of the tape path

Heat zone: The part of the tape path that is directly heated

Nip point: Also known as the nip line, it represents the area of tape that is in immediate contact with the laminate substrate and is pressed on by the compaction element

Deposition zone: The substrate that has been laid up in previous winding passes

Each zone harbors various behaviors and effects that must be understood and controlled in order to achieve a synergistic and reliable manufacturing process.

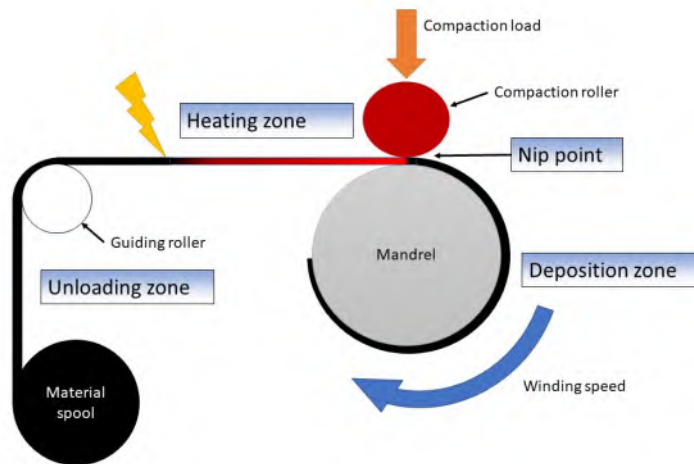


Figure 2.2: Schematic of the tape winding process, with specific process zones

2.4.1. Unloading zone

Given that the tape winding process is a continuous process, it requires UD continuous fiber reinforced tapes. These tapes are commonly produced by either hot melt coating or pulltrusion [17]. An example of the required setup is shown in Figure 2.3. Firstly, multiple tows of sized carbon fibers from various bobbins are spread to the desired tape width, which can vary from 60 mm to 1300 mm, while closely monitoring the areal fiber density. After having a spread of UD carbon fiber, the thermoplastic resin is introduced, either as a film of extruded melted polymer which permeates the tow using compaction pressure induced by the tow being tensioned over rollers, or as a pool through which the tow is calendared. The impregnated tape is further passed through calender rolls under tension to ensure sufficient consolidation and reach the desired tape thickness, most commonly around 0.15 mm and fiber volume fraction. Thus, industrially manufactured thermoplastic UD tape is well consolidated and incorporates a low amount of defects. Generally, low-width prepreg tapes, such as the widely commercialized 1/4 inch tape, or 6.35 mm, are made from slitting wider tapes to measure, which can affect the morphology of tape edges. The resulting cut tapes are wound on a material spool and passed over for the manufacturing of parts.

Although not part of the unloading zone directly, the storage of the material spools can have an impact on final part quality, through the absorbed moisture content. If transported or kept in humid conditions, polymer matrix can absorb moisture from the environment as diffused water molecules, especially in the case of polymers made from polycondensation reactions, such as polyamides and polycarbonates. These plastics contain polar groups that better attract water molecules, making them hygroscopic. As it will be expanded when discussing tape deconsolidation behavior, this entrapped moisture leads to the formation of pores down the production line.

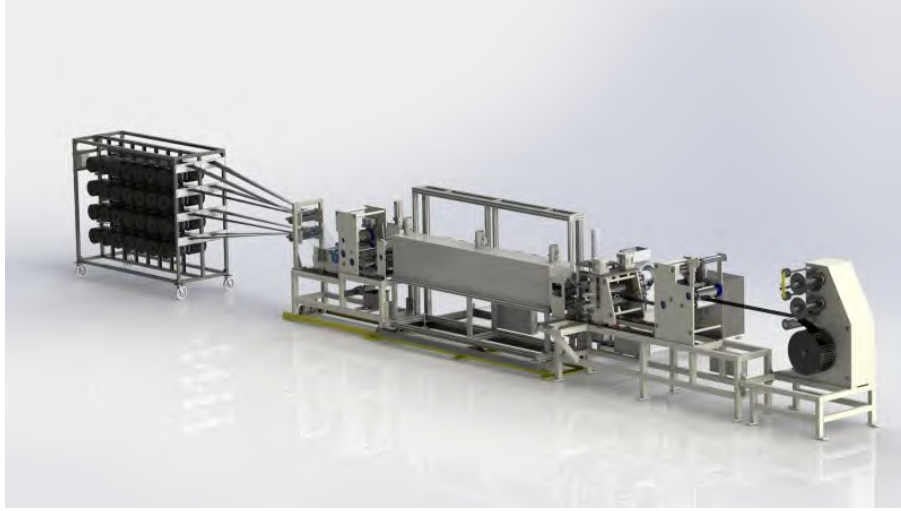


Figure 2.3: Thermoplastic tape line and slitter designed by Cygnet Texkimp, showing material creels, heat shielded impregnation unit, calender rolls, and the final accumulation spool, reproduced from [18]

Thus, keeping material spools in a dry environment is encouraged.

Prepreg UD thermoplastic tape, and especially the ones containing high performance thermoplastics such as LM-PAEK, PEEK AND PEKK, regain significant high stiffness despite their slenderness. Accordingly, great care must be put into tape alignment within the unloading zones. Lateral misalignment between subsequent rollers in the path tape must be absolutely minimized. Otherwise, under the influence of tow tension, the tape can either impinge on roller side walls or lie under variable radius curvatures that concentrate tape tension to one edge or introduce out of plane loading, resulting in tape splitting, which is highly undesirable. Furthermore, depending on polymer type, fiber volume content and areal density, tapes may have different bending radii under which breaking occurs, which has to be taken into account when planning for a tape path. Additionally, reasonable limitations regarding tape twist and tape length for certain twists in the tape path must be considered.

Along the length of the unloading zone the tape tension is usually set, with the help of an electronically controlled break. Within this region tape tension readings are also taken, either using a load cell and an arrangement of rollers, or by using tensiometers specially designed for measuring tow tension about an axis. It should be noted here that the roughness and amount of rollers can greatly influence the tape tension, by the action of friction.

2.4.2. Heating zone

To reach the high temperatures required to melt the thermoplastic matrix, sometimes even exceeding 350 °C as in the case of PEEK, heating sources such as hot gas torches, pulsed light lamps, infra-red heaters, and focused lasers are used. These heat sources are placed in close proximity to the nip point and are required to ensure that the temperature at the nip point is within the processing temperature range of the deposited material. In this state, also known as melt state, the polymer chains within the matrix are highly mobile, and the material is able to flow, and thus be molded into the desired shape. Thus, it is imperative that the tape must be in a melt state when it arrives under the influence of the compaction pressure at the nip point.

In the region within the heat zone but preceding the nip point, tape deconsolidation is highly likely to occur. This phenomenon occurs as the thermoplastic matrix is able to flow while the tape is not subjected to any out of plane loading. In turn, the tape experiences morphological changes such as a sharp increase in porosity, increased surface roughness and tape waviness, as well as considerable thickness expansion. By investigating laser heating of 6.35 mm thick UD CF-PEEK tapes, Çelik et al. found that heating length and heating rate, which is equivalent to deposition rate, have a significant impact on tape morphology, with heating length greatly influencing waviness and roughness. Moreover the local discrepancies in heating due to unevenly rough tape surface leads to locally exacerbated deconsolidation [19].

The deconsolidation behaviour has been attributed to multiple concurrent causes. The increased void content can be linked to diffused or pre-existing entrapped foreign substances. In the case of already present pores, an increase in temperature would lead to the entrapped gas expanding in volume until a pressure equilibrium is reached, as shown in Figure 2.4a. Besides entrapped air, diffused moisture can play a role in the rise of void content during deconsolidation. As the polymer reaches temperatures above T_g , diffusion of water molecules is facilitated by the increased mobility of polymer chains. By studying CF/PEEK multi-layer preform blanks, Slangue et al. observed that these mobile water molecules coalesce at the interface between layers to form voids and voids channels, which eventually reach the limits of the blanks and degas, leaving behind a network of voids [20]. The phenomenon is illustrated in Figure 2.4b. Additionally, by monitoring the thickness change in real time, it was observed that deconsolidation occurs instantaneously once T_m is reached.

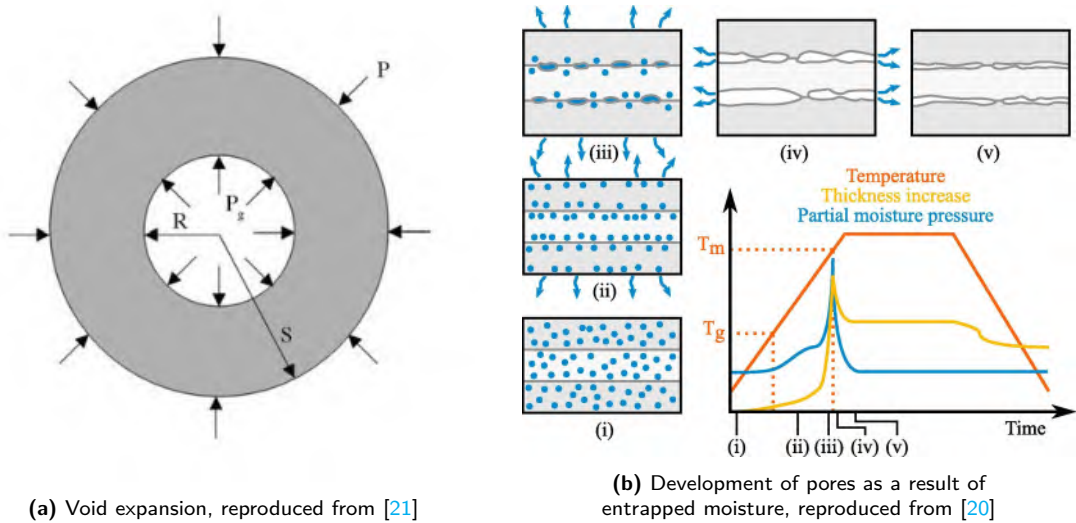


Figure 2.4: Void development mechanisms taking place in the presence of high temperatures

Furthermore, the release of frozen residual stresses introduced to the tape during tape manufacturing may also play a role in the morphological change of consolidated tape. As the matrix becomes soft and malleable, residual stresses maintained within the highly stiff carbon fibers may greatly displace matrix, increase tape thickness and roughness, and enlarge other created voids [19].

In a subsequent study, Çelik et al. studied the compaction behavior of deconsolidated CF-PEEK tape. It was determined that morphological changes at the meso-scale, such as waviness, due to deconsolidation, were reversible under compaction held above T_g , while micro-scale morphological changes, such as surface roughness and porosity, became partially reversible only after reaching

T_m [22]. Using optical microscopy together with image analysis techniques, the study demonstrated that high-power heating deconsolidation above the melt state increases void content by an order of magnitude as compared to as-received tape. A similar trend was also found when analyzing tape roughness. Ultimately, it was shown that, apart from roughness, as-received tape and consolidated tape become statistically indistinguishable if compacted with enough pressure for an extended period of time.

Excessive heating can lead to degradation of the polymer matrix, which can yield significant increases in viscosity, decreased crystallinity, and even loss of polymer mass, affecting laminate performance and life span. For high performance thermoplastics, such as PEEK and PAEK, it is known that prolonged dwell times above 340 °C in an oxidative atmosphere can lead to chain cleavage and subsequent crosslinking, which highly increases the complex viscosity of the melt, lowers the crystallizability of the material, and changes its color, without noticeably reducing the mass of the polymer [23]. Besides dwell times at temperatures above the melting point, it has been shown that the heating rate can also greatly influence the thermal degradation phenomenon. In a study performed on PEEK degradation, Gaitanelis et al. showed that high-rate heating had a lesser influence on the degree of crystallinity as compared to slow-rate heating methods [24]. This is attributed to a lower duration spent at high temperatures, and thus a decrease in time where the crosslinking due to degradation could take place. This would favour higher heating rates methods, such as laser-based and induction or electrical conductivity.

2.4.3. Nip point

The bonding between incoming melted tape and the laminate substrate occurs at the nip point, and is largely characterized by two phenomena, namely the development of intimate contact, and autohesion at the polymer interface [25]. Both of these stages of bonding are illustrated in Figure 2.5. These processes are interdependent, as autohesion requires the formation of intimate contact between the lower side of the tape and the upper surface of the substrate. As these physical phenomena are the basis of interlaminar bonding, sufficient understanding is required in order to effectively promote bonding, and thus, increase part quality and mechanical properties.

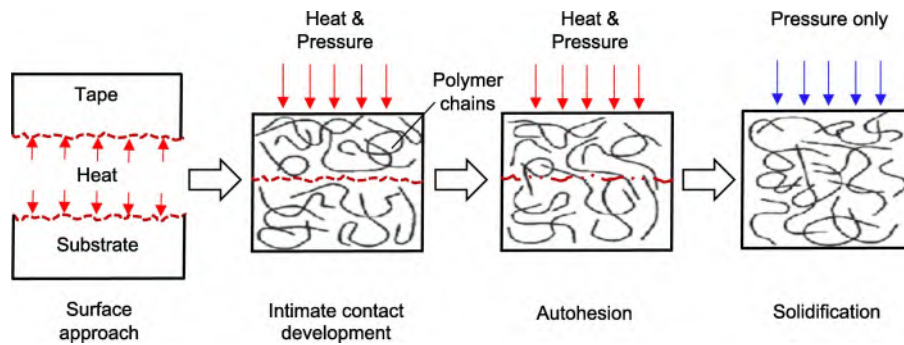


Figure 2.5: Schematic of the bonding mechanism of thermoplastic reinforced tape, reproduced from [25]

Intimate contact represents the coalescence of subsequent laminate plies, and is generally measured by the degree of intimate contact, which is defined by the area of immediate contact between the tape and substrate divided by the total available interface area [26]. Insufficient intimate contact can lead to insufficient interlaminar bonding, lowering interlaminar shear strength, and also to the entrapment of air at the interface, thus resulting in pores between laminas that can act as stress

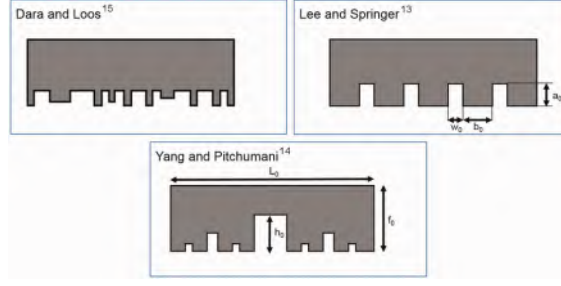


Figure 2.6: Surface models schematic representations, reproduced from [28]

concentrators and yield delaminations.

Multiple models have been developed in order to simulate the development of intimate contact, yet the majority of the models are based on the same physical phenomena. The tape is simulated with a certain surface quality, containing various-sized asperities at the micro-scale. As the tape is heated, the thermoplastic matrix becomes mobile, and is able to flow under an external load. Accordingly, the tape surface asperities flatten to form intimate contact. In order to model the deformation of such asperities, the flow of the viscoelastic mixture of melted matrix and fibers is assumed to behave as a Newtonian squeezing flow of an equivalent homogeneous fluid between two rigid plates. The governing equations upon which squeeze flow is based are obtain from conservation of mass and laminar flow condition, with the latter being considered descriptive of such a slow-moving, highly viscous flow as the one for the matrix-fiber mixture. [Dara and Loos](#) first developed the model and described the asperity profile of the tape by matching a Weibull Density Function to a histogram of experimentally measured relative tow heights [26]. [Lee and Springer](#) simplified the model by describing the asperity distribution as a sequence of equally spaced and identical rectangles, with a_0 initial height, b_0 initial width, and w_0 gap distance as defining characteristics [27].

Thus, the expression for the degree of intimate contact (D_{IC}) was simplified to Equation 2.1, with μ_{mf} being the equivalent transversal viscosity of the melted matrix-fiber mixture, P_{app} being the applied consolidation pressure, and t being the duration of maintained contact.

$$D_{IC} = \frac{1}{1 + \frac{w_0}{b_0}} \left[1 + 5 \left(1 + \frac{w_0}{b_0} \right) \left(\frac{a_0}{b_0} \right)^2 \int_0^{t_c} \frac{P_{app}}{\mu_{mf}} dt \right]^{0.2} \quad (2.1)$$

Further simplifying the expression by assuming constant pressure and viscosity during contact duration t_c , the time to obtain intimate contact can be described as in Equation 2.2. This could be argued as a valid assumption for fast processes, such as in-situ tape winding. For validation purposes, [Lee and Springer](#) showed accordance with hot press consolidating of APC-2 (PEEK) CF preforms, with full intimate contact forming in the order of tens of seconds for processing temperatures exceeding 350 °C and consolidation pressures exceeding 0.27 MPa.

$$t_{IC} = \frac{\mu_{mf}}{5P_{app}} \frac{1}{1 + w_0/b_0} \left(\frac{b_0}{a_0} \right)^2 \left[\left(1 + \frac{w_0}{b_0} \right)^5 - 1 \right] \quad (2.2)$$

[Yang and Pitchumani](#) described the surface roughness of the tape as a Cantor set fractal after observing that the distribution of the Fast Fourier Transform of the surface profile after the spatial dimension of asperities follows a power-law variation. In turn, the power spectrum of the Fourier transformed tape surface roughness can be described by Equation 2.3, with C a fitting constant, ω the frequency in the asperity length scale, and D the fractal dimension [29].

$$S(\omega) = \frac{C}{\omega^{5-2D}} \quad (2.3)$$

Furthermore the fractal is further defined by the scaling ratio between two adjacent generations of asperities, f , and the number of generations on a repeating Cantor set s [29]. Thus the case for a scaled Cantor set fractal was made and successfully validated using non-destructive ultrasonic measurements of D_{IC} after hot press consolidation. The final expression for the D_{IC} is given by Equation 2.4, with n representing the n -th generation of the Cantor set. Accordingly, the determination of the D_{IC} is done sequentially, set generation by set generation, as large asperities have to collapse first before shorter asperities have the chance to be loaded.

$$D_{IC}^{(n)} = \frac{1}{f^n} \left[1 + \frac{5}{4} \frac{f^{\frac{2sD}{2-D} + n + 4}}{(f+1)^2} \int_{t_{n+1}}^{t_n} \frac{P_{app}}{\mu_{mf}} dt \right]^{0.2} \quad (2.4)$$

Although squeeze flow was assumed to be the primary viscoelastic deformation mechanism to take place at the nip point, Kirchhoff et al. makes the case for matrix percolation in continuous high-speed manufacturing processes, based on three arguments. Firstly, a scaling analysis relating percolation flow and squeeze flow theoretically suggests that the former is favorable over the latter. Secondly, given the fibers always extend in areas of the tape where the enclosing matrix is solidified, the equivalent viscosity of the melted area should be corrected accordingly, increasing in value, thus favoring percolation. Lastly, through observations of Scanning Electron Microscopy images of cross-sections of consolidated laminates, it has been noted that the propensity of resin-rich areas to form in interlaminar regions. This phenomenon is argued to be the result of percolation flow of melted thermoplastic through a rigid fiber bed. Thus, a model was developed based on Darcy's law of permeability, as shown in Equation 2.5, with \mathbf{u} local velocity vector, \mathbf{K} the permeation tensor of the fiber bed, V_f the fiber volume content, and P the local pressure vector [30].

$$-\mathbf{u} = \frac{-\mathbf{K}}{\mu(1 - V_f) \nabla P} \quad (2.5)$$

By assuming the resin front travels only along the thickness of the tape, and that the resin front conserves its mass, it is possible to obtain the height of an asperity in relation to its original height, as shown in Equation 2.6, where ζ is asperity height, ζ_0 is the tape thickness, ζ_i is the initial tape asperity, K is the permeability of the fiber bed, and μ is the matrix viscosity.

$$\zeta(t) = \zeta_0 - \sqrt{(\zeta_0 - \zeta_i)^2 + \frac{4K}{(1 - V_f)} \int \frac{P(t)}{\mu(t)} dt} \quad (2.6)$$

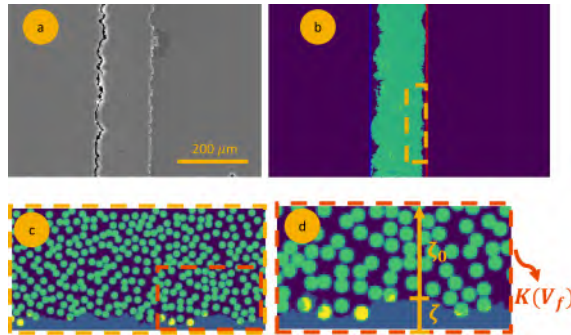


Figure 2.7: a) SEM scan of tape cross-section, b) isolated and segmented image with maximum width range marked by vertical lines, c) zoomed tape section illustrating fibers, matrix, and embedding resin, d) definition of local asperity height ζ , taken as the difference between the maximum width limit, and the tape width ζ_0 , reproduced from [30]

Thus, intimate contact is reached through percolation when $\zeta(t)$ reaches zero. Using this method over the entire width of the 1D flow front, the D_{IC} is described by Equation 2.7.

$$D_{IC} = \frac{1}{w} \int_0^w H \left(1 - \frac{\zeta(t)}{\zeta_i} \Big|_x \right) dx \quad (2.7)$$

Further assuming the applied pressure and viscosity remain constant during the process, the required time to achieve intimate contact over a segment of tape width is given by Equation 2.8. A similar analysis over the entire width of the tape can be done to evaluate the overall time to reach total time to intimate contact, by taking the maximal value.

$$t_{IC} = \frac{(1 - V_f)\mu}{4K\Delta P} (2\zeta_i\zeta_0 - \zeta_i^2) \quad (2.8)$$

Using these insights, [Kirchhoff et al.](#) simulated the percolation of a LM-PAEK CF reinforced tape processed at 400 °C and found that the required time to intimate contact using 0.96 MPa compaction pressure would be around a couple of tenths of a second at maximum, depending on fiber volume fraction and tape roughness [30].

It is clear that the surface roughness of the tape plays a large role in the formation of intimate contact. A tape with closely packed slender asperities would require much shorter times under consolidation pressure to achieve full intimate contact as compared with a tape with widely distributed short and bulky asperities. As it has been previously discussed, the deconsolidation phenomenon, which occurs right before the nip point, increases the tape roughness significantly and thus can cause ineffective formation of intimate contact. It is important to note that both models for intimate contact were validated using hot press consolidation, where deconsolidation cannot occur, unlike in continuous tape winding. Thus, in the case of tape winding, the surface roughness taken as model input should be the one of a deconsolidated tape in order to effectively achieve any valid information regarding D_{IC} . Another noteworthy observation in regarding to deconsolidation is that tape waviness, as induced by deconsolidation, is not considered in these models. Thus, even though previously discussed studies showed that waviness is totally reversible after consolidation, there is no indication how tape waviness would affect the results of these models.

The other factors influencing the development of intimate contact are related to directly controlled process parameters. Firstly, the time to achieve full intimate contact is inversely proportional to the applied consolidation pressure. Thus, two avenues to achieve complete intimate contact arise, either using intense pressure for short times, akin to fully rigid contact, or using lower pressure while maintaining contact for longer durations, akin to conforming soft contact. Secondly, the duration of total intimate contact is proportional to the viscosity of the melt-fiber mixture. This parameter can be indirectly controlled using the tape heating rate, by establishing the desired tape temperature at the nip point. Yet, this method of influencing D_{IC} is more cumbersome as compared to the previous strategy, as temperature variations during continuous fiber laying or winding processes are widespread, even more so for high speed processes. Furthermore, discrepancies between tapes, such as fiber distribution across tape profile, adds further variance. Thus, it is thought that an achievable influence on D_{IC} , and in turn, on interlaminar porosity and bonding, can be done through the choice of pressure element and applied consolidation load.

[Zhao et al.](#) Investigated interlaminar bonding of CF-PPS laminates using laser-assisted in-situ AFP with a solid roller at various deposition speeds and processing temperatures [31]. They showed that porosity increases with winding speed for all processing temperatures, yet the rate of porosity increase decreases with an increase in nip-point temperature. Retrofitting the data resulted from

this study showed that the relationship between porosity and deposition speed was best described by a power law, irrespective of the used nip-point temperatures. The tape placement speeds considered were limited to 60 mm/s, 100 mm/s, and 200 mm/s. The same study showed that the surface profile approximation of Lee and Springer yielded more accurate intimate contact results in experimental trials as compared to the one developed by Yang and Pitchumani. Yet, the surface profiles which was simplified to be used in the intimate contact model were taken from pristine tape and not from deconsolidated tapes Khan also encountered a gradual increase in laminate porosity with increasing deposition speed when validating a void content development model for hot gas torch AFP, based on the expansion of pre-existing voids within the prepreg thermoplastic tape until equilibrium is reached with the surrounding compressed melted tape [32]. It was determined that initial lamina tended to have lower porosities as compared to final plies.

In a prior study, Zhao et al. investigated process parameters such as applied compaction load, laser temperature, tool temperature, and placement speed for laser assisted AFP using CF-PPS tapes [33]. It was determined that the compaction load and winding speed were the most significant impact factors on laminate porosity. Samples produced during this study at increasing levels of compaction pressure are shown in Figure 2.8. By evaluating the interlaminar shear strength of the laminates, it was shown that crystallinity did not correlate with ILSS, and it was proposed that porosity might be the most influential factor in this regard.

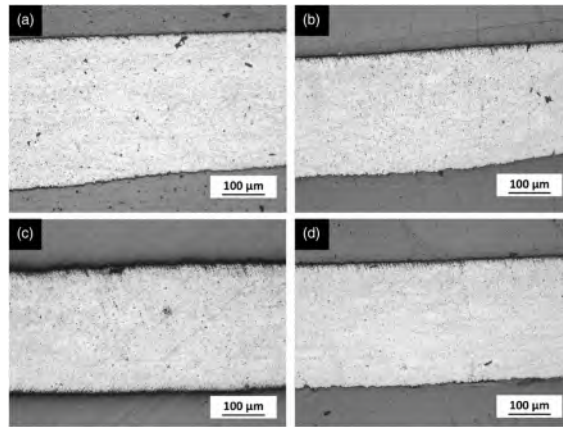


Figure 2.8: SEM micrographs of CF-PPS laminates consolidated at various levels of compaction force, namely a) 500 N, b) 1000 N, c) 1500 N, and d) 2000 N, reproduced from [33]

Heathman et al. also varied the applied compaction pressure in a study on consolidation quality using laser-assisted in-situ AFP in conjunction with a 25 Shore A hardness roller on flat CF-LMPAEK laminates [34]. The findings show that the compaction force had a negligible effect on porosity when compared to processing speed and processing temperature. It is presumed that this is due to an insufficiently long compaction length, such that the tape is still above T_g after it exits the consolidation area.

The application of consolidation pressure is done through the inclusion of an actuated pressure element, most often a freely rotating roller, which activates above the point of contact between the incoming tow and the substrate, also known as the nip point. Besides promoting intimate contact, consolidation pressure is also meant to close and fill the voids already present in the deposited tape, mostly formed during deconsolidation. In turn, the temperature at the nip point must be ensured to be above T_m in order to provide the polymer flow required to close such pores. Given these high processing temperatures, compaction rollers are often manufactured using high heat-resistant materials in order to maintain adequate contact between roller and laminate during the process, and to avoid the inclusion of foreign material or residue in the laminate itself. Here,

the distinction between conforming and non-conforming pressure elements must be made, as their main differences are exacerbated by the curved nature of the mandrel.

Conforming rollers, most often made out of various silicone polymers, are quite flexible under the applied loads, and can better dissipate the consolidation pressure over the contact area, leading to a more uniform pressure distribution. Conformable pressure elements can also adapt to surface discontinuities, such as layer drops, and can maintain contact even in these circumstances. Depending on the stiffness of the material and applied load, the width and, more importantly, the length of the contact area can greatly vary. The expanding contact area will further lead to lower average consolidation pressures. In order to characterize a conformable roller regarding this aspect, the Shore A Hardness grading is largely used, with higher values being an indicator of a more rigid material.

Non-conforming rollers are rigid elements, and they are often made out of either hard polyurethane or various metals and alloys. Non-conforming rollers, as the name implies, do not drastically change their shape when pressed onto a curved surface, leading to a line surface contact. This makes it so that the contact surface is of significant lower length as compared to the conformable roller. This also generally yields much higher average consolidation pressures given the same load range. Non-conformable rollers are also prone to insufficient contact, as slight angle misalignments between the axis of rotation and the surface can cause partial contact, which is undesirable. This can also occur in the case of surface discontinuities and concave profiles. In the case of metallic rollers, special considerations must be made regarding the heat transfer between the roller and substrate. Because of the great thermal mass these rollers can provide, heat absorbed through contact from the tape close to the nip point can create sudden drops in tape temperature and prevent matrix melting, causing improper bonding.

Besides rollers, very few other designs have been considered in literature for compaction elements. A notable exception is found in the work of [Lamontia et al.](#), which developed conformable line and area compactors by having a series of sliding thin shims vertically supported that could independently adapt to the curvature imprinted by the substrate [35]. In turn, the time under which the tape was subjected to consolidation pressure was massively extended as compared to the use of a single roller. These pressure elements were designed for automated fiber placement processes, where non-axisymmetric complex geometry is covered by an applicator mounted on a robotic arm or hanging on a gantry. Furthermore, the pressure element was temperature-controlled for even more precise process control. A schematic of the compaction system can be found in Figure 2.9.

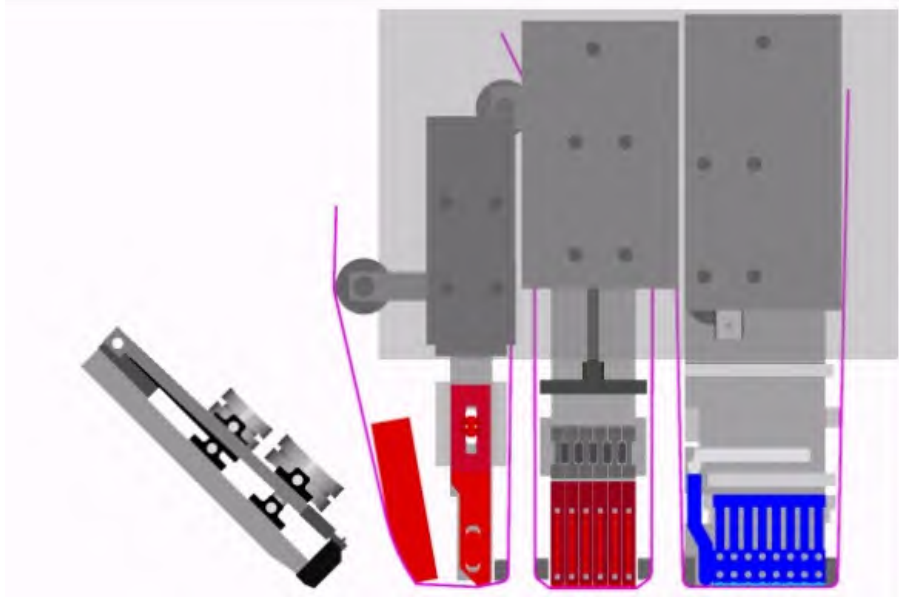


Figure 2.9: Accudyne surface compactor used with AFP manufacturing, with temperature-controlled hot and cold zones, reproduced from [35]

The second major physical phenomenon to lead to interlaminar bonding is autohesion. As the polymer interface between the tape and substrate is closed, and intimate contact is achieved, polymer chains can interdiffuse across the interface, and due to increased chain mobility at high temperatures, can become entangled. This leads to the fusion of the two surfaces without the emergence of any seam. Note that autohesion can occur only in the presence of matrix, making it impossible to eliminate an interface between fibers. The mechanics of autohesion are based on the on polymer chain reptation theory developed by [de Gennes](#), which follows the movement of large macromolecules under Brownian motion in a temperature dependent manner [36]. As aforementioned, the crossing of the glass transition temperature leads to a sharp increase in free volume within the amorphous part of a thermoplastic polymer, which leads to high chain mobility by reptation. It was believed that semi-crystalline thermoplastics undergo autohesion only above the melting temperature of crystalline domains, as it was believed these crystallites would pose as obstacles in chain movement and impede interdiffusion. But, [Stokes-Griffin and Compston](#) showed that as long as the melting point of an infinite perfect crystal T_m^∞ is reached during tape heating, bonding would still occur even at sub-melt temperatures, above T_g [37]. Once the interdiffused polymers create an entanglement network around the previous interplay interface, they can be subsequently cooled below T_g and form a stiff solid, completing the bond. This occurs in the last area on interest of the tape winding process.

As aforementioned in the discussion of intimate contact, the melted tape undergoes transverse squeeze flow under the application of out of plane load. This phenomenon is not limited to the immediate surface of the tape, aiding in intimate contact, but takes place throughout the thickness of the tape. In turn, noticeable width increases and thickness decreases can be observed, and are mostly attributed to squeeze flow mechanics [38] [39]. Although, most literature regarding transversal squeeze flow has been validated on hot press forming processes, and transverse squeeze flow models applied to continuous fiber placement processes have showed significant discrepancies when compared to experimental measurements of tape width [32][40]. Thus, it is believed that other flow mechanics are at play, with [Kok](#) identifying tow spreading prior to the nip point within the heated length as the tape comes in contact with the pressure roller [40].

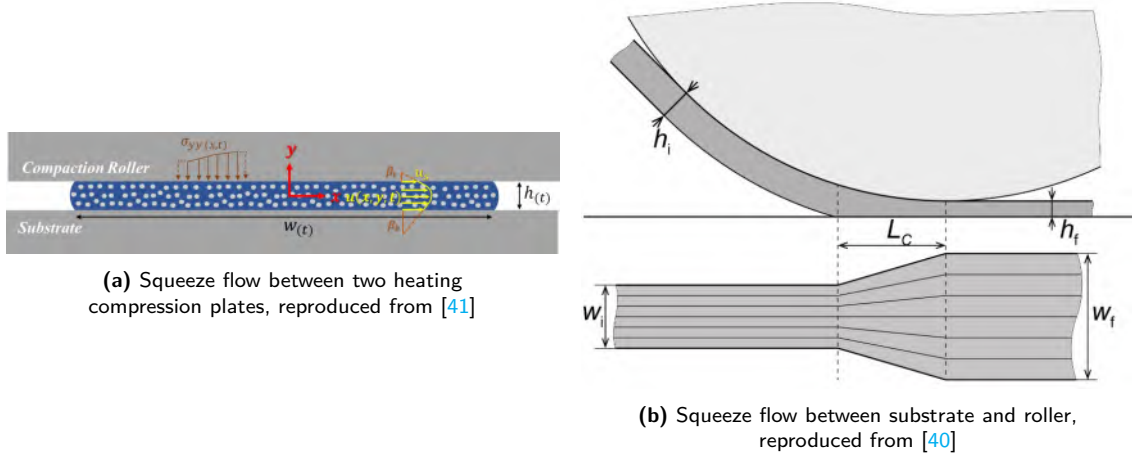


Figure 2.10: Behaviour of tape width change due to transversal squeeze flow phenomena

If this width change is not taken into account during layup, it can cause the development of gaps and overlaps, which account for the majority of laminate defects in automated tape laying and automated fiber placement processes [42]. Furthermore, such gaps and overlaps in adjacent tapes can drastically reduce the compressive strength of laminates by introducing out-of-plane fiber waviness regions that may act as inception spots for damage [43]. Such features can be seen in Figure 2.11. Agarwal investigated tape width increase during in-situ AFP using Toray 1225CT CF-LMPAEK tapes of quarter inch width, or 6.35 mm [44]. It was shown that heated length, tape temperature, and applied pressure can greatly affect the width change of the tape at the nip point, with registered width increases up to 12%. Moreover, it was found that for heated lengths exceeding 45 mm, the tape width change rate seemed to gradually decrease for either increases in consolidation load and nip point temperatures above T_m , and the tape width seemed to stabilize around 7.1 mm.

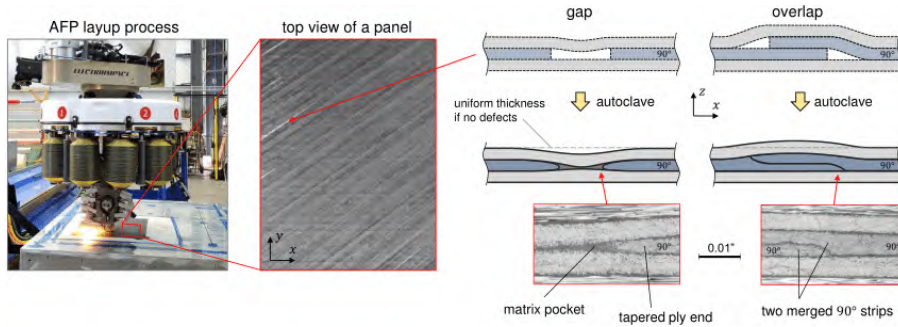


Figure 2.11: Example of visible gaps in AFP-manufactured laminates and the schematics of gap and overlap influence on ply morphology prior to and following consolidation, reproduced from [45]

2.4.4. Deposition zone

After the tape is placed on the tooling, following the nip point, it encounters rapid cooling due to heat conduction through the substrate and into the tooling, which is generally a great heat sink in such processes. In turn, cooling rates exceeding 500 °C/sec have been recorded in laser AFP applications at deposition speeds around 100 mm/sec, and are expected to greatly increase with deposition speed [46].

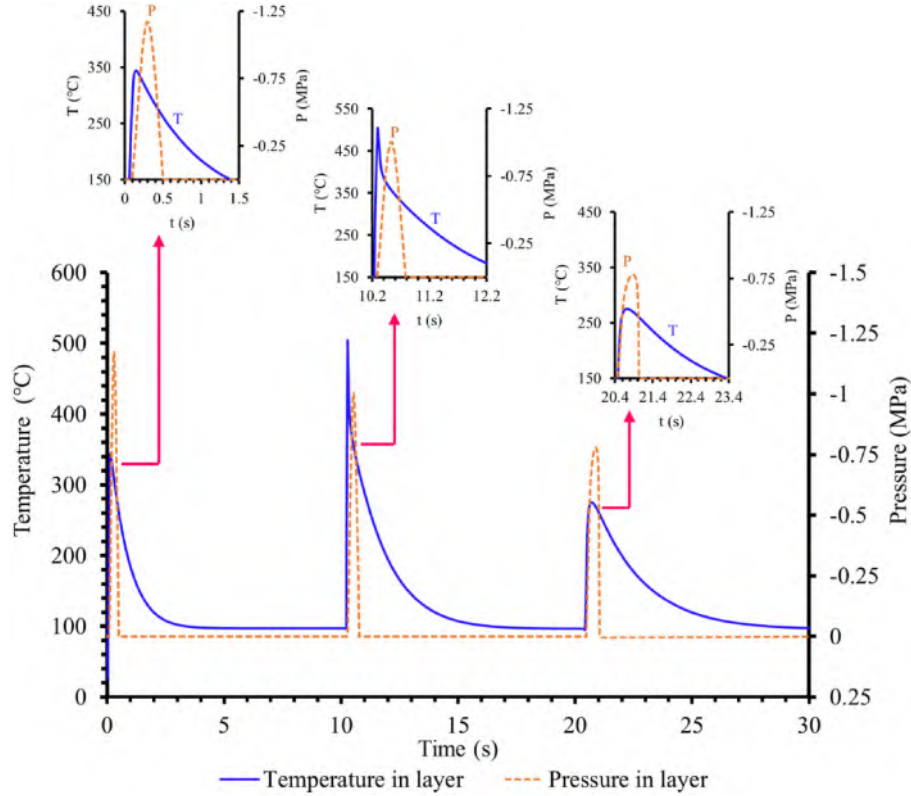


Figure 2.12: Simulated compaction and heating cycles during laser-assisted in-situ AFP, reproduced from [34]

Dong et al. investigated the influence of tooling temperature on interlaminar shear strength on tape wound CF-PEEK rings using laser heating [47]. It was determined that mandrel temperatures far above T_g have a large beneficial influence on laminate ILSS, with stress increases of above 50% as compared to trials using tooling temperatures below T_g . In turn, high mandrel temperatures are deemed to promote interlaminar bonding, and thus, aid in the removal of interlaminar voids.

In the case of semi-crystalline thermoplastics, which represent the majority of high-performance plastics, the cooling rate dictates the degree of crystallinity, and in turn, key mechanical properties such as stiffness, strength, hardness, and impact resistance. PEEK has been widely investigated for its performance appeal, and it has been showed that adequate crystallization occurs for cooling rates below $0.3^\circ\text{C}/\text{sec}$ [23]. It is thus of interest for in-situ tape placement procedures to maintain temperature control of the laminate even beyond the heating zone, as long as the laminate is within the crystallization temperature range. This poses a great challenge for high-speed in-situ production, which aim for fast processing and autoclave-like laminate quality.

Once the deposited tape is bonded to the substrate, it will be subjected to additional passes under the consolidation element as the subsequent layer is placed. Furthermore, under the influence of heating elements such as laser and flash lamps, the substrate will also be heated above T_g for a few passes after being deposited, as shown in Figure 2.12. These additional passes are thought to further decrease void content, promote interlaminar bonding and fiber bridging between plies, and lead to cold crystallization [34]. Furthermore, Shadmehri et al. investigated the effect of additional hot repasses on in situ consolidated CF-PEEK laminates, where the AFP process was continued without deposition [48]. It was observed that by only using one repass treatment the void content can be halved and the surface roughness of the part can be drastically reduced. On the other hand, the laminate crystallinity was actually lowered with each repass treatment [48]. Moreover, if the substrate is kept above T_g beyond the nip point, deconsolidation could take place in the

deposited plies and increase the void content of the laminate.

2.5. CoRe HeaT method

Continuous Resistance Heating Technology has been in development for the past decade at the ZLP in Stade, Germany. It represents a novel, state-of-the-art technique for extremely rapid heating of carbon fiber reinforced tows in order to enable fast and energy-efficient fiber reinforced composite automated production. The fundamental principle of CoRe HeaT lies in the Joule effect, namely the conversion of electrical energy into thermal energy as a current flows through an electrically conductive medium. In turn, CoRe HeaT manages to make use of the electrical resistivity of carbon fibers in order to intrinsically heat material tows. Benchmarking CoRe HeaT on dry carbon fibers heated until 180 °C has yielded heating rates beyond 100.000 K/sec [49]. Such high heating rates can be leveraged in favor of high-speed tape laying processes, with usual high-performance thermoplastics process temperatures of the order of 450 °C being reached in mere milliseconds. Moreover, accurate and strategic placement of heating zones along the tape path is possible by modifying the placement of electrodes. Thus, short heated lengths can be located in the immediate proximity of pressure elements without having the drawbacks of insufficient heating at the nip point.

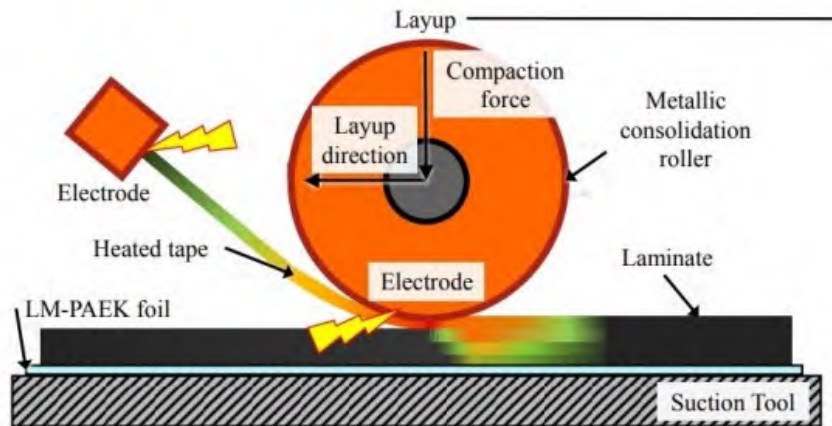


Figure 2.13: Schematic of the CoRe HeaT technique utilised in AFP manufacturing of flat panels, reproduced from [50]

The initial implementation of CoReHeaT took place on an AFP head mounted on a robotic arm for the purposes of dry fiber placement. This process used CF tows with a low content of thermoplastic binder, and resulted in preforms that were to be infused with resin to achieve solid laminates. Subsequently, [von Heusinger and Grohmann](#) substituted the dry fiber for Toray TC1225 CF-LMPAEEK 145gsm UD tapes in order to study the effect of CoRe HeaT pulse parameters on flat thermoplastic preforms. A schematic of the process is provided in Figure 2.13. The tape was heated using a repeating sequence of electrical pulses, to achieve a consistent above-melting-point nip point temperature [51]. The consolidation pressure was delivered through a solid metallic roller, and the tape was laid on an unheated flat tooling. In turn, much necessary information was developed regarding the preferred range of CoRe HeaT parameters for the processing of thermoplastic tape under continuous layup at high speeds, namely 500 mm/sec.

Following successful AFP trials, the technology was adapted to fiber winding processes, using the same Toray TC1225 CF-LMPAEEK 145gsm UD tapes, for the production of CFRP open-ended

tubes. As winding processes can be maintained with constant feed velocity, the CoRe HeaT technology could be effectively leveraged to achieve the upper echelon of deposition speeds used in industry. The fiber winding process did not include in-situ consolidation, was performed at constant tow tension, and the tooling temperature was maintained the same for all specimens. After incipient trials, it was determined that an additional processing step of post-consolidation was required in order to achieve adequate laminate quality [52]. In the spirit of process integration, and to avoid autoclave needs, this post-processing step took the form of winding the preform CFRP tube with shrinktape, and applying a heat cycle to the part. As the laminate would be heated above T_m , the mandrel would expand according to its thermal expansion coefficient, while the shrinktape would contract, thus exerting consolidation pressure on the melted laminate. Once a certain dwell time is reached, the laminate could be cooled in a controlled manner in order to reach a desired degree of crystallinity.

By investigating the effects of mandrel wall thickness, dwell time, dwell temperature, and cooling rate, Khan established that laminate quality similar to well-established out-of-autoclave post-consolidation methods could be matched using a minimum of 60min of dwell time at 340 °C [53]. Dwell times below 60min led to high porosity and a drastic decrease in interlaminar shear strength. It was thus established that the diffusion of pores was primarily influenced by the viscosity of the matrix and, thus, the post-consolidation temperature. However, elevated temperatures led to the partial degradation of the auxiliary material used to provide post-consolidation pressure and to exacerbate laminate surface waviness. Thus, to be able to reduce processing times for lower temperature ranges and avoid these undesirable effects, Khan recommended that efforts should be made to obtain lower porosity preforms.

Chapter 3

Research complex

Past literature on the topic of consolidation of thermoplastic laminates, continuous in-situ tape winding processes, and CoRe HeaT development aided in the identification of relevant knowledge gaps, as presented in this chapter. Considering such knowledge gaps, the objective of this research paper is established, as structured around some main research questions. Hypotheses based on the research questions are formulated and are to be challenged against experimental data in order to attempt to close the targeted knowledge gap.

3.1. Knowledge gap

Moreover, given the unique capability of CoRe HeaT to reliably reach considerably higher heating rates than other conventional AFP heating methods, there is a need to research the impact of various consolidation strategies on high-speed wound laminates. There is little research done on high-speed laminate production, with lay-up speeds exceeding 300 mm/s, due to inherent limitations of current AFP machines, such as size, intermittent movement, and slow heating methods. In the literature, only a small number of theoretical papers based on physical models even address this range of production speeds. Since CoRe HeaT enables this range for tape winding, it is of interest to check the efficacy of consolidation strategies and the paths that would lead to an improvement in laminate quality.

As previously described in Section 2.5, CoRe HeaT has been successfully implemented to high-speed fiber winding processes using CF reinforced thermoplastic UD tapes. Yet, the sub-par quality of preforms requires the addition of a post-consolidation step, which increases processing times and can have a bad influence on laminate surface morphology and layer crumbling. In turn, it would be of great advantage if the preform laminate quality were to be improved during the tape winding process. By doing so, the post-consolidation step could be shortened, processing time and energy requirements could be cut, and the effects on the laminate surface could be minimized or avoided entirely. In order to achieve these quality improvements, it is required to investigate the impact of relevant in-situ consolidation parameters on wound tubes using CoRe HeaT.

3.1.1. CoRe HeaT deconsolidation

Since CoRe HeaT is a novel tape heating method, not much is known about its deconsolidation mechanisms and effects. As opposed to thoroughly studied laser heating methods, which directly

heat the upper fibers within the tape, which are immediately visible to the laser source, CoRe HeaT acts on all carbon fibers within the tape and heats the tow from the inside. In turn, it is not known if the well-observed mechanisms of tape deconsolidation in the case of laser heating can be directly transferred to CoRe HeaT deconsolidation. And as it has been discussed in Subsection 2.4.3, the consolidation quality can be directly affected by changes in tape surface morphology, void content, and tape width that arise through deconsolidation. Thus, the impact on the deconsolidated tape structure of heating parameters such as heating rates and maximum temperature ought to be investigated and quantified.

As seen in Subsection 2.4.2, process parameters besides heating-related ones can have a great impact on deconsolidation mechanics. It was shown that moisture content can greatly influence tape porosity and thickness [20]. In turn, it is noteworthy to analyze this behaviour in combination with the high heating rates of CoRe HeaT. Moreover, the release of internal stresses from the tape manufacturing process was shown to affect tape morphology [19]. Thus, it is of interest to assess if fiber displacement could be curtailed during deconsolidation by the application of high tape tension, which can be easily tuned during the manufacturing process.

3.1.2. Consolidation elements influence

Previous studies on flat AFP laminates performed by [von Heusinger and Grohmann](#) used a rigid metallic roller as a compaction device while utilizing CoR HeaT. Yet, this is the maximum extent of investigation allotted to compaction devices in regard to CoRe HeaT continuous tape processing. And, as elaborated in Subsection 2.4.3, a large variety of compaction elements have been engineered in literature, with individual advantages and shortcomings. In turn, an opportunity arises to analyze the adaptation of several compaction element designs and strategies to the high speed CoRe HeaT tape winding process. By varying the shape and constitution of pressure elements, important consolidation parameters can be influenced, such as applied consolidation pressure and consolidation time.

Since the previous tape winding production series performed by [Khan](#) used constant tow tension for consolidation purposes, there is little information on the influence of both applied consolidation pressure and tape tension on laminate quality. As aforementioned, tape tension is investigated for having an effect on consolidated tape morphology. Yet, tape tension alone could not guarantee adequate preform laminate quality. It is of interest to assess by which manner would applied consolidation pressure further improve the laminate quality.

3.1.3. Tooling temperature

Other scientific work has observed laminate quality improvements by increasing tooling temperature, as seen in Subsection 2.4.4. Moreover, maintaining laminate temperatures above T_g after deposition has been showed to still allow for interlaminar bonding, especially in subsequent pressure element passes [34][37]. Yet, sudden deconsolidation after tape placement, as well as insufficient ply cooling in order to accommodate interlaminar bonding after chain interdiffusion, remain risks against reaching good laminate quality. Thus, investigating the impact of high tooling temperature, especially above the T_g of the polymer matrix, on laminate quality remains a significant point of contention.

3.2. Research objective

The objective of this research paper is twofold:

1. Investigate the deconsolidation behaviour of UD CF-reinforced thermoplastic tape using CoRe HeaT and relate it to laminate preform quality.

2. Assess the influence of consolidation parameters, such as pressure element, applied pressure, consolidation duration, and tow tension, on quasi-90deg preform laminate quality manufactured using CoRe HeaT based tape winding.

3.3. Research questions

In order to address all aforementioned research goals, the following research questions and sub-questions were formulated:

RQ1 *How does CoRe HeaT influence the deconsolidation behaviour of prepreg thermoplastic tape within the heating zone?*

SQ1.1 *How effective is preconditioning the tape against moisture buildup for achieving low porosity, waviness and roughness after deconsolidation?*

SQ1.2 *How does tape tension, heating rate, and tape temperature influence tape deconsolidation?*

RQ2 *How can different consolidation strategies affect laminate quality (i.e., porosity, surface quality, fiber distribution) of tape-wound CF-LMPAEK preforms?*

SQ2.1 *How do different pressure elements (i.e. rigid, hard conformable, soft conformable) affect laminate quality?*

SQ2.2 *What is the relationship between applied consolidation pressure, tape tension, and laminate quality?*

RQ3 *What is the influence of heated tooling on preform quality?*

3.4. Hypotheses

Based on the established research questions and considering the past work of the researchers presented in Chapter 2, it is possible to establish a set of hypotheses. These statements will be addressed again after the results of this research paper are presented and discussed, in order to assess the validity of the hypotheses.

Hypothesis 1: The deconsolidation of tapes using CoR HeaT is expected to be highly dependent on moisture content, maximum tape temperature, and heating rate, while only the tape morphology is expected to be impacted by tape tension.

As moisture content is a characteristic of the tape and not of the heating method, it is believed that the moisture content impact will be similar to the deconsolidation behaviours of other heating methods. The maximum temperature will determine the viscosity, and thus flowability, of the matrix, as well as the expansive capacity of entrapped moisture and air. Furthermore, the increase in heating rate will exacerbate hot spots, which will amplify the local increase in porosity. Lastly, the tape tension that can be realistically applied to the brittle tape during the tape winding process is thought to be unable to prevent the release of frozen fiber stress, but it is believed to be enough to restrain large morphological changes, such as waviness and perhaps even roughness.

Hypothesis 2: The use of pressure elements with either high consolidation pressure or long consolidation times will have a major impact on preform porosity.

Based on previous work on preform tape wound CFRP tubes done by [Khan](#), it is believed that most pores are a result of entrapped air during the manufacturing process. In turn, strategies to increase intimate contact will have a drastic effect on the amount of interlaminar pores. As discussed in Chapter 2, the degree of intimate contact is thought to be proportional to applied pressure and consolidation duration. Thus, both strategies of increasing pressure consolidation and time duration should have a favourable impact on laminate porosity.

Hypothesis 3: Conformable pressure elements with longer contact lengths would prove more effective in void closure than conformable pressure elements with shorter contact lengths and solid rollers, when used at high deposition speed.

Since void diffusion is a dynamic process, which requires sufficient time for matrix viscous flow, it is believed that prolonged consolidation time will be a highly influential factor for high deposition rate processes. In turn, conformable pressure elements, which will generate a longer contact surface, will be more effective in void diffusion as compared to rigid rollers, which will be in contact with the laminate for a very short duration. This occurs as the rigid roller cannot readily deform to lengthen the contact zone to the laminate, unlike the conformable pressure elements. Moreover, rigid pressure elements would be unable to exert uniform compaction pressure when acting on uneven surfaces, which may lead to parts of the laminate being under less or even negligible compaction. Furthermore, conformable pressure elements with longer compaction lengths would be able to extend the consolidation duration far beyond those with shorter compaction lengths, yielding lower laminate void content.

Hypothesis 4: Increased tape tension will have a beneficial effect on lowering interlaminar porosity, as long as the tape is not damaged prior to deposition.

As presented by both intimate contact models discussed in Section 2.4, tape roughness is believed to have immediate effects on intimate contact and time to obtain intimate contact. In turn, if *Hypothesis 1* holds true regarding tape tension deconsolidation, it is believed that increasing tape tension will be beneficial to improving laminate quality.

Hypothesis 5: High mandrel temperatures are expected to aid in the dissipation of voids within lower laminate layers.

If the deposited lamina would remain above T_g for subsequent pressure element passes, it is believed that intimate contact, interlaminar bonding, and void diffusion would be further promoted, as shown by [Stokes-Griffin and Compston](#) and [47]. Yet, this effect is considered to decrease with an increase in laminate thickness. Thus, noticeable improvements are expected only in the first few lamina.

Chapter 4

Methodology

This chapter presents the practical aspects of answering the aforementioned research questions. The chapter is structured around the experiments performed, and describes the motivation for performing the experiment, the experimental setup, the Design of Experiments (DoE), and the evaluation method used to extract relevant experimental data.

4.1. Static deconsolidation

In order to try to answer **RQ1**, the deconsolidation conditions experienced by the tape prior to the nip point shall be simulated under controlled conditions. In order to isolate the impact of controlled parameters from other variables, such as tension or temperature variability due to winding speed, the test was performed under static settings. Thus, to correctly reflect dynamic conditions, the following requirements shall be fulfilled:

- The heating length of the tape shall be comparable to the heating length maintained during the manufacturing process
- The tape shall be free of any out-of-plane constraints or loading.
- The tape shall be heated to processing temperatures

4.1.1. Experimental Setup

A strip of tape measuring 70 cm in length was cut to size from the material roll and fixed at one end through clamping. The tapes used in this experiment are 145 g/m² T700GC SM CF-LMPAEK UD Toray Cetex TC1225. Some important product characteristics can be found in Table 4.1. More information on the used materials can be found in the material data sheets provided by the Original Equipment Manufacturer (OEM), in Chapter A.

Table 4.1: Characteristics provided by OEM of all deconsolidated tapes

Material	T_g [°C]	T_m [°C]	T_p [°C]	Tape width [mm]	Tape thickness [mm]	V_f [%]	Density [g/cm^3]
TC1225 CF-LMPAEK	147	305	340-385	6.35	0.15	58	1.59

The tape to be consolidated was fixed at one end by clamping. The other end was left suspended from a plastic roller positioned so that the horizontal part of the tape would be level. A scientific

weight was attached to the free end of the rope in order to control the tow tension.

Custom-designed supports were 3D printed and fixed 90 mm apart in order to maintain a consistent heating length. These were used to support suspended P1P Parker pneumatic actuators in line with the electrodes used for heating the tape. The electrodes consisted of two copper bars, sanded for a flat finish, electrically connected at one side using a nut and screw. The tape was then clamped in between the two flat plates and placed under the piston of the actuator. Thus, when the pneumatic cylinders were actuated, they would ensure sufficient clamping force to enable the current to flow from the electrode to the tape and vice versa. Moreover, sufficient clamping force was required in order to ensure even clamping pressure along the width of the contact. This was done to level the contact resistance between the copper bars and the tape, which will improve the even distribution of current through the tape.

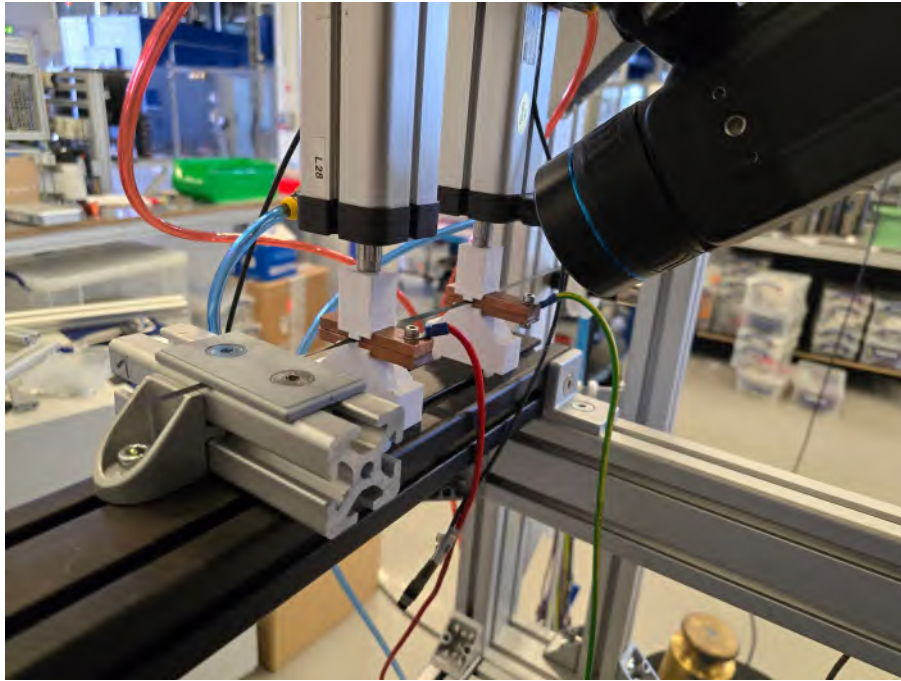


Figure 4.1: The deconsolidation setup, showing in the foreground the fixed tape, the pneumatic actuated electrodes, the thermal camera used for temperature readings, and in the background the weight used to tension the tape.

The tape would first be loaded in tension by the hanging weight, and then clamped at the electrode positions using 7 bar of pressure, which translates to 563 N, in order to maintain the tape in a tensioned state. The tape was then subjected to a single electric pulse of a certain voltage and duration, in order to reach the desired maximum temperature and heating rate. The required voltage and pulse duration were experimentally determined to reach a desired temperature. After the pulse was sent, the tape was cut at the electrodes, and the sample was kept for analysis.

4.1.2. Design of experiments

The parameters to be studied were chosen to be: moisture content, maximum tape temperature, heating rate, and tow tension. As-received tapes, which were not deconsolidated, were taken as reference. The parameters were varied in two sets. The parameters and values used can be found in Table 4.2.

Table 4.2: Static deconsolidation test matrix

Run	Tension [N]	Heating rate [°C/sec]	Temperature [°C]	Moisture
0	0	0	0	Ambient
1	10	~ 2	T_m	Ambient
2	10	~ 2	T_m	Soaking
3	10	~ 2	T_m	Oven dried
4	10	~ 2	120% T_m	Ambient
5	100	~ 40	120% T_m	Ambient
6	100	~ 40	T_m	Ambient
7	100	~ 2	120% T_m	Ambient

The first set, containing Runs 0 through 3, was used to evaluate the effect of moisture content. While the ambient tapes were used directly after being cut from the material roll, which was kept at ambient conditions, the soaked tape was conditioned in a water bath overnight. Conversely, the oven-dried samples were kept overnight in an 80 °C and deconsolidated immediately after being removed from the oven.

The second set, containing Runs 1, 4, 5, 6, and 7, was assembled to evaluate the influence of tape tension, heating rate, and temperature on tape deconsolidation behaviour. Both pairs of Runs 4 and 7, Runs 5 and 7, and Runs 5 and 6 can be compared to determine the influence of each parameter, in isolation from the other two.

4.1.3. Evaluation

The temperature was monitored during the entire deconsolidation process using a FLIR A615 series infrared thermal camera. By doing so, it is possible to detect non-uniformities in heat distribution along the tape, such as gradients and hot spots. The camera was used within a temperature range of 100 °C to 650 °C, thus covering the desired temperature space. The main regions that were recorded were the longitudinal and transversal axes of symmetry, as well as the hottest regions. Furthermore, the temperature of the tape was taken as the average temperature of a wide rectangle covering the middle region of the tape. The tape extremities were discarded from the measurement due to optical effects errors close to the slightly curved edge. A representative area of measurement can be seen in Figure 4.2 as the rectangle with white borders.

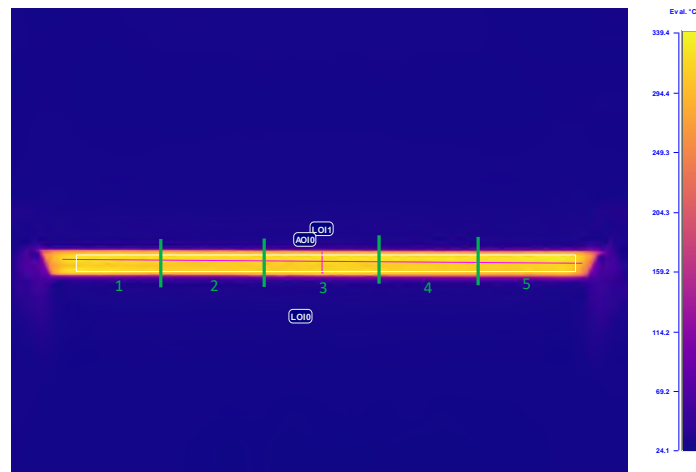


Figure 4.2: Visual of the deconsolidated tape using the FLIR thermal camera, as the maximum temperature is reached. The white rectangle represents the area used to estimate average tape temperature, while the green lines represent the delimitation location for the five microscopy samples.

After cutting the region of the tape that has been deconsolidated, the tape is further subdivided in five pieces of equal length, as shown in Figure 4.2. The samples were then embedded in fast-curing 2K epoxy resin while supported by a circular 3D printed clamp support, in order to maintain the samples straight and vertical. After curing, the samples were polished using increasingly higher grit diamond suspensions as abrasion agents on an ECO-MET30 semi-automated table grinder. The intermediary embedding step and the result of the polishing process can be seen in Figure 4.3.

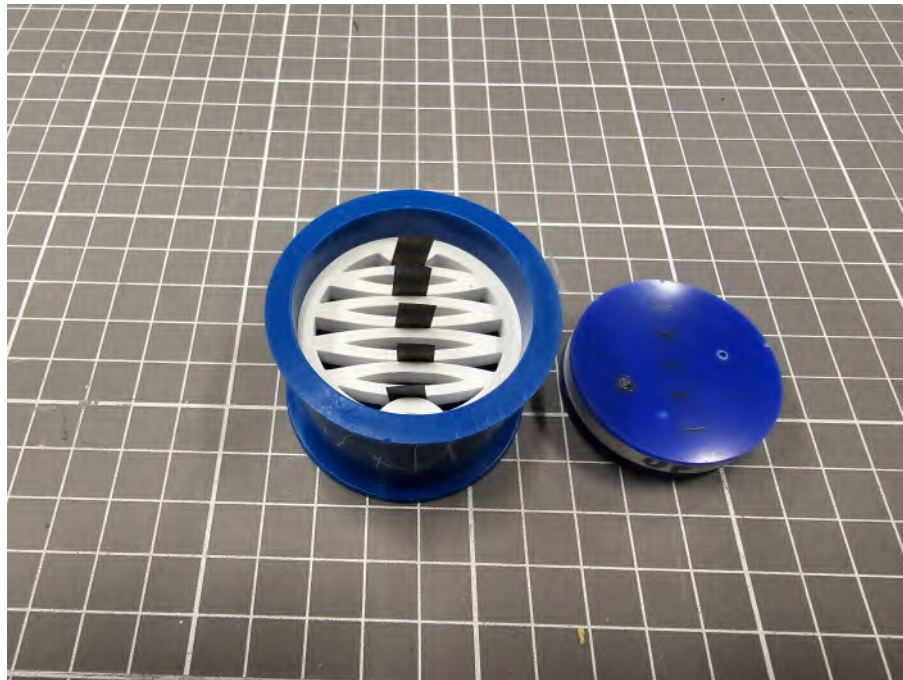


Figure 4.3: Single tape embedding setup (left) and a polished micrograph-ready disc (right)

Micrographs of the polished surface of the tape were generated using a Keyence VHX 5000 optical microscope, under 500x magnification and using a mix of mostly edge lighting and ring lighting. In turn, five micrographs were made for each deconsolidated tape. This was done in order to capture the variability across the heating zone. Additionally, given the reduced size of the features of interest, it was considered that using such a high number of samples was enough to statistically identify emerging trends. An example of such a micrograph is given in Figure 4.4.



Figure 4.4: Micrograph of sample 2 of Run 2, taken at x500 magnification, with resolution of 0.44 μm per pixel

Once the high magnification micrograph is generated, the tape is isolated from the background, consisting of embedding resin, using the open source image processing software ImageJ. For this purpose, the built-in wand tracing tool was used. The wand tool requires a pixel chosen by the user and a numerical value, which is taken as tolerance. In turn, the tool selects the largest contiguous area of pixels with values within the starting pixel \pm the tolerance value that also contains the starting pixel. In turn, one can take advantage of the fact that the interface between the tape sample and embedding resin is darker than the thermoplastic matrix by choosing a bright fiber pixel. Moreover, increasing the tolerance in order to decrease the threshold enough to contain a 'border' pixel would lead to a traced area that visibly includes a large swath of the embedding resin. This is because the embedding resin also has higher pixel values as compared to 'border' pixels. In turn, a clear limit to the acceptable tolerance is established in order to attain sufficient tracing accuracy. The results of this process are shown in Figure 4.5. After the tape is selected, the outside can be cleared, resulting in an isolated tape cross-section, as shown in Figure 4.6.



Figure 4.5: Entire tape cross-section being selected using the ImageJ wand tracing tool



Figure 4.6: Isolated tape cross-section

Much information can be extracted once the tape profile is clearly isolated from the background. The tape upper and lower surfaces can be located in the XY plane using the scale of the image in order to obtain profilometry data. Obtaining the moving delta between the absolute position of the upper and lower profiles yields the local thickness of the tape. Moreover, measuring the distance between the first and last element shared by the upper and lower profiles will yield the maximum tape thickness.

By further processing the profilometry data of the deconsolidated tapes, it is possible to obtain quantifiable data regarding tape surface roughness and surface waviness. This is done in accordance with ISO4287 [54]. Namely, the profilometry data is transposed in the spatial frequency domain using a Fast Fourier Transform algorithm. The roughness profile was isolated by means

of a high-pass filter, which would only allow the transmission of high-frequency elements. The waviness profile was constructed by centering the original surface profile around its mean, and then subtracting the roughness data from it. By doing so, a low-pass filter complementary to the high-pass filter used for roughness estimation was effectively used, so that no information in the surface profile would be lost. The cut-off frequency for the two filters, which specifies the frequency where the filter allows for the transmission of 50% of the amplitude of the signal as seen in Figure 4.7a, was deliberately chosen in order for the waviness and roughness profiles to contain the desired surface features. For the purposes of surface analysis of deconsolidated tape, the central cut-off frequency was chosen as 0.8mm, similarly to the work of Çelik et al.[22]. The other marginal cut-off frequencies were discarded by using one sided filters, in order to preserve the entirety of the information contained by the surface profile. An example of the filters used on the FFT series of the upper surface of the specimen shown in Figure 4.4 is provided in Figure 4.7b.

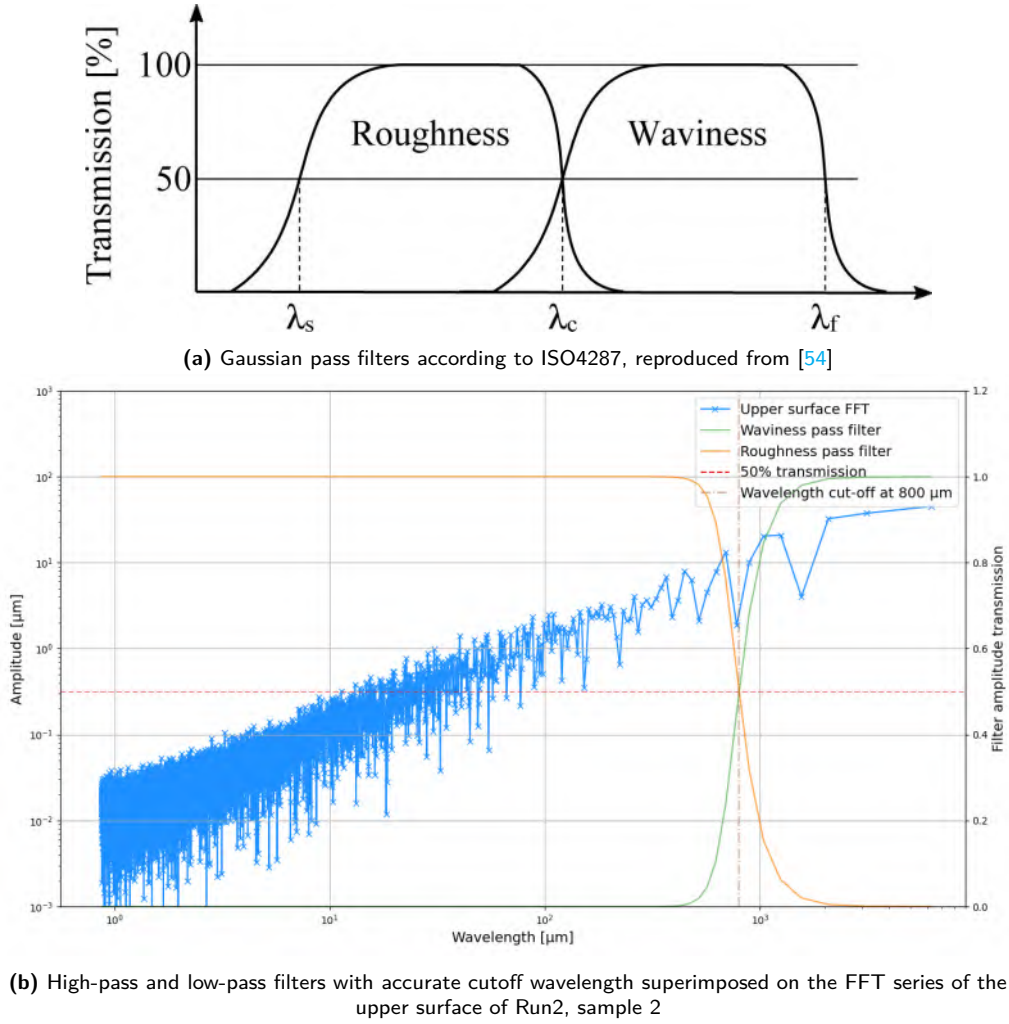


Figure 4.7: Method used for separating roughness from waviness

The resulting surface profile breakdown, as applied on the upper surface of the specimen shown in Figure 4.4 is presented in Figure 4.7b. After filtering, the root mean square roughness, R_q , and waviness, W_q are calculated. Equation 4.1 can be applied to either profile to obtain the aforementioned indicators of interest, with l_s the sample length being the width of the tape, and $Z_{(x)}$ being either the positive or negative deviation from the average of surface height at x . For the

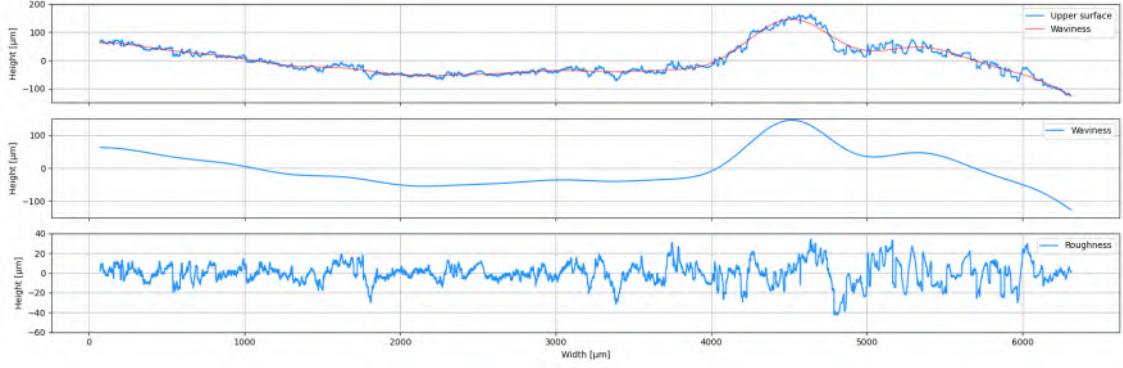


Figure 4.8: Roughness profile (down), waviness profile (middle), and the comparison between the original surface and the waviness profile (up)



Figure 4.9: Detailed view of sample 2 of Run 2 after segmentation

purposes of the deconsolidated tape, only the lower surface was analysed. This was done, as the lower surface is critical for intimate contact and bonding, while the upper surface will morph to accommodate the surface of the pressure element used in winding before becoming the substrate for subsequent layers.

$$S_q = \sqrt{\frac{1}{l_s} \int_0^{l_s} Z_{(x)}^2 dx} \quad (4.1)$$

The porosity and local fiber volume fraction are determined using a retrofitted feature segmentation tool developed by [55]. The tool consists of a convolution-based machine learning algorithm organized under a U-Net architecture with a Dilated Neighborhood Attention Transformer (DiNAT) backbone. Using labeled training data, the model is capable of identifying and categorizing pixels belonging to significant features, such as 0 deg, 45 deg, and 90 deg fibers, matrix, cracks, voids, and other minor elements such as dust and scratches. Once all image pixels are attributed to one of these categories, further image processing can yield volumetric pore content, spatial distributions of pores, as well as volumetric fiber content, and heatmaps of local fiber content. An example of the output of the segmentation process is shown in Figure 4.9.

The model was originally designed to detect cracks created under thermal loading in CFRP thermoset tubes, which were wound and then cured in the autoclave. In turn, the original labeled training data did not contain a significant amount of pores. Thus, in order to adapt the model to be able to detect pores that are a result of the manufacturing process, a new set of training data was created. This training data was created using microscope images of both post-consolidated

tubes with high pore content produced by Khan, and of micrographs of single deconsolidated tapes. This was done in order to increase the robustness of the model, since the pores from the two categories vary in appearance, even under similar magnification and lighting conditions. The training data was initially segmented by the model, and then corrected by manual labeling. Validation testing performed after training gained a void precision, which measures the accuracy of true predictions, of 97.02%, and a void recall, which measures the completeness of true predictions, of 98.72%.

The significance of the influence of tape tension, heating rate, and maximum temperature on porosity, lower surface roughness, and surface waviness is determined by using the signal-to-noise ratio (S/N). This method is able to determine the amount of variance around a target value within an experiment series caused by one specific parameter. In this case, as the target would be minimizing these features, the signal-to-noise ratio is given by Equation 4.2, where x is the desired indicator to be evaluated of one sample from the five per each tape, t is the target value, and n is the number of samples evaluated from a single tape. Thus, a more negative signal-to-noise ratio would be associated with a larger variance from the targeted value. In case the desired indicator is to be minimized, such as in the case of porosity, the target values shall be set to zero.

$$S/N = -10 \log_{10} \left(\frac{\sum_i^n (x_i - t)^2}{n} \right) \quad (4.2)$$

The signal-to-noise values are averaged for all experiments within the second set about each level of the aforementioned parameters. A large difference between the signal-to-noise ratios of different parameter levels would thus be attributed to a large change in data variance. In turn, the larger the delta between the average signal-to-noise ratios of the two levels, the more influential the parameter.

Whisker box plots are used in order to better visualise the porosity, roughness, waviness, and thickness data from the multiple samples belonging to each run. Figure 4.10 shows the type of boxplot used throughout this thesis. The box marks the region between the first quartile and the third quartile, with the inter-quartile range (IQR) being the difference between the two. The horizontal line within the box marks the median value, while the \times indicates the mean value. The whiskers extend until the most marginal data points lying within 1.5IQR of the box. All other data points exceeding this range are marked as outliers.

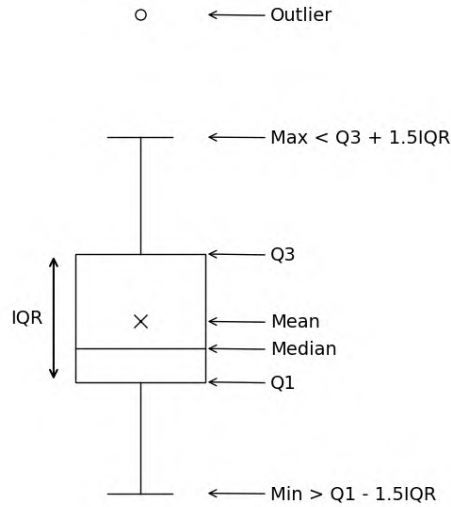


Figure 4.10: Whisker box plot used for data visualisation, with annotated important characteristics

4.2. Static compaction

It has been established in Subsection 2.4.3 that a valid strategy for influencing major consolidation parameters such as consolidation pressure, pressure distribution, and duration of compaction, is to modify the geometry and material constitution of the compaction element. In turn, this led to the establishment of **SQ2.1**. Yet, in order to evaluate the impact of singular consolidation parameters on preform quality, as mentioned in **SQ2.2** and **SQ2.3**, it is necessary to accurately characterize each compaction element in regard to such parameters. This was performed using experimental evaluation methods, under static conditions, using the same set-up used for the final production of CFRP wound tubes.

4.2.1. Experimental Setup

Pressure impressions against the curved mandrel were obtained from each compaction element used for winding. This was done using the FujiFilm Low Pressure Prescale films, which are able to correlate film pigmentation to applied pressure through the use of breakable capsules containing reactive pigments. The Prescale use by this study is able to detect applied pressure values in the range of 2 MPa to 10 MPa. In turn, relevant information regarding the shape of contact, as well as the pressure distribution, can be extracted from the imprint.

The pressure elements were attached to the custom-built deposition head, which will be further described in Section 4.3, and were actuated by a FESTO ADNGF-63-20-PPS-A compact pressure cylinder controlled using compressed air. The pressure cylinder has a stroke of 20 mm, a cylinder active surface of 3117 mm², and an operating compressed air range of 0.1 MPa to 1 MPa. This yields a theoretical applied load range of 312 N to 3120 N. The pneumatic actuator was positioned centered to all compaction elements and to the tooling, a chrome-plated steel alloy (E355, EN10305-1) thick-wall hollow cylinder of 100 mm diameter, respectively. The mandrel wall thickness was measured to be 15 mm.



Figure 4.11: Setup for the static compaction trials, showing a slider lying above the Prescale films placed on the mandrel

The tests were performed in static conditions. Since the actuator is pressure (load) controlled, precautions were taken so that full contact between the pressure element and mandrel is achieved before the maximum stroke length is reached. A constant cylinder pressure was maintained for a duration of 2 min measured from the point of contact.

4.2.2. Design of experiments

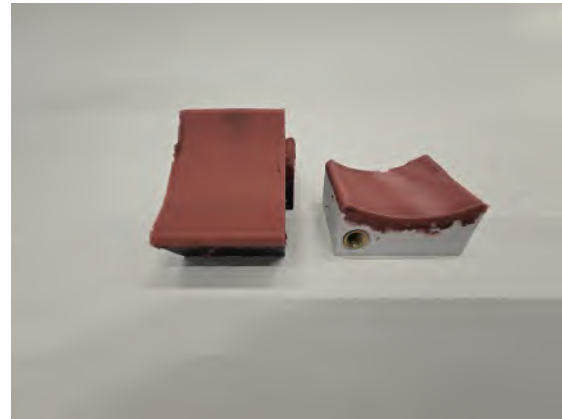
Multiple concepts were employed to generate consolidation elements that would vary in compaction characteristics, most notably average compression pressure and compaction surface length given a certain applied load. All pressure element options are provided in Table 4.3, alongside some initial rough considerations regarding their compaction behaviour. All compaction elements are shown in Figure 4.12

Table 4.3: General description of compaction behavior of considered compression elements

Material Geometry	Copper	Soft silicone	Hard silicone
Roller	Very high pressure Very short duration	Low pressure High duration	High pressure Low duration
Slider	—————	Very low pressure Very high duration	Low pressure Very high duration

Three types of materials were considered for the pressure elements used in this study. The aim is to cover non-conforming, as well as conforming materials. For the non-conforming material, copper was used in the form of a solid metallic roller. As to the conforming materials, two types of high-temperature resistant two-component silicones were considered, namely Troll Factory Typ 3, of 33 Shore A Hardness, and Wacker Elastosil M4370, of 55 Shore A Hardness. As the hardness of these silicones varies by quite some margin, it was thought that the conforming compaction characteristic will vary in accordance, as shown in Table 4.3.

As inspired by the work of [Lamontia et al.\[35\]](#), an area compactor was considered as a possible compaction element geometry besides the ubiquitous roller. This pressure element shape, referred to from now on as a slider, is manufactured to be able to entirely cover the curvature of the mandrel for an arc span of 50° and a width of 35 mm. This allows for a dramatic increase in contact duration, but comes with the disadvantage of decreased compaction pressure. Yet, it is expected that the distinct shape would maintain a similar size contact area irrespective of the applied load within the practical range of the setup. Thus, the applied pressure and compaction duration are able to be decoupled, and the effects of the applied pressure alone can be analyzed.

**(a)** Roller pressure elements**(b)** Area compaction elements**Figure 4.12:** All considered compaction elements, grouped after geometry

Severe difficulties were experienced during the process of reaching sufficient adhesion between these silicones and any metallic or plastic surface. Adhesion tests were performed on polished, unpolished, and anodized aluminum, copper, smooth PLA, smooth PETG, textured PLA and textured PETG, PAHT-CF, and PA12-CF, with unsatisfactory results. In turn, a single-component high-temperature silicone adhesive was chosen as an intermediate, namely, Welkem WK-15-300. The 1K silicone was able to adhere to 3D printed PLA and could be co-cured with the 2K silicone. To increase bonding surface and overall adherence, the 3D printed part was retrofitted with slight

protuberances, as shown in Figure 4.13. In the case of rollers, the PLA 3D printed support was further bonded to an aluminum ring using a cyanoacrylate adhesive.

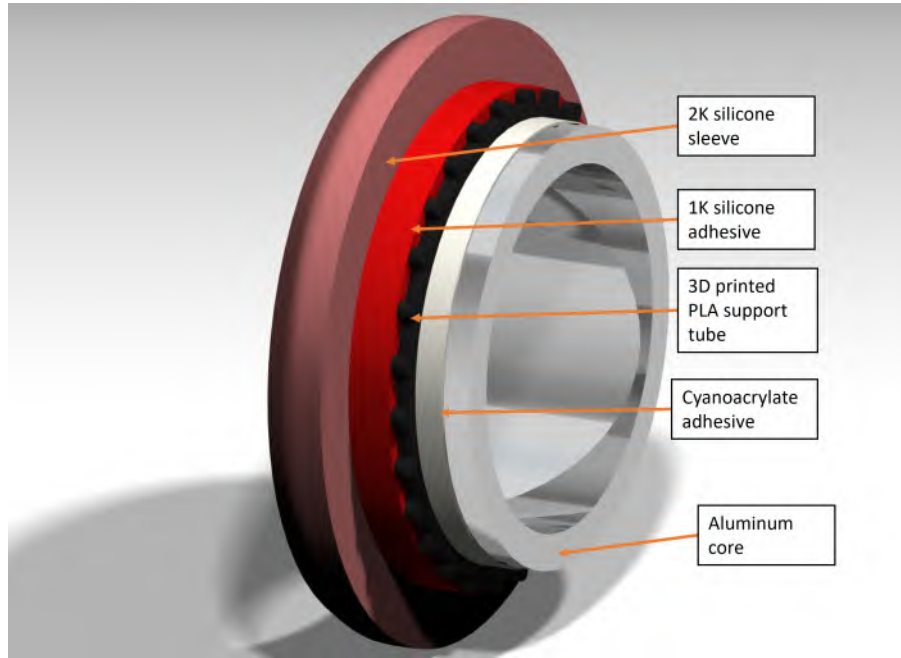


Figure 4.13: Layers of a compaction roller, from interior to exterior: aluminum tube, cyanoacrylate adhesive, 3D printed PLA tube, 1K silicone adhesive, and 2K silicone

The methods of silicone casting were kept similar for both rollers and sliders. They involved coating the 3D printed PLA support part with a thin layer of 1K silicone by removing excess silicone using a low-tolerance 3D printed scraping tool. Afterwards, the PLA support part was placed in a purpose built mold made of 3D printed PETG parts. The surface quality of the silicone was imparted by a custom 1-layer thick 3D printed sleeve containing the negative of the desired pressure element surface. The sleeves were printed using 0.8 mm, which is the minimum operational layer height available to the Bambu X1E 3D printer, used for the majority of prints. This was done in order to obtain the smoothest possible roller and slider surfaces. After assembling the mold around the 1K covered PLA support, the 2K silicone was mixed and degassed under vacuum for 2 min to 3 min. The mold was then filled with 2K silicone, either poured through the upper vent gap, in the case of the soft silicone roller, or injected into the mold, as in the case of the hard silicone roller and both types of sliders.

The reasons behind using injection moulding for the hard silicone roller and not for the soft silicone are twofold. Firstly, the hard silicone is much more viscous as compared to the soft silicone. Thus, the difficulty of removing all entrapped voids after pouring the silicone mixture into the mould drastically increases, which makes injection moulding a more reliable method. Secondly, the silicone layer thickness of the hard silicone roller was decreased from 8 mm, the silicone layer thickness of the soft roller, to 3 mm. This was done in order to avoid tearing the much harder Wacker silicone while being loaded under compaction while winding at high speeds. As an unforeseen effect, the decrease in silicon layer thickness further accentuated the difference in compaction characteristics between the soft silicone roller and the hard silicone roller.

For the silicone sliders, a layer of AIRTECH Tooltec CS5 woven high temperature resistant PTFE tape was draped over the silicone layer. This was done with the idea of decreasing friction between

the melt tape and the pressure element surface for winding trials. As the deposited tape would slide under the pressure element, high friction could lead to matrix being squeezed out of the tape, fibers being displaced and damaged, and silicone particles being sliced off from the compaction element and included in the laminate as foreign objects. In turn, the tape was used for the compaction testing in order to reflect process conditions.

All pressure elements were tested at four levels of increasing actuator loading, using a factorial experiment design. The list of all parameters and their respective levels is seen in Table 4.4. It is important to note that the compaction load was not measured experimentally and was derived mathematically based on the certification load provided by the OEM, at 6 bars of pneumatic pressure. A linear relationship was assumed between the applied pneumatic pressure and the delivered load, considering that the cylinder area would remain constant. This ignores the effect of friction within the pressure cylinder.

Table 4.4: Parameters and their respective levels used to characterize the compaction behaviour of compression elements

Level \ Parameter	Pressure element type	Pneumatic pressure [bar]	Equivalent compaction load [N]
1	Soft silicone roller	1	312
2	Hard silicone roller	2	623
3	Copper roller	3	935
4	Soft silicone roller	6	1870
5	Hard silicone roller	_____	_____

4.2.3. Evaluation

After maintaining constant actuation load for 2 min, the widths and lengths of the imprints were measured by hand using a caliper. The average compaction pressure was derived from dividing the compaction load by the area of the imprints. The duration of consolidation was derived as the length of the imprint, divided by the deposition speed used in subsequent winding trials.

4.3. Preform winding

In order to reliably test the impacts of high values of compaction loading, tow tension, and mandrel temperature at high winding speeds in a safe and repeatable manner, and to be able to answer **RQ2**, **RQ3**, and **RQ4**, a custom-built tape winding machine was built. This required a fully enclosed machine in order to ensure safety in case of high-velocity projectiles expelled during the winding process. The machine was to employ a modular design that would allow for fast replacement of compaction elements, be highly automated to allow for series production, while maintaining consistency between production runs. Moreover, the machine was to incorporate sensors measuring important process parameters, such as deposition speed, tow tension, tape, laminate, and tooling temperature, as well as input energy from the CoRe HeaT module during winding. Lastly, in order to facilitate post-consolidation for future trials, post-consolidation capacities were to be integrated into the machine independently of the tape winding assembly. By doing so, post-consolidation could be performed immediately after winding, without major operator interference.

4.3.1. Experimental Setup

The new machine was built within a frame of ITEM aluminum profiles, in order to be fully enclosed using sliding double doors. The frame measures roughly 3.2 m in length, 1.3 m in height, and 1.3 m in width. The box design is further reinforced on three lateral sides with additional aluminum profiles at a height of 0.7 m. The sliding doors were placed on both long lateral sides and are able to fully open in order to allow for maintenance and set-up adjustments between production runs.

Along the length of the machine, two zones can be defined. The frontal zone is where all winding subsystems are located and it is where the tape winding process takes place. It includes all motors, the mandrel and its supports, the deposition subsystem, the post-consolidation subsystem, which includes the tooling heating assembly, as well as other elements specific to the CoRe HeaT module. The aft zone of the machine contains additional space for subsystem stowing and maintenance, as well as an electric cabinet and data modules, which are easily reachable and reconfigurable. Cables leading out of the electric cabinets, data modules, and motors are redirected towards an external Siemens PLC, which is used for controlling the machine.

The mandrel is heightwise located at the middle level of the machine. It is secured using two Zentra DIN6350 3-jawed chucks measuring 200 mm. The chuck teeth clamp down on the mandrel ends from the exterior. Thin slotted rings made of wound CF-PEEK are used between the mandrel and chuck teeth in order to prevent mandrel surface damage during clamping, accelerating, and braking. Currently, this set-up restricts the maximum tooling temperature to temperatures below 300 °C, in order to prevent excessive softening of the melting CF-PEEK laminate, which could introduce unwanted eccentricities to the mandrel rotation. The chucks are fastened to EN10305 steel alloy shafts, each supported by a pair of pillow blocks. One shaft is connected to a Siemens SIMOTICS S-1FG synchronmotor, which drives the rotational motion of the mandrel through a reducing gearbox. The other shaft is free to rotate, and is placed together with its supporting pillow blocks on a moving cart made of ITEM aluminum profiles. The cart is propped on two FESTO EGC toothed belt linear axes, mounted on the lowest level of the machine. This allows for translating the chuck cart along the length of the machine and conveniently fixing it at any desired longitudinal position. In turn, various sizes of mandrels up to 1.3 m and 200 mm in diameter can be effortlessly installed to the machine.

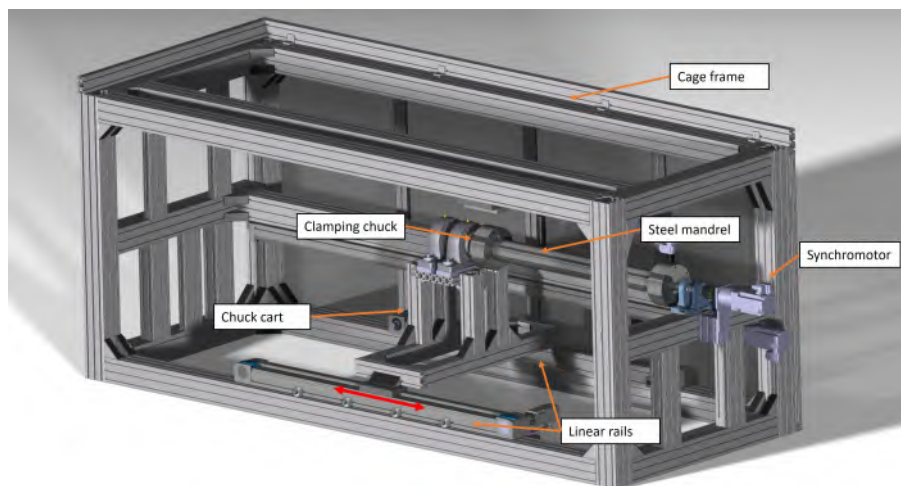


Figure 4.14: Render of the mandrel supports and frame

Two additional FESTO EGC toothed belt axes are installed on either side of the machine, and span the entire inner length of the frame. These two linear axes support the deposition and

post-consolidation assemblies, respectively. In turn, both constructions can effectively process the entire length of the longest usable tooling and also be moved beyond the chuck cart to the aft of the machine to be maintained, repaired, and modified if need arises. Each of these linear axes are actuated by a Siemens SIMOTICS S-1FK synchronmotor through a reducing gearbox. Each axis is able to move independently of the other, while matching the rotational speed of the mandrel at a rate controlled by user input. Specifically, both axes are programmed to translate so as to wind a mandrel with a given diameter using a tape with a given width without gaps or overlaps. The set-up has the theoretical capacity to reach winding speeds of up to 5 m/s, yet it has been successfully tested while filament winding, without in-situ consolidation, for speeds up to 2 m/s.

The entirety of the unloading zone is contained by the mobile deposition assembly, including the material spool itself. The reasoning behind this decision is twofold. Firstly, this allows for limiting the tape length that is kept in the unloading zones at a time, improving resource efficiency. Secondly, and more importantly, the tow tension can be better maintained constant during layup. In the case of a static material spool, passes where the nip point travels away from the spool unwind extra tape length that has to be used by the receding layer pass without decreasing tape tension. In turn, having a traveling material spool maintains the unloaded tape length constant during the entire process.

As post-consolidation was not approached within the span of this research, a detailed description of the post-consolidation assembly is out of the scope of this paper. Instead, the focus will be mainly placed on the tape deposition assembly. Besides the motorized linear axis, the deposition construction, assembled using ITEM aluminum profiles, was further supported by a Kamp & Kötter KPNR 2 m long passive linear rail. This was done in order to increase the stiffness of the construction, given the envisioned high load use case.

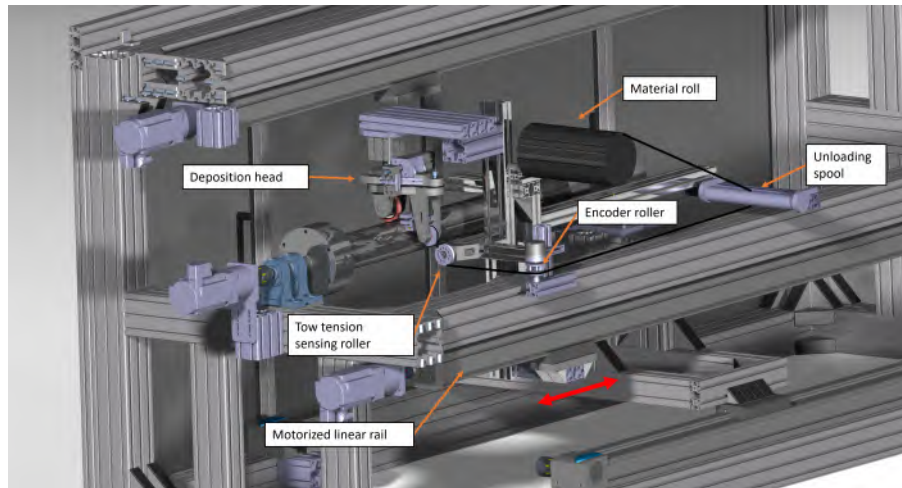


Figure 4.15: Deposition assembly in position to the side of the mandrel.

In order to control the tow tension during winding, the material spool is mounted on a shaft connected to a magnetic powder brake. The production run was started using an IBD Wickeltechnik B.121 brake with 12 N m maximum torque, but the brake setup was changed mid-run for a more powerful IBD Wickeltechnik B.351 brake with 35 N m maximum torque. Both brakes were controlled using constant DC voltage and amperage. This resulted in a slight increase in tow tension during the winding process, as the material spool would decrease in diameter. The tape was unloaded from the spool using a long, slender plastic roller in order to eliminate the

lateral tape travel given by the layup of the material spool for the downstream rollers. The tape then passes around three additional 50 mm in diameter flat plastic rollers before reaching the nip point. Attached to these rollers are various sensors, including a Honigmann RFS-150 radial force measuring sensor. During the production run, two such sensors were used due to initial technical difficulties. The production run started with a 50 N maximum load sensor mounted under a contact angle of 30 deg with the tape, yielding a maximum measurable tow tension of 96.6 N, but was changed mid-production for a 600 N maximum load sensor mounted under a contact angle of 90 deg with the tape, increasing the maximum measurable tow tension to 425 N. Nevertheless the sensors were previously calibrated and their positions were verified using millimeter accuracy.

A deposition head was developed in order to be able to change the winding angle during the winding process while maintaining compaction at the nip point. The design followed the idea of having the entire head be actuated by a pneumatic cylinder. A render of the construction can be in Figure 4.16. Two 20 mm thick plates are connected at one point by a large screw with an axial ball bearing tightly clamped between the plates. Two additional industrial ball transfer units were added between the plates to maintain a stable and even gap. In turn, one plate can rotate about the axial bearing while still transmitting a compression load to the other fixed plate. This rotation is driven by a smaller pneumatic cylinder mounted on the fixed upper plate. On the lower plate are attachment points for the pressure element, as well as an uptake roller. The role of the uptake roller is to maintain the tape as vertical and in line with the axis of rotation of the lower plate. This is done to neatly twist the tape instead of bending it in-plane, which can locally increase internal stresses in the tape and cause tape damage under tensioned winding conditions. The uptake roller is also set to match the height of the nip-point, in the case of the rollers, or the plane tangential to the mandrel, where the slider makes first contact, in the case of the area compaction elements. CoRe HeaT modules are also attached to the deposition head, as well as around the mandrel, in order to heat the tape preceding the nip point.

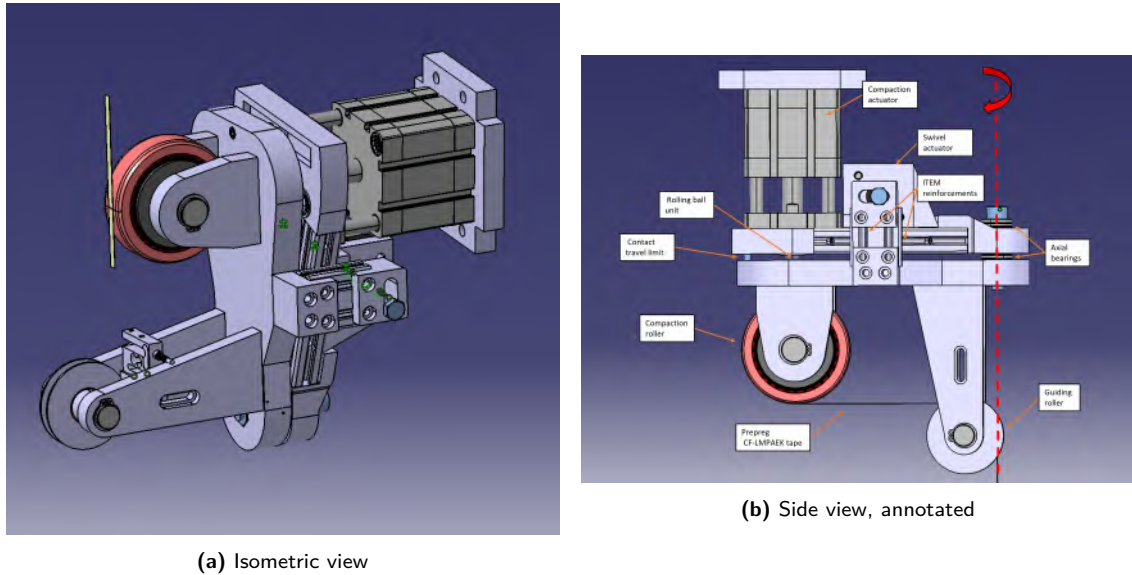


Figure 4.16: Deposition head, with a roller compaction element installed

During tape winding, important process temperatures are continuously monitored, using optical temperature sensing techniques. The mandrel is overlooked by an FLIR A615 thermal camera within the sensing range of 100 °C to 650 °C. Using real time camera feed, the tape temperature preceding the nip point can be observed for most of the length of the layup. This measurement was

used during tape winding to modify CoRe HeaT parameters in order to keep the tape temperature within the processing temperature window.

The mandrel temperature was monitored using an Optris OPTCTLLTFCF3 pyrometer, pointed at a thin silicone band positioned towards the end of the mandrel. Although a lag between the mandrel temperature and the pyrometer readings could be detected using a thermocouple, due to the heat transfer between the steel and the silicone, this measurement method was preferred over measuring the mandrel directly. This is because metallic surfaces are characterized by high reflectivity and low emissivity in the IR frequency range, which makes optical thermal measuring difficult. In turn, the silicone surface is much of a better emitter than the mandrel surface. Nevertheless, due to the large thermal mass of the chucks, the thermal distribution of the mandrel was found to follow an inverted bath curve, making the pyrometer readings under-representative for the region of interest of the mandrel, namely its center. This effect was felt even more intensely for high mandrel temperatures, as a 50 °C difference between center and mandrel end was noted for a center temperature around 280 °C, taken by a thermocouple. Thus, winding was started with silicone band readings below the target temperature, for example starting at 80 °C in order to have a central mandrel temperature somewhat higher than 100 °C.

Another Optris pyrometer, of model OPTCT3MLCF1, ideal for close range, was mounted to the deposition head and was pointed at the laminate immediately succeeding the nip-point. This pyrometer, as well as the one used for mandrel temperature monitoring, was provided with emissivity based on past experience in similar tape winding settings, using identical materials. It is worth noting here that accurately calibrating such optical devices can become quite tricky, as emissivity is influenced not only by material type but also by surface finish, incidence angle, and temperature.

In preparation for winding, the mandrel was coated with two subsequent layers of Haufler HT400 release agent, which were left to cure at a tooling temperature around 120 °C. Pipes measuring 100 mm in internal diameter and 100 mm in length were wound using 8 layers arranged in a quasi-90° layup. Toray Cetex TC1225 UD 145gsm T700GC Standard Modulus CF-LMPAEK tapes were used for the entirety of the production run. The pipes were wound using a constant winding angle of 88.72°, corresponding to a perfect spiral coverage using a tape thickness of 7 mm on a 100 mm diameter. This winding angle was chosen based on the results of [Agarwal](#) on tape widening during consolidation [44]. Of course, this perfect layup is achievable only for the first layer, as the increase in laminate diameter would require an increasing winding angle to maintain perfect coverage, which is practically unachievable using the current setup.

After winding, the mandrel is cooled using cooled compressed air, and the laminate is manually removed from the tooling. To this end, the imbalance between the coefficient of thermal expansion (CTE) between the laminate and the mandrel is used. The CTE of steel is around 12×10^{-6} m/mK, while the CTE of UD CFRP of high fiber volume content is around the order of -1×10^{-6} m/mK. In turn, after winding is complete and the setup is brought to ambient temperature, the steel mandrel would contract while the laminate will slightly expand, ideally creating just enough clearance in order to slide the laminate off the mandrel. Some laminates are wound using higher compaction pressure and tape tension, requiring keeping the mandrel and laminate in a freezing chamber in order to generate enough clearance. In such cases, after defrosting the mandrel, an additional layer of release agent was applied.

4.3.2. Design of experiments

The main parameters which were varied during preform production followed directly from RQ2 and RQ3. These were the compression element type, the applied cylinder pressure, the winding speed, the tow tensions, and the mandrel temperature. The final production parameter set is

shown in Table 4.5, and can be subdivided into four subsets according to the consolidation aspect under investigation.

Table 4.5: Preform tape winding parameter set

Run	Pressure element type	Cylinder pressure [bar]	Winding speed [mm/s]	Tape tension [N]	Mandrel temperature [°C]
1	Soft silicone roller	2	200	15	100
2	Hard silicone roller	1	200	15	100
3	Soft silicone slider	1	200	15	100
4	Copper roller	1	200	15	100
5	Soft silicone roller	2	500	15	100
6	Hard silicone roller	1	500	15	100
7	Soft silicone slider	1	500	15	100
8	Copper roller	1	500	15	100
9	Hard silicone slider	1	500	15	100
10	Hard silicone slider	3	500	15	100
11	Hard silicone slider	6	500	15	100
12	Hard silicone slider	1	500	45	100
13	Hard silicone slider	1	500	80	100
14	Hard silicone roller	1	500	15	200

The first subset contains Runs 1 through 8, and was designed to answer **SQ2.1** and **SQ2.3**. A change in winding speed would directly lead to a change in compaction duration, in accordance with the compaction length of each compression element. This is so as the applied load to each compaction element is maintained constant, and thus the imprint size would also remain constant. Yet, given the expected variance in imprint sizes between compaction elements, the average consolidation pressure exerted at the nip point would also vary accordingly. Thus, it is possible to study the effect of decreasing compaction duration for different levels of consolidation pressure. Moreover, it is possible to evaluate the efficacy of the various pressure elements, which exhibit vastly different compaction behaviors, at identical machine parameters under increasing winding speeds.

The second subset is built around investigating the impact of compaction pressure on laminate quality, and spans Run 9 through 11. As it will be shown in Section 4.2, the slider footprint size does not significantly change with the applied load. In turn, the compaction average pressure and

compaction duration can be effectively decoupled. This made the slider element an ideal candidate for evaluating the influence of applied pressure alone on the laminate quality.

The third subset is, similarly to set three, focused on the influence of a single winding parameter, namely the tow tension. The set is made of Runs 9, 12, and 13. The slider was used for this set as well, as the deposition head containing the slider is built so that the tape is more accurately placed onto the mandrel in a tangential fashion. This is believed to help in effectively determining the influence of tow tension on laminate quality. Alternatively, due to the deformation of the rollers, the tape would be subjected to unwanted out-of-plane bending immediately before the nip point.

The fourth and last subset of this experimental production run is set to answer **RQ3**, namely the extent to which the mandrel temperature is affecting the laminate quality. Runs 6 and 14 are to be compared, as only the initial mandrel temperature differs between them. The temperature set was chosen to have one data point below the T_g of LMPAEK, namely 147 °C as shown in Table 4.1, and one data point above T_g , but below T_m , which reaches 305 °C.

4.3.3. Evaluation

The evaluation of significant laminate quality indicators, namely volumetric void content, porosity distribution, surface roughness and waviness, as well as laminate thickness, was performed using the methods employed for single tape analysis described in Section 4.1.

Arc samples were cut from the pipes using a custom-built CNC cutting machine developed by [Khan](#), and depicted in Figure 4.17 [53]. The cutting machine uses two Dremel 8260 cordless rotary tools fitted with diamond cutting discs and actuated by pneumatics in order to cut test samples from pipe-shaped laminates accurately. The preform was placed on a rotary 3D printed spindle and secured through a tight fit, while the blade mount was able to translate along the length of the laminate for precise location positioning and cutting.

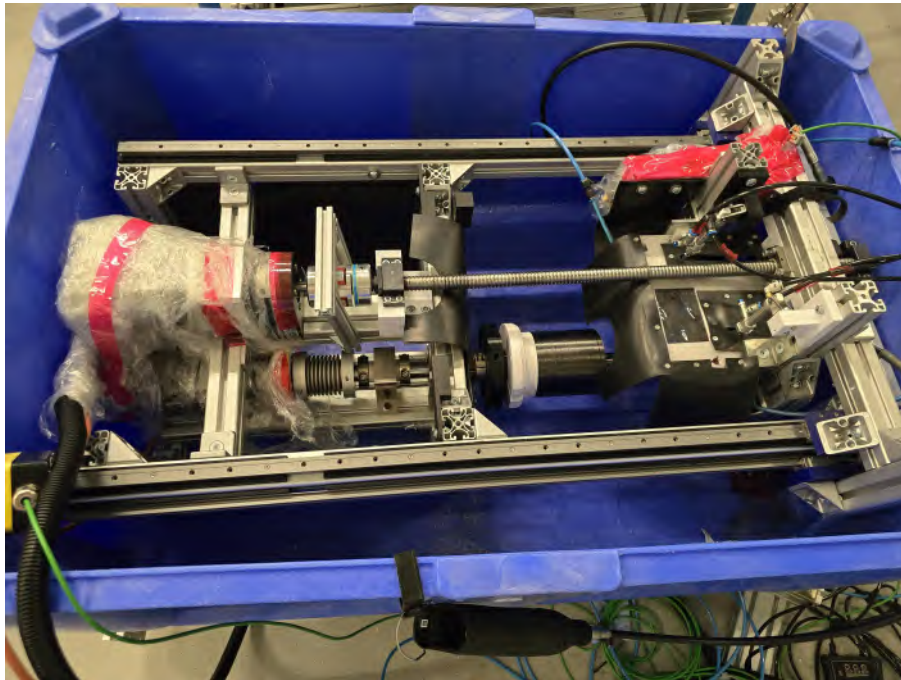


Figure 4.17: CNC-controlled cutting machine

Five samples, measuring roughly 10 mm in width and 20 mm arc length, were cut from the central ring of the pipe, taken at equidistant angles with 72° increments all around the pipe. Four out of five samples, chosen at random, were then embedded, polished, and micrographed using the same method as for the deconsolidated tapes. Thus, micrographs taken at 500 magnification were obtained. The end regions measuring roughly 5% sample width were not captured in the micrograph, as they would be more likely to suffer damage as a result of the cutting process itself, and not from manufacturing.

The laminates were then isolated from the background embedding resin using the magic wand tool within ImageJ, and were segmented using the algorithm developed by [Naumann\[55\]](#). The void content and void distribution were determined using the segmentation data, and information regarding the surface finish and laminate thickness was obtained by processing the upper and lower profiles of the isolated laminate. For more information regarding this method, see Subsection 4.1.3. A deviation from the aforementioned methodology was made when defining the cut-off wavelengths for the filters used in roughness and waviness calculations. In order to contain lower wavelength information within the waviness indicator, as in the case of gaps within the outermost lamina, the central cut-off wavelength was decreased from 0.8 mm to 0.4 mm.

Chapter 5

Results

The most relevant results are presented in this chapter. They are organized around the main experiments described in Section 4.1, Section 4.2, and Section 4.3, respectively. All subsequent analyses will be performed based on the data outlined in this chapter.

5.1. Static deconsolidation

Pre-tensioned CF-LMPAEK tapes of various moisture content were deconsolidated using an electrical pulse set for a specific heating rate until a desired temperature threshold measured over the surface of the specimen was reached. The numerical results of the deconsolidation trials are presented in Table 5.1. The values are presented as averages and standard deviations of all samples produced from each deconsolidated tape. The data was trimmed of outliers using two methods. Firstly, in order to account for segmentation model inaccuracies, the volumetric fiber content was used as the trimming indicator. Since all samples were taken from the same batch of UD prepreg tape, they ought not differ in fiber volume content by a statistically significant amount. In turn, all samples that had a fiber volume content exceeding or subceeding the global average by three standard deviations were ignored for porosity calculations. This led to the exclusion of two samples from the global 35, each belonging to one run. Secondly, in order to account for embedding misalignment and thus morphological inaccuracies, all samples exceeding or subceeding the global average of the width by three standard deviations were omitted from the geometrical measurements. Thus, one sample was trimmed from the data set.

Table 5.1: Static deconsolidation parameter set and results, with averaged values and standard deviations given

Run	Tape tension [N]	Heating rate [°C/ms]	Max Temp. [°C]	Moisture	Average width [mm]	Average thickness [μm]	Average R _q [μm]	Average W _q [μm]	Average void content[%]
0	0	0.0	0	Ambient	6558.48 ±21.15	150.41 ±1.91	4.91 ±1.34	8.37 ±5.72	0.29 ±0.15
1	10	1.7	303	Ambient	6349.83 ±114.58	156.03 ±8.06	7.84 ±2.25	47.40 ±19.46	4.26 ±2.59
2	10	1.7	306	Soaking	6378.48 ±104.27	168.83 ±10.64	7.73 ±1.16	30.91 ±13.46	8.14 ±5.39
3	10	1.7	304	Oven-dried	6383.91 ±84.60	157.12 ±4.01	7.65 ±0.55	36.46 ±12.27	2.58 ±0.22
4	10	2.0	360	Ambient	6596.35 ±77.16	163.46 ±2.69	10.99 ±1.17	65.29 ±16.54	6.25 ±1.33
5	100	32.8	361	Ambient	6242.00 ±40.67	178.56 ±2.18	10.61 ±1.16	27.16 ±7.38	7.76 ±1.46
6	100	42.9	309	Ambient	6363.13 ±38.49	166.74 ±3.38	9.87 ±1.03	17.78 ±3.36	5.32 ±1.02
7	100	2.1	382	Ambient	6174.96 ±86.57	180.42 ±2.97	11.62 ±1.95	24.63 ±13.57	4.69 ±0.61

The eight specimens considered most representative for their respective runs are shown in Figure 5.1. They were chosen as their volumetric void content was the closest to their run's average.

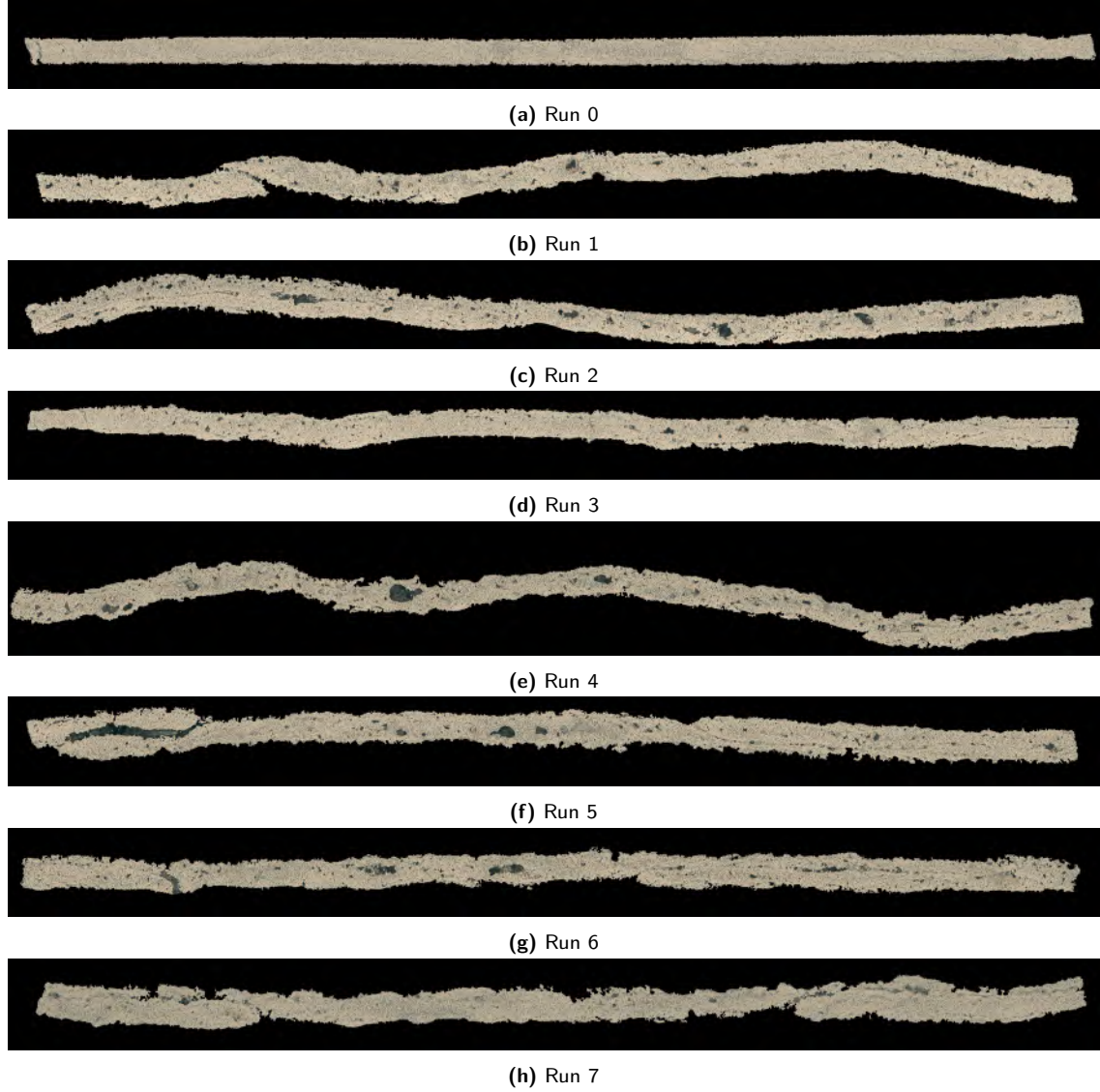


Figure 5.1: Representative specimens for all runs used in the deconsolidation study

The influence of moisture content on porosity can be seen in Figure 5.2. The pristine tape contained the lowest amount of porosity, well below 0.5%, as expected, and was also very consistent from sample to sample. This can be seen as the basis for establishing confident observations regarding the influence of external factors, such as moisture, on deconsolidation porosity. The tape kept under ambient conditions showed an increase in porosity of almost 15-fold, while the water-soaked tape had an increase in porosity of double this amount. In fact, the soaked tape was shown to have the largest increase in porosity among all runs. The deconsolidation also greatly increased the variance in porosity values for both the ambient tape and the soaked tape by a similar order of magnitude. Once the moisture within the tape was removed, the variance in porosity was lowered to an amount comparable to the pristine tape. Yet, an increase in porosity in the oven-dried tape could be observed as compared to the pristine tape by roughly one order of magnitude. Nevertheless, the porosity of the oven dried tape is much lower than both other deconsolidated

tapes.

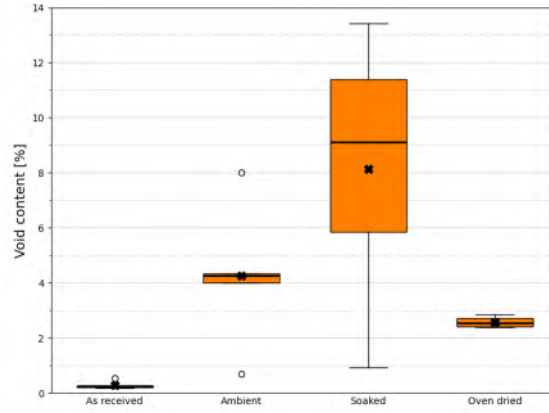


Figure 5.2: Effects of moisture content on deconsolidated tape porosity, compared to pristine tape

The overall surface roughness of the tape was seen not to follow a distinct trend related to the moisture content, as it can be observed in Figure 5.3a. The average of all deconsolidated tapes hover somewhere in between $7\text{ }\mu\text{m}$ to $8\text{ }\mu\text{m}$, in the same neighborhood as one carbon fiber diameter, and close to double the RMS roughness of the as-received tape. Similarly to porosity, the oven-dried samples showed the least variability out of the deconsolidated runs. As to the waviness of the deconsolidated tape, displayed in Figure 5.3b, it can be seen that all deconsolidated tapes greatly surpass the waviness of the as-recieved tape. Surprisingly, the soaked tape showed the lowest average out of all deconsolidated tapes, at around $30\text{ }\mu\text{m}$.

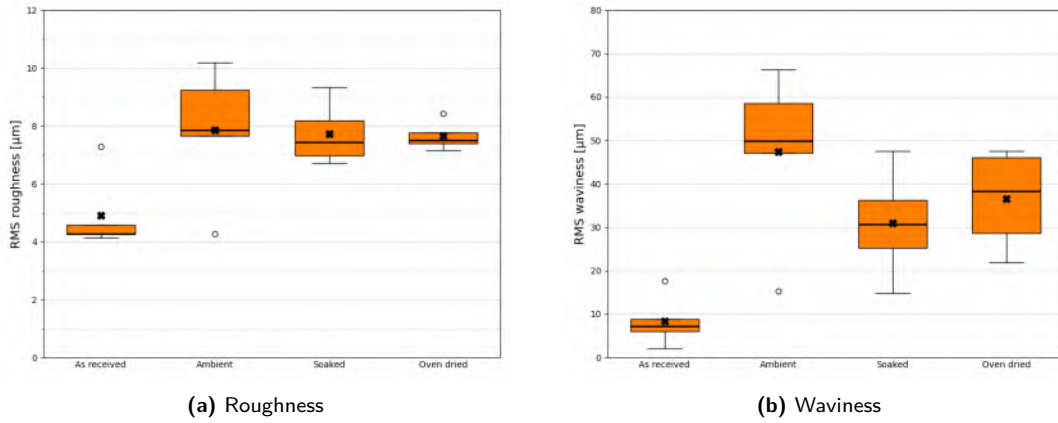


Figure 5.3: Effects of moisture content on deconsolidated tape surface quality.

For the effect of tape tension, Runs 4 and 7 were compared. These trials were conducted at a low heating rate and a maximum temperature well above T_m . The porosity change with increasing tape tension can be seen in Figure 5.4. A clear decrease in porosity can be seen with increasing tape tension, as well as a more uniform distribution of voids along the length of the deconsolidated tape. Note that the increase of tow tension by an order of magnitude led only to a decrease of 25% in tape porosity.

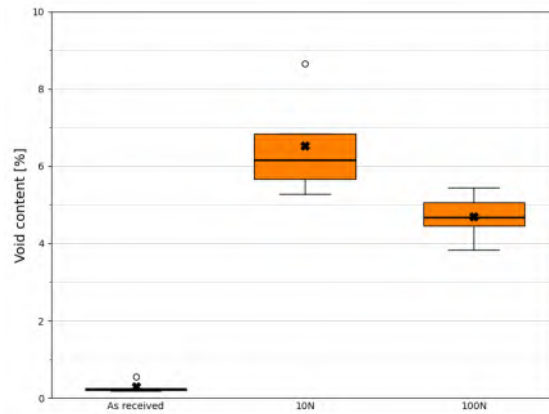


Figure 5.4: Effects of tape tension on deconsolidated tape porosity at low heating rate and above melt temperature, compared to pristine tape

Roughness and waviness results presented in Figure 5.5a and Figure 5.5b, respectively. A slight increase in roughness could be identified. Yet given that the two runs differed by more than 20 °C, and that the roughness will be seen to be more influenced by maximum temperature, little conclusive evidence can be drawn. Waviness could be seen to strongly decrease with an increase in tape tension, dropping by more than 75%, even though porosity was only decreased by 25%. In fact, the lowest W_q was encountered at high tape tension settings, namely with Run 6, which is comparable to the as-received tape.

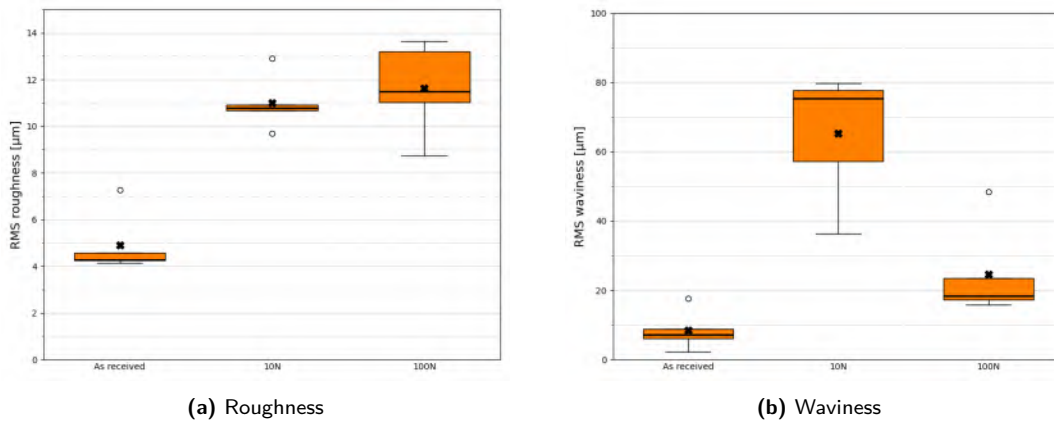


Figure 5.5: Effects of tape tension on deconsolidated tape surface quality.

The tape tension was found to greatly decrease the deconsolidated tape width for samples heated under similar conditions. As shown in Figure 5.6, increasing the tape tension from 10 N to 100 N led to a decrease of 5% in tape width. It is worth noting that the samples deconsolidated under 10 N shown in Figure 5.6 yielded, quite surprisingly, a slight increase in width as compared to the as-received samples, even if in all other morphological qualities, i.e., porosity, roughness, and waviness, they registered clear increases.

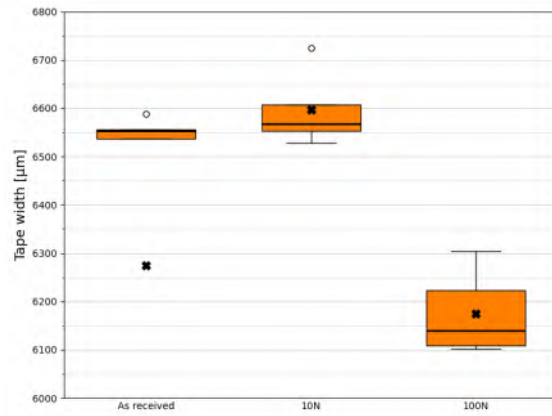


Figure 5.6: Effects of tape tension on deconsolidated tape width.

The influence of heating rate can be determined when comparing Runs 5 and 7, as both were conducted at 100 N tension and temperatures far above T_m . Their void contents are compared in Figure 5.7, and show a strong positive correlation with heating rate. Moreover, the porosity range also seems to increase with an increase in heating range. In fact, Run 5 had the highest increase in porosity out of all tapes kept at ambient storage conditions.

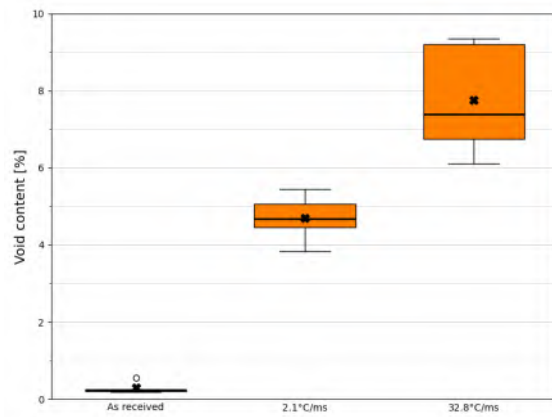


Figure 5.7: Effects of heating rate on deconsolidated tape void content at 100 N tape tension and far above melt temperature, compared to pristine tape

On the other hand, the impact of the heating rate on tape morphology was found to be inconclusive. As Figure 5.8a and Figure 5.8b both show, only slight differences in waviness and roughness were seen with increasing heating rate. Yet, the variance of Rq was strongly reduced with an increase in heating rate.

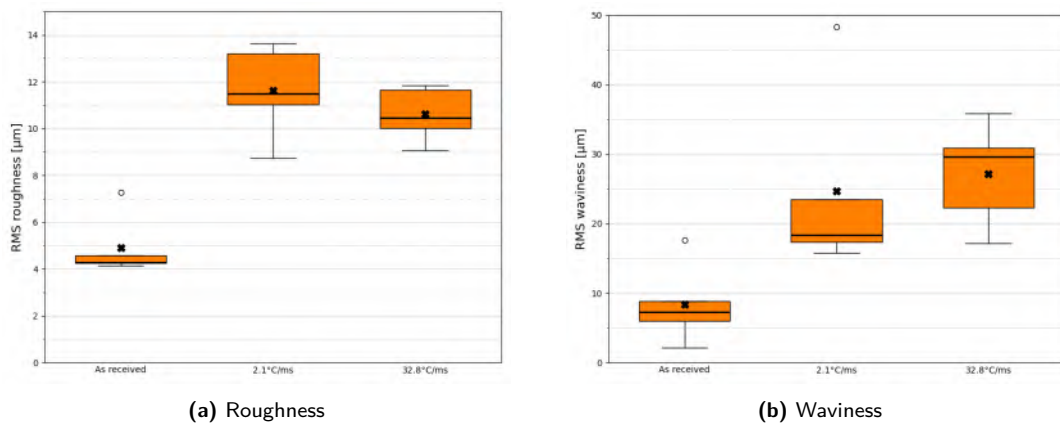


Figure 5.8: Effects of heating rate on deconsolidated tape surface quality.

The impact of maximum tape temperature can be evaluated by comparing Run 6 and 5, as both tapes were loaded by 100 N and heated at a high rate. The porosity change between runs can be seen in Figure 5.9. Distinct increases in both average values as well as variance can be seen with an increase in maximum temperature.

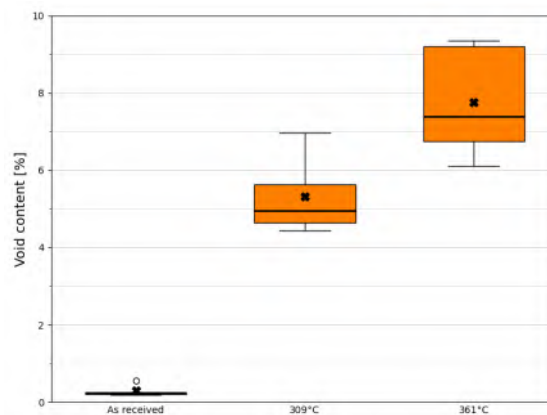


Figure 5.9: Effects of maximum temperature on deconsolidated tape porosity at 100 N tape tension and high heating rate, compared to pristine tape

As can be seen in Figure 5.10a, no significant changes in tape roughness could be seen when increasing the maximum tape temperature. On the other hand, waviness seemed to greatly increase, both by average value and by data spread.

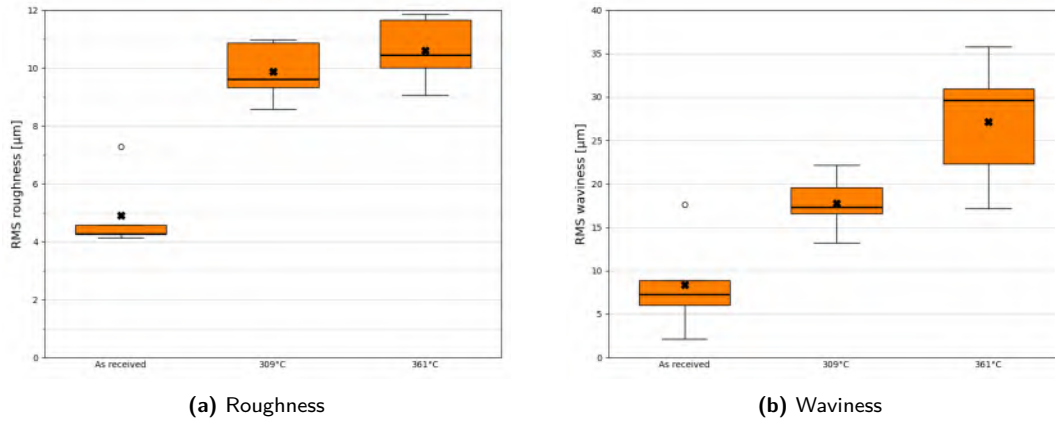


Figure 5.10: Effects of maximum temperature on deconsolidated tape surface quality.

5.2. Static compaction

Different pressure elements of various geometries and material compositions were activated by increasing loads on pressure-sensitive films in order to evaluate their compaction imprint areas. The outcomes of the static compression trials are shown in Table 5.2. Unfortunately, the achievable compaction pressures with the current setup largely fell short of the 2 MPa minimum pressure limit that would allow for an in-depth analysis of pressure distribution as a function of prescale film pigmentation intensity. Although such an analysis could not be performed accurately, the resulting imprints were visible enough to obtain an estimate for imprint size, and thus, the mean compaction pressure could be derived.

Table 5.2: Static compaction results

Compaction element	Cylinder pressure [bar]	Compaction force [N]	Imprint length [mm]	Imprint width [mm]	Compaction pressure [MPa]
Soft silicone roller	1	312	24	25	0.52
Soft silicone roller	2	623	27	28	0.82
Soft silicone roller	3	935	29	30	1.07
Soft silicone roller	6	1870	31	30	1.98
Hard silicone roller	1	312	13.6	24	0.94
Hard silicone roller	2	623	16	25	1.56
Hard silicone roller	3	935	18	25	2.08
Hard silicone roller	6	1870	18	25	4.16
Copper roller	1	312	3.8	18	4.56
Copper roller	2	623	3.8	19	8.49
Copper roller	6	1870	3.8	19	25.37
Soft silicone slider	1	312	41.5	36	0.21
Soft silicone slider	2	623	42	36	0.41
Soft silicone slider	6	1870	44	36	1.18
Hard silicone slider	1	312	40	35	0.22
Hard silicone slider	2	623	40.5	36	0.43
Hard silicone slider	3	935	41.2	36	0.63
Hard silicone slider	6	1870	42	36	1.22

The compaction length of each pressure element plotted against their respective theoretical applied load can be seen in Figure 5.11. The copper roller imprint seems not to change in length for the range of applied loading used. The compaction length of the soft roller is roughly twice the compaction length of the hard silicone roller, although that difference becomes smaller with increasing loading. This is reasonable, given the stiffness and silicone thickness differences between the two compaction elements. The difference between the two types of sliders remains minimal

for all considered loads. Note that the spread of values between all compaction elements provides a good range to evaluate the influence of compaction length on preform quality.

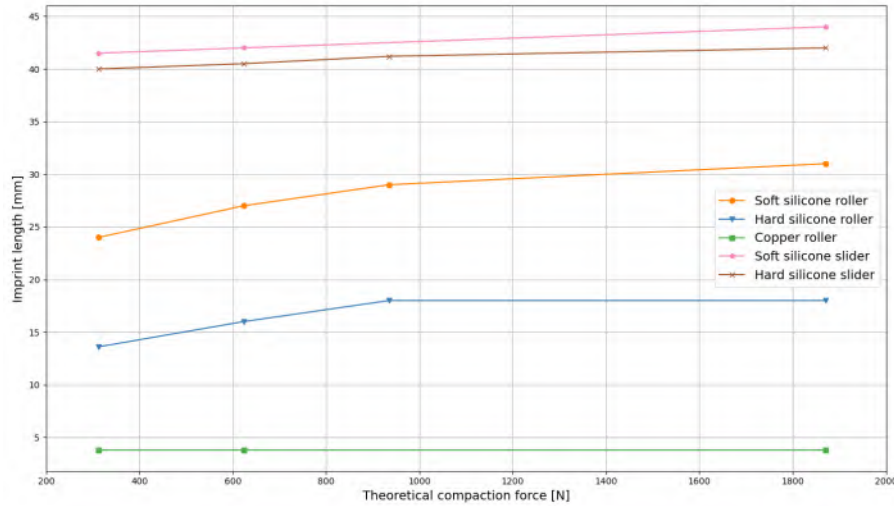


Figure 5.11: Average compaction length as a function of theoretical compaction load for each compaction element, fitting curves

The relation between theoretical compaction load and average compaction pressure can be found in Figure 5.12. The compaction behaviours of the two sliders were determined to be very similar, irrespective of cylinder pressure. This can be attributed to their silicon layer shape, as the shape constricts any meaningful shape changes that would arise from the difference in silicone material stiffness. In turn, for the purposes of evaluating compaction effects, they can be assumed to be identical.

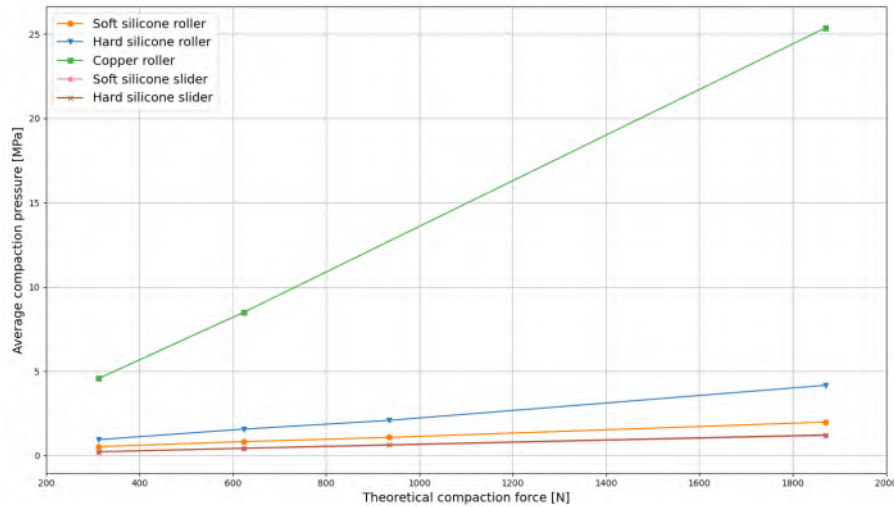


Figure 5.12: Average compaction pressure as a function of theoretical compaction load for each compaction element

5.3. Preform winding

CF-LMPAEK pipe preforms consisting of 8 quasi 90° layers were tape-wound using CoRe HeaT. The parameters that were varied were the pressure element type, the applied average compaction

pressure, tow tension, and tooling temperature.

During tape winding of the preform pipes, the soft silicone roller was not able to maintain its integrity for the duration of one trial. Two iterations were made for this pressure element, but due to time constraints, the two runs using the soft silicone roller were omitted, namely Run one and Run five from Table 4.5. This lowered the number of winding trials to twelve, which were relabeled from Run 1 to Run 12. A brief discussion regarding the possible cause of failure is given in Section 6.2. Nevertheless, the remaining three consolidation element types exhibit such different compaction behaviour that the results extracted from the remaining runs would be able to form the basis for reasonable conclusions. Furthermore, during high applied pressure trials using the sliders, severe damage occurred to the ToolTec tape layer, which is further discussed in Section 5.2. In turn, for Run 11, the ToolTec layer was replaced with a 2 mm thick teflon plate, which was able to be bent to the shape of the silicone surface.

For all winding trials, the CoRe HeaT module placed before the nip point, which introduces current to the tape created some friction, and thus, additional tape tension. A load cell was positioned in line to the tape to measure this friction loading. Thus, the final tow tension at the nip point was taken as the sum of the readings between the tensiometer presented in Section 4.3 and this load cell. Prior to pipe winding, the required breaking control settings to reach the tape tension values provided in Table 4.5, as read using the tensiometer, were determined experimentally. Thus, the final tow tensions consistently exceed the values provided in Table 4.5 by an even amount. Furthermore, the extra friction is the reason as to why the tow tension measurements between sliders and rollers may differ, even though the same breaking force was used. Nevertheless, the tension differences are of the order of 15 N, and thus should not invalidate the test runs.

The dataset was searched for outliers similarly to the single tape deconsolidation results, namely, the volume fiber content was verified to be within three standard deviations from the global mean. The average fiber content of all laminates was found to be 58.4%, with a standard deviation of 1.41%. No outliers could be identified.

All relevant controlled variables and final results for the preforms produced using tape winding are given in Table 5.3. The values of the laminate quality key indices are provided as averaged values from the samples of each pipe, along with their respective standard deviations.

A global comparison between the laminate thicknesses of each run is provided in Figure 5.13. As specified by the manufacturer, the consolidated ply thickness of this kind of prepreg tape ought to be 140 μm . Accordingly, a laminate with 8 plies ought to have a thickness of 1120 μm . It can be seen that most laminates are either fairly close to this threshold, or are exceeding it, with the notable exception of Run 11. This is so because the deposition of the last layer was halted halfway through the process as the upper limit of the tape tension limit was reached, which engaged a built-in emergency stop. Another notable mention is Run 4, which has the largest positive difference in average laminate thickness. Nevertheless, the laminate thickness cannot be used alone to judge the quality of the laminate, and must be aided by waviness measurements. A fairly well consolidated laminate with gaps in the upper plies could have a lower average thickness as compared to a poorly consolidated laminate with compounded faults, high waviness, but an acceptable average thickness.

Table 5.3: Tape winding final parameter set and results, with averaged values and standard deviations given

Run	Pressure element	Compaction pressure [Mpa]	Winding speed [mm/s]	Compaction duration [ms]	Tape tension [N]	Mandrel temperature [°C]	Void content %	Rq [μm]	Wq [μm]	Thickness [μm]
1	Hard silicone roller	0.94	200	68.0	31.60	100	1.48 \pm 0.44	4.45 \pm 0.49	29.83 \pm 12.38	1102.92 \pm 70.22
2	Soft silicone slider	0.21	200	207.5	16.34	100	2.97 \pm 0.83	4.60 \pm 1.10	35.27 \pm 10.06	1145.18 \pm 9.53
3	Copper roller	4.56	200	19.0	25.52	100	0.43 \pm 0.34	2.64 \pm 0.14	9.99 \pm 2.55	1099.94 \pm 2.36
4	Hard silicone roller	0.94	500	27.20	30.02	100	2.53 \pm 1.15	6.73 \pm 0.75	40.14 \pm 11.47	1205.11 \pm 9.22
5	Soft silicone slider	0.21	500	83.0	17.73	100	4.87 \pm 0.64	4.37 \pm 1.12	26.91 \pm 4.79	1116.63 \pm 13.21
6	Copper roller	4.56	500	7.6	25.86	100	1.13 \pm 0.55	2.27 \pm 0.21	9.50 \pm 2.55	1132.75 \pm 2.48
7	Hard silicone slider	0.22	500	80.0	17.15	100	4.74 \pm 1.77	4.59 \pm 0.70	26.00 \pm 8.01	1173.08 \pm 15.12
8	Hard silicone slider	0.63	500	81.0	18.01	100	1.29 \pm 0.34	4.26 \pm 0.30	33.44 \pm 7.34	1102.68 \pm 7.93
9	Hard silicone slider	1.22	500	82.4	27.50	100	0.75 \pm 0.32	2.27 \pm 0.20	13.76 \pm 5.62	1112.33 \pm 7.04
10	Hard silicone slider	0.22	500	80.0	63.05	100	1.29 \pm 0.61	4.47 \pm 0.73	25.78 \pm 6.00	1108.23 \pm 3.49
11	Hard silicone slider	0.22	500	80.0	103.45	100	2.07 \pm 0.43	3.90 \pm 0.52	33.64 \pm 9.13	993.49 \pm 4.71
12	Hard silicone roller	0.94	500	27.2	30.00	200	2.64 \pm 0.97	5.71 \pm 0.86	33.45 \pm 7.26	1167.82 \pm 5.35

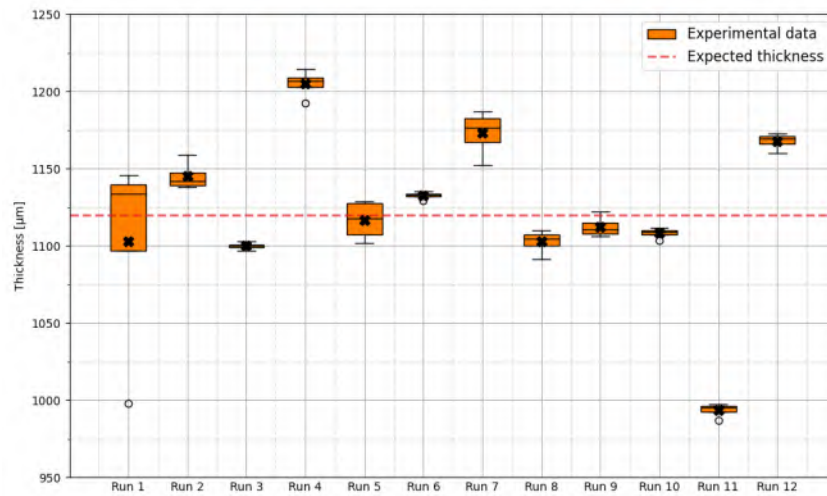


Figure 5.13: Laminate thicknesses of all pipes, with the ideal laminate thickness provided at $1120\ \mu\text{m}$

A general comparison between the three compaction behaviours at similar machine settings can be done through Runs 1 through 6. The representative specimens for these runs are shown in Figure 5.14. Their respective porosities are shown in Figure 5.15, and display the expected trend of increasing porosity with an increase in winding speed. Additionally, both the silicone and copper rollers show a great increase in variance with an increase in winding speed, while in the case of the slider, the spread change does not seem statistically significant. When comparing the compaction elements, the copper roller was able to produce the lowest porosity, followed by the hard silicone roller and the slider, with the difference seeming to increase with increasing winding speeds.

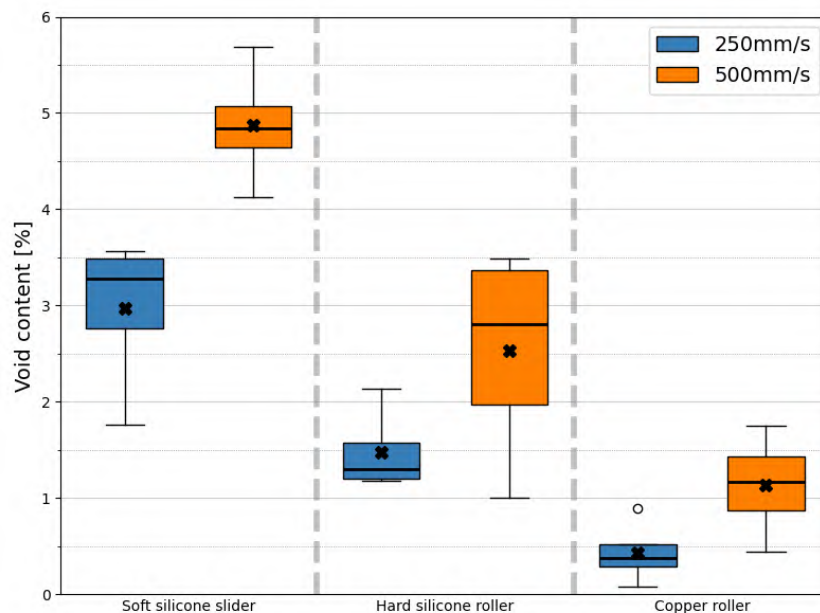


Figure 5.15: Void content spread for each pressure element at increasing winding speeds

In regard to the laminate surface quality, the copper roller was able to achieve the best results, far from all other compaction elements. The roughness and waviness of these runs can be found

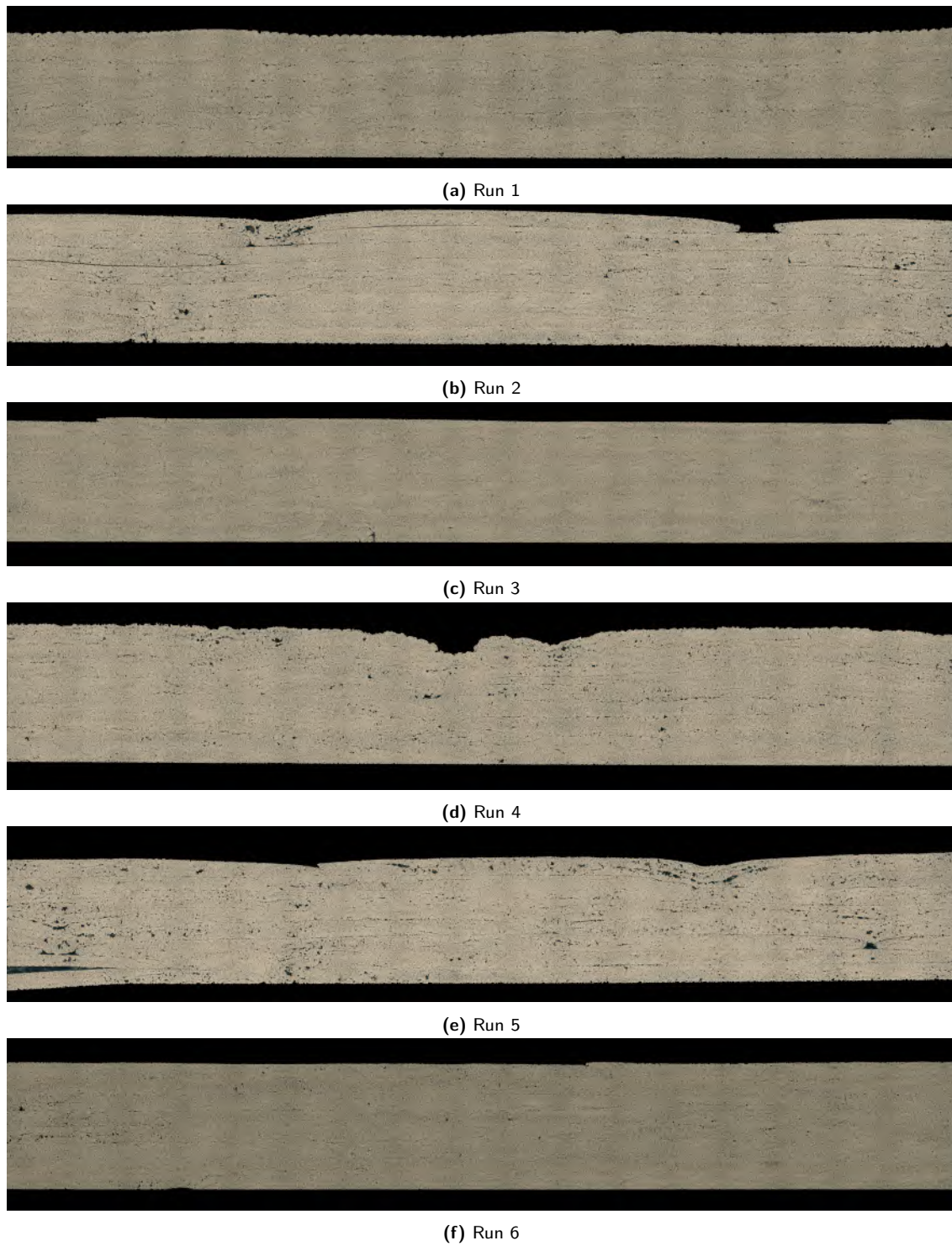


Figure 5.14: Representative specimens for winding runs 1 through 6

in Figure 5.16a and Figure 5.16b, respectively. For both the slider and copper roller, the surface quality seems to either remain constant or improve, while for the hard silicone roller, a deteriorating trend was observed. In fact, the worst waviness profile of all laminates was observed for the run using the hard silicone roller at 500 mm/sec.

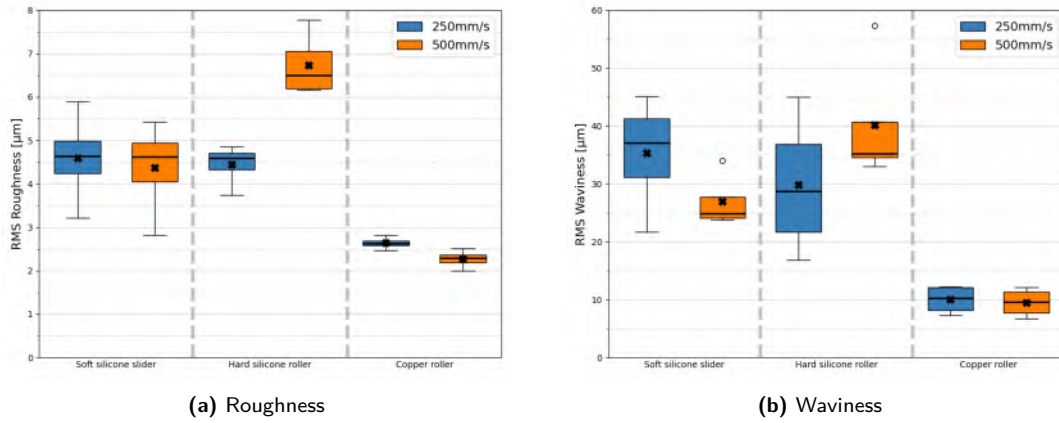


Figure 5.16: Effects of different pressure elements used at increasing winding speeds on laminate surface quality.

As discussed in Section 2.4, the influence of compaction pressure can be seen when comparing Runs 7 through 9. The representative specimens for these runs are shown in Figure 5.17. The porosities of these laminates are shown in Figure 5.18. A clear trend of decreasing porosity with an increase in compaction pressure can be identified, as expected. A large decrease in porosity can be seen with an increase from 0.22 MPa to 0.63 MPa, yet the difference seems to taper off from 0.63 MPa to 1.22 MPa. Taking this trend into account, a power law fitting for the averages of all these runs was found to best represent the impact of compaction pressure on porosity, with a coefficient of determination of 0.9976. A similar trend can be seen in void content variance among the investigated samples. Note that the run using 1.22 MPa compaction pressure produced the lowest void content of all runs, and the lowest sample variance of all runs conducted at 500 mm/s.

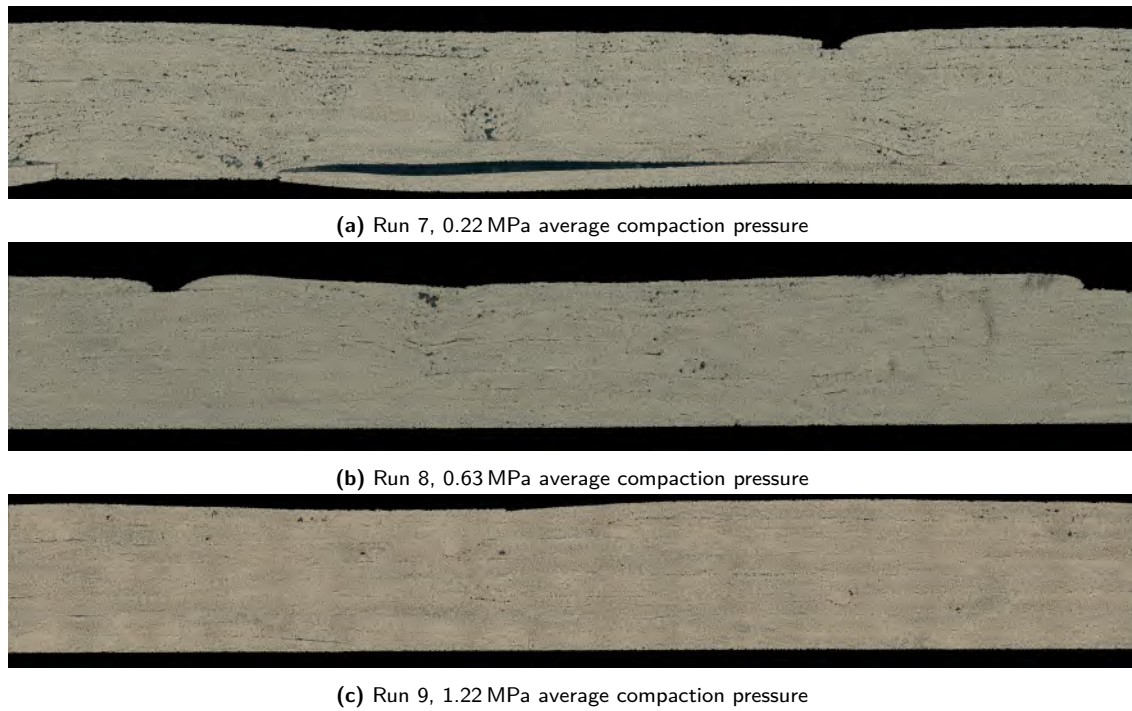


Figure 5.17: Representative specimens for winding runs 7 through 9

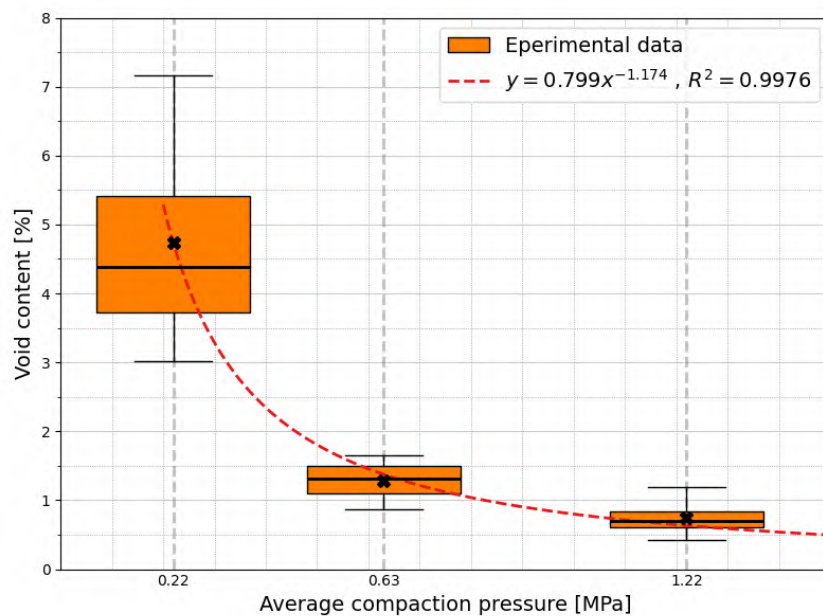


Figure 5.18: Effects of compaction pressure on porosity of preform wound laminates, using a hard silicone slider, with power law fitting curve provided

The surface quality key indicators for these trials are displayed in Figure 5.19a and Figure 5.19b, respectively. The surface roughness seems to greatly decrease with increasing pressure, even more so where the average compaction pressure is doubled from 0.63 N to 1.22 N. The surface waviness is also greatly decreased once the highest level of compaction pressure is reached. The variance

across samples is also shown to react positively to an increase in pressure.

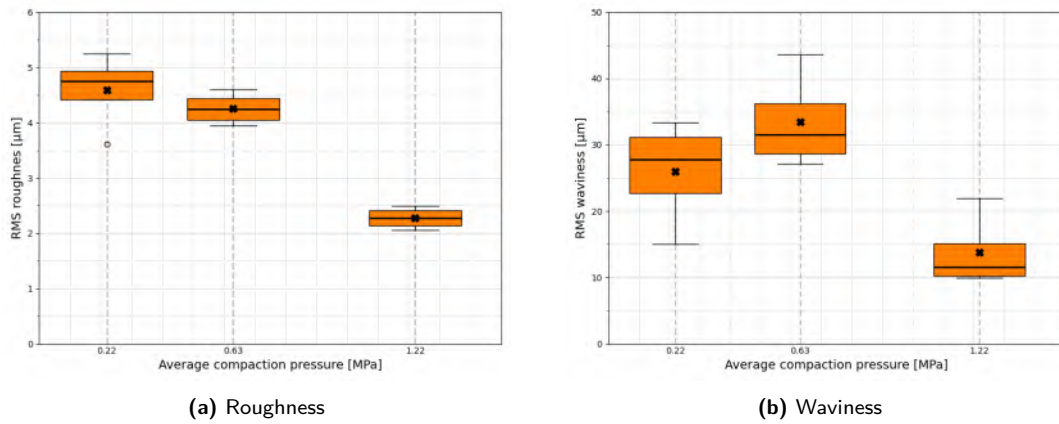


Figure 5.19: Effects of increasing average compaction pressures, using a hard silicone slider, on laminate surface quality.

The impact of tape tension was evaluated based on Runs 7, 10, and 11. The representative specimens for these runs can be found in Figure 5.20. The void content ratios of these runs are shown in Figure 5.21. Given that increasing tow tension would also increase the compaction pressure applied by the deposited tape on the laminate substrate, it was expected that the porosity would follow a similar power law trend as in the case of increasing compaction pressure. Yet, an increase in porosity can be seen from 63 N to 103 N, yielding a subpar power law coefficient of determination of 0.863. It is thus the case that another mechanism is at play, which would determine this unexpected rise in void content.

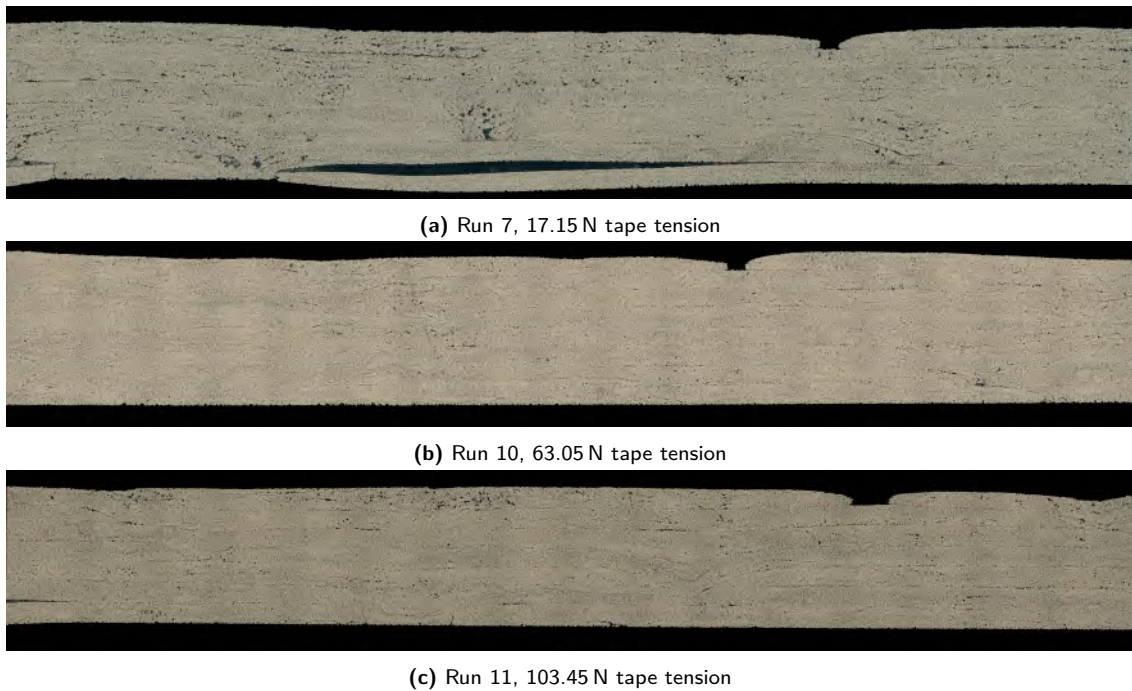


Figure 5.20: Representative specimens for winding runs 7, 10, 11

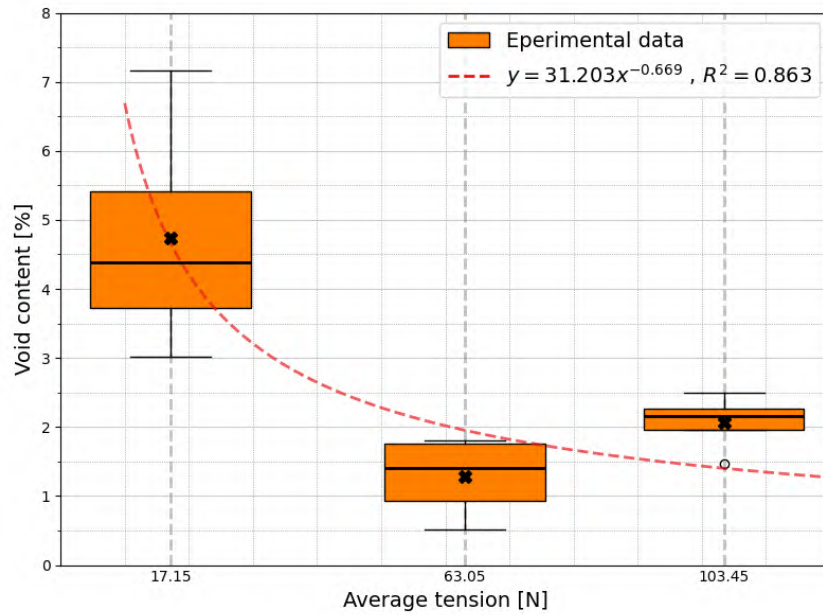


Figure 5.21: Effects of tension on porosity of preform wound laminates, using a hard silicone slider

The root mean square roughness and waviness measurements of Runs 7, 10, and 11 are shown in Figure 5.22a and Figure 5.22b. The increase in tape tension seems to have a negative effect on the surface roughness of the laminate, while no particular trend could be observed for mean waviness. The largest waviness variance of all runs was encountered in the laminate produced with the highest tape tension, meaning that this run was more prone to gaps.

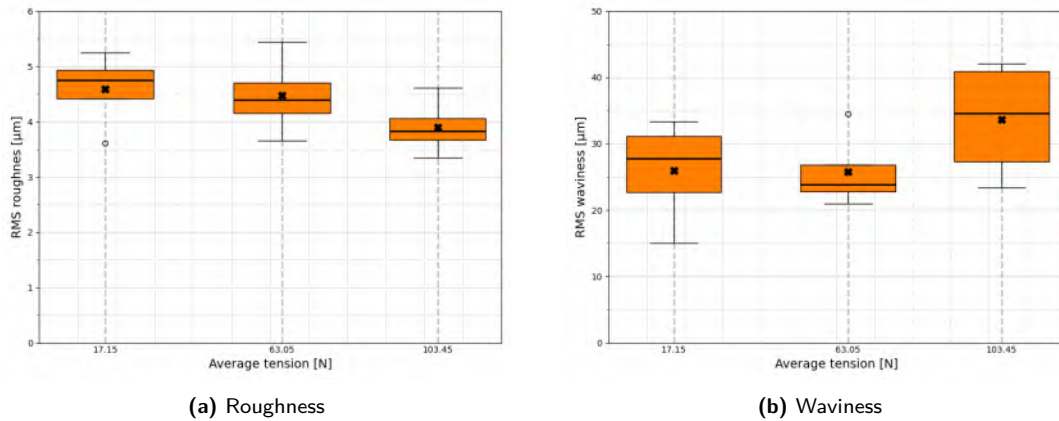


Figure 5.22: Effects of increasing tape tension, using a hard silicone slider, on laminate surface quality.

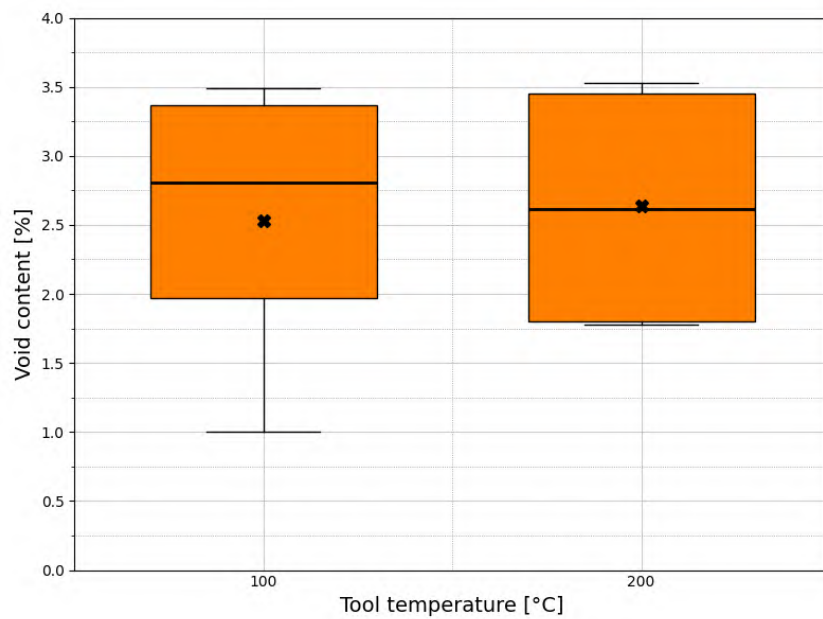
The initial mandrel temperature was increased from below T_g to above T_g between Runs 4 and 12. The representative specimens for these runs are shown in Figure 5.23. The porosities of these two trials are shown in Figure 5.24. Both laminates displayed the same average void content, with an insignificant relative difference of 2%. A slight decrease in sample variance could be seen, but not to a significant level.



(a) Run 4, 100 °C mandrel temperature



(b) Run 12, 200 °C mandrel temperature

Figure 5.23: Representative specimens for winding runs 4 and 12**Figure 5.24:** Effects of increasing mandrel temperature on porosity of preform wound laminates, using a hard silicone roller

Tooling temperature was found to slightly decrease surface roughness, as shown in Figure 5.25a. Yet, the hotter mandrel trial shows a higher roughness variance among samples. Regarding waviness, displayed by Figure 5.25b, a slight decrease in mean value could be seen, with little change in variance.

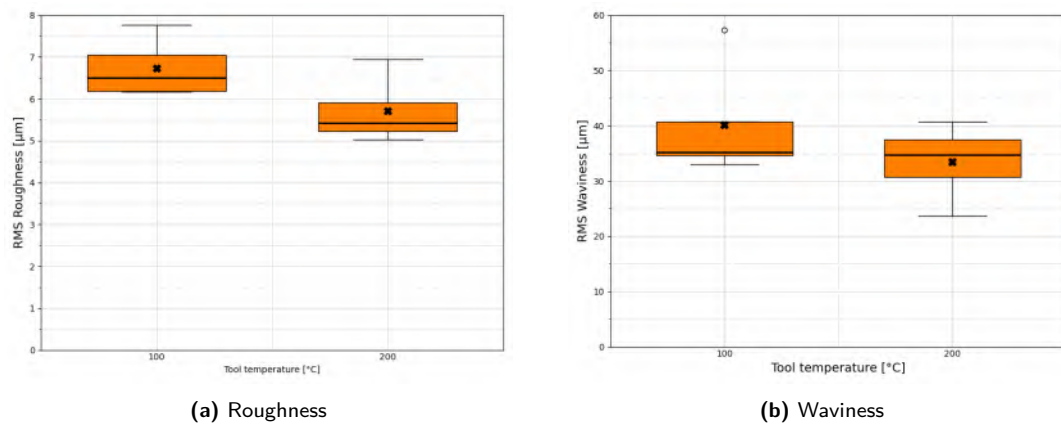


Figure 5.25: Effects of increasing mandrel temperature, using a hard silicone roller, on laminate surface quality.

Chapter 6

Discussion

The most relevant findings presented in Chapter 5 are further analyzed and interpreted in this chapter. The discussion follows the structure of the previous chapter. Section 6.1 dissects the results of the deconsolidation trials. Section 6.2 covers technical aspects regarding the use of the custom-built compression elements. Section 6.3 treats the findings of the winding trials and brings into focus possible physical causes for the observed effects. The chapter is closed by Section 3.4, in which all hypotheses previously stated in Chapter 3 are evaluated against the findings of this research work.

6.1. Tape deconsolidation

The tape moisture content can be clearly seen as a great influence on the porosity of deconsolidated tape. This effect is evident in Figure 5.2, and is in line with findings from [Slange et al.](#). The large variance in data pertaining to high moisture content tape seems to indicate that localized effects contribute the most to the final void content. In fact, these tapes were seen to contain much larger pores as compared to tapes kept in ambient or dried conditions. A peculiar example of such a phenomenon can be seen in Figure 6.1. The large pore seems to follow a distinct delineation along the width of the tape that splits the sample in half. It is believed that this resin-rich divide within the tape is a result of the manufacturing process, and poses as a void nucleation interface similar to the inter-ply borders in prepreg stacks investigated by [Slange et al. \[20\]](#). In turn, it can be assumed that dissolved moisture molecules contained within the matrix diffuse across the tape and travel to such void nucleation interfaces. The dissolved moisture can then further expand upon reaching high enough temperatures and displace tape material unimpeded by external loads to form pores of great size. It is possible that the large variation of porosity along the length of the tape could indicate the propensity of dissolved water to travel in a lengthwise manner, as this path would be aligned with the fiber direction and thus create much less resistance to movement.

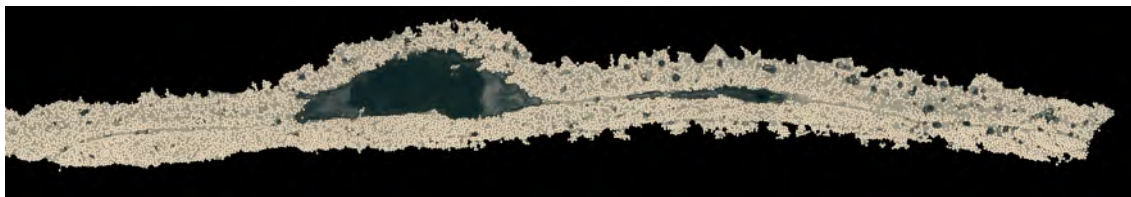


Figure 6.1: Sample of deconsolidated tape with high moisture content, displaying a large-size pore

Once the internal moisture is removed from the tape, the distribution of pores seems to become much more uniform along the length of the tape. Thus, pore expansion mechanisms that are more uniform along the tape, such as pre-existing pore expansion and the release of internal fiber stresses, become the driving factors in final void content. This interpretation is further strengthened by the low porosity variance of the pristine tape, which would contain only pores resulting from insufficient matrix permeation during the manufacturing stage.

Utilizing the data represented in Table 5.1, it is possible to assess the significance of each quantifiable controlled parameter on the variance of the test results by determining the range of signal-to-noise for an increase in parameter level. As a minimum void content is desired, the target for porosity when calculating the signal-to-noise ratios was set to 0. The same target was chosen for both roughness and waviness assessments. The signal-to-noise ratios corresponding to the porosity of each tape, along with the amount of variance attributed to each parameter is shown in Table 6.1.

Table 6.1: Signal-to-noise analysis of the void content of deconsolidated tapes

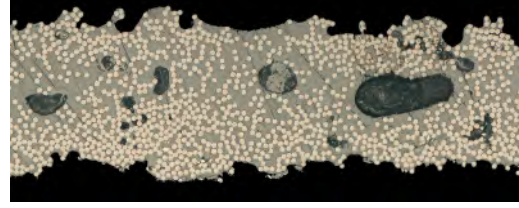
Run	Tension		Heating rate		Temperature		S/N
1	10N		low		T _m		-13.72
4	10N		low		120%T _m		-16.43
5	100N		high		120%T _m		-17.91
6	100N		high		T _m		-14.65
7	100N		low		120%T _m		-13.49
Levels	10N	100N	Low	High	T _m	120%T _m	
Avg. S/N	-15.07	-15.35	-14.54	-16.28	-14.18	-15.94	
$\Delta S/N$	0.28		1.74		1.76		
Normalized $\Delta S/N$	0.16		0.98		1.00		

It is clear that both the maximum reached temperature, as well as the heating rate used to reach that temperature, are greatly correlated to the increase in tape porosity. This is in line with the one-to-one comparison displayed in Figure 5.7 and Figure 5.9. This is also consistent with the findings of Çelik et al., which correlated the increase in porosity with the increase in heating rate and maximum temperature, although this study did not isolate the effects of these parameters. On the other hand, Table 6.1 shows that tape tension accounts for a lesser impact on void content as compared with temperature and heating rate.

The influence of temperature can be attributed to the requirement of matrix mobility for the formation of pores. As the matrix viscosity drops, entrapped gases and the release of internal stresses of constricted fibers face less resistance to movement and are able to displace the matrix-fiber phase in which they are contained more readily. Moreover, increasing the maximum tape temperature raises the temperature of entrapped moisture and volatile vapor, and thus increases the internal pressure of these gaseous pockets. The increase in pressure, in conjunction with the lower viscosity of the matrix, will increase the volume required by the emerging void to reach a pressure equilibrium with its surroundings, thus leading to larger pores. This may explain the prevalence of large, round-shaped pores close to resin-rich areas within samples 4 and 5, which were heated far above their melting point, as shown in Figure 6.2.



Snippet of run 4, specimen 4



Snippet of run 5, specimen 1

Figure 6.2: Examples of large, well-rounded pores, within tapes heated far above melting temperature

The high impact of heating rate can also be attributed to the influence of matrix temperature and viscosity on void inception and growth. Increasing the amount of power used to heat the tape is likely to lead to the presence of hot spots within the tape, especially in fiber-rich regions, close to the outer edges of the tape. It can be the case that the current introduced by the contact electrodes may be spread unequally along the width of the tape, greatly influenced by the gradient of contact pressure at the interface between the electrode and the tape. A higher contact pressure would decrease the contact resistance across the interface between the electrode and the carbon fibers at the edges of the tape, which would lead to more current, and conversely, more heat, going to those fibers as compared to those subjected to lower contact pressures. This effect would be further exacerbated at higher power settings, leading to more pronounced hot spots, where the previously mentioned effects would increase porosity locally.

The results of the signal-to-noise analysis regarding tape roughness are shown in Table 6.2. Both maximum temperature and tape tension seem to be highly influential on low wavelength morphology changes, while the heating rate does not seem to have a statistically significant influence. This is, again, in line with the findings of Çelik et al., who found that highly deconsolidated tape under high heating power to high maximum temperatures has a much rougher surface than slightly deconsolidated tape under lower heating power to temperatures just above melting. Yet, this signal-to-noise analysis indicates that the increase in surface roughness seems to be caused overwhelmingly by temperature effects, and not by heating rate influences. As discussed in Subsection 2.4.3, the small wavelength characteristics of deposited tape play a larger role in the development of good intimate contact, and thus interlaminar bonding. The fact that such morphological tape characteristics seem not to be greatly influenced by heating rate proves advantageous in the case of high-speed processes, where high heating rates are required to reach the melt temperature at high deposition speeds.

Table 6.2: Signal-to-noise analysis of the surface roughness of deconsolidated tapes

Run	Tension		Heating rate		Temperature		S/N
1	10N		low		T_m		-18.17
4	10N		low		120% T_m		-20.86
5	100N		high		120% T_m		-20.55
6	100N		high		T_m		-19.93
7	100N		low		120% T_m		-21.40
Levels	10N	100N	Low	High	T_m	120% T_m	
Avg. S/N	-19.51	-20.63	-20.14	-20.24	-19.05	-20.94	
$\Delta S/N$	1.11		0.10		1.89		
Normalized $\Delta S/N$	0.59		0.05		1.00		

Tape tension seems to gain a significant influence on large wavelength tape morphology changes,

as it can be seen in Table 6.3. This is self-explanatory, as tension introduces resistance in out-of-plane fiber movement, which would conserve the flat shape of the tape. This is in line with the comparison shown in Figure 5.4. The heating rate applied to the tape also seems to have a significant impact on surface waviness, yet unlike tape tension, higher heating rates yield increases in waviness, as shown in Figure 5.8b. Furthermore, heating rate and, partly, maximum temperature, impact the tape waviness indirectly through void formation. Large voids that form within the tape can locally increase waviness by affecting tape thickness, while voids that are able to be evacuated to the outside environment create deep indentations that are largely counted towards large wavelength measurements, as shown in Figure 6.3b. On the other hand, the lack of tape tension allows for global tortuosity to occur, as in Figure 6.3a.

Table 6.3: Signal-to-noise analysis of the surface waviness of deconsolidated tapes

Run	Tension		Heating rate		Temperature		SN
1	10N		low		T_m		-34.06
4	10N		low		120% T_m		-36.57
5	100N		high		120% T_m		-28.93
6	100N		high		T_m		-25.12
7	100N		low		120% T_m		-28.77
Levels	10N	100N	Low	High	T_m	120% T_m	
Avg SN	-35.32	-27.61	-33.14	-27.02	-29.59	-31.42	
$\Delta S/N$	7.71		6.11		1.83		
Normalized $\Delta S/N$	1.00		0.79		0.24		



(a) Run 1, specimen 1, deconsolidated in the absence of high tape tension under low heating rate until just above melting, shows global crinkling.



(b) Run 5, specimen 2, deconsolidated in the presence of high tape tension under high heating rate until far above melting. The right-hand side annotation shows a very large pore, while the left-hand side annotation shows deep grooves left by void evacuation, both capable of influencing surface waviness.

Figure 6.3: Comparison between the impact of lack of tension (a), and of severe deconsolidation due to heating method (b) on surface waviness.

Lastly, the width deformation data were used to generate a signal-to-noise analysis, using as the target value the mean width of all pristine tapes instead of zero, like in previous cases. The results of this analysis are shown in Table 6.4.

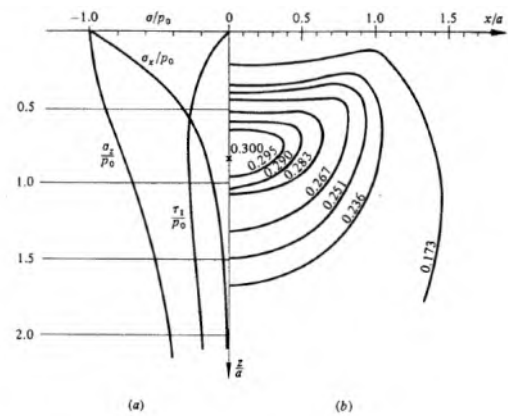
Table 6.4: Signal-to-noise analysis of the width of deconsolidated tapes

Run	Tension		Heating rate		Temperature		SN
1	10N		low		T_m		-47.33
4	10N		low		120% T_m		-37.92
5	100N		high		120% T_m		-50.06
6	100N		high		T_m		-45.95
7	100N		low		120% T_m		-51.85
Levels	10N	100N	Low	High	T_m	120% T_m	
Avg SN	-42.55	-49.20	-45.62	-47.92	-46.55	-46.53	
$\Delta S/N$	6.65		2.30		0.02		
Normalized $\Delta S/N$	1		0.35		0.00		

The tape tension was shown to be the primary influencing factor in deconsolidated tape width change. Indeed, looking at the width measurements shown in Table 5.1, tapes loaded under high tension were more prone to have a lower width than those loaded by lower tensions. This effect can be analogously compared to the necking behaviour in tensile test specimens. High tensile loads may compact the fibers spread along the tape width once the matrix viscosity decreases. As the loading was maintained until the tape cooled below T_g , the fibers were immobilized in the solid matrix, and thus the width decrease remained after the removal of the load. Interestingly, temperature does not seem to play a significant role in width deformation, within the above T_m temperature range considered in this study.

6.2. Compaction elements

As mentioned in Section 5.2, the soft silicone roller was not able to withstand the applied loading during the tape winding process. Figure 6.4 shows the damaged soft silicone roller after trying to complete Run 1. It can be seen that the 2K silicone layer was forcefully ripped away from the 1K silicone adhesive, leaving behind a thin residual layer of soft silicone still attached to the inner silicone.

**Figure 6.4:** Critically damaged soft silicone roller**Figure 6.5:** Contact theory of two aligned cylinders: a) internal stress distribution taken along the symmetry line, b) contour plot of principal shear stresses, reproduced from [56]

The mechanism of failure is believed to be attributed to three main reasons at interplay with each other. Firstly, the region at the interface between the silicone layers was not fully cured, as the surface of the residual 2K silicone was found to be tacky to the touch. This may come as a result of an interaction between the two silicones while co-curing, creating a sort of hybrid layer of silicone that would not fully cure. Secondly, the two silicones vary greatly in hardness and, more importantly, stiffness. Thus, it may be the case that the strain of the 2K silicone could not be matched by the 1K silicone, causing tears close to the interface, which further devolved to complete rupture. Lastly, the maximum principal shear stress, as according to Hertzian contact theory of two cylinders, happened to act fairly close to the interface between the two silicones. As shown in Figure 6.5, the location of maximum principal shear stress is dependent on the factor a , which is related to the reduced stiffness modulus of the two bodies, and in turn, the stiffness of the roller.

This failure mechanism did not occur in the other roller manufactured with hard silicone. It is believed that the thinner layer of 2K silicone used for this roller, as well as the stiffer 2K silicone itself, increased the reduced stiffness module and thus changed the point of action of the maximum principal shear in such fashion that the silicone interface was not overloaded. Additionally, the lower mismatch between the stiffness of the 1K and 2K silicone is believed to have maintained the structural integrity of the roller through even more demanding production trials.

The manufacturing process of silicone casting used for the hard silicone roller was seen to have a direct impact on the surface roughness of the laminates, especially on Run 1, which was performed at a lower winding speed. Given that the casting mold was made using 3D printing techniques, the surface of the roller was imprinted with a rugged and repeating finish given by the layered deposition of the 0.8 mm PETG filament. This surface pattern could be clearly seen in Figure 5.14a, on the laminate's upper surface. Figure 6.6 shows how this repeating imprint accounts for mostly the entire roughness profile. Considering that all deposited layers may have received such an imprint, it is safe to assume that this level of roughness contributed towards the porosity of the laminate, and it is expected that using a more advanced mold, with polished metal surfaces, for example, would aid in achieving lower void content while using a silicone conformable roller. Further experimental work is thus recommended.

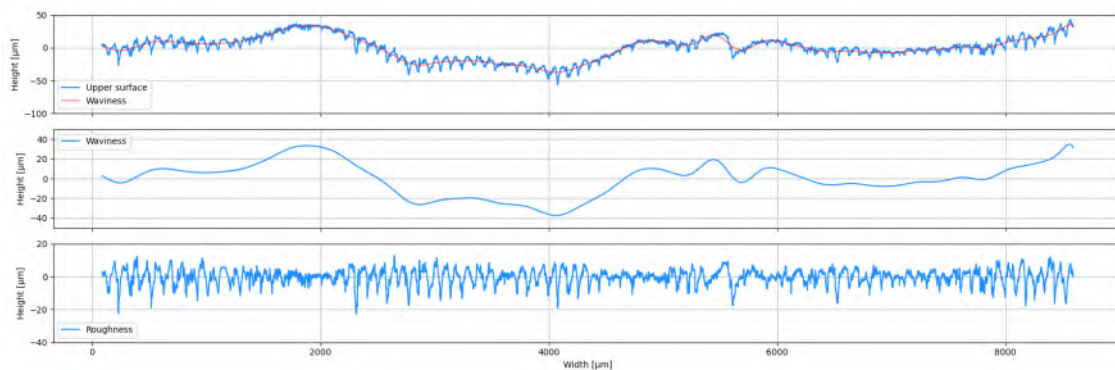
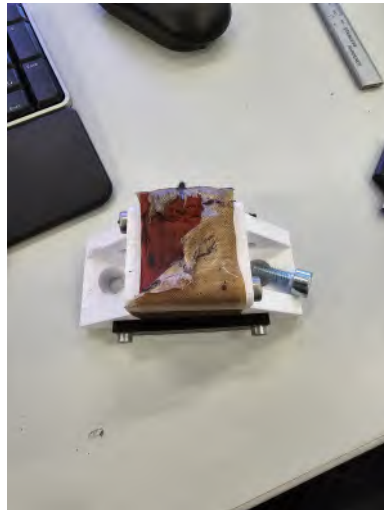


Figure 6.6: Upper surface profile analysis of a specimen belonging to Run 1, with a repeating pattern of roughness imparted by the silicone roller

The sliders also faced technical issues, as the friction of the sliding melted tape caused severe damage under high compaction loading, as presented in Figure 6.7. While using one layer of tape, the ToolTec was completely ripped apart, and some silicone residue could be seen being imparted to the laminate. This is highly undesirable, as it can drastically affect mechanical performance. The silicone was able to be protected by the inclusion of another layer of ToolTec tape, yet the consolidation quality could be negatively affected by an inconsistent pressure distribution caused

by the surface height difference seen in Figure 6.7b. Indeed, the perforation in the first layer of ToolTec tape, as well as the wrinkles that succeed it, are believed to be the cause for the increase in roughness and waviness seen for the 0.63 MPa run, as shown in Figure 5.19a and Figure 5.19b.



(a) Single ToolTec layer



(b) Double ToolTec layers

Figure 6.7: Damaged sliders loaded under high compaction loading

Under closer inspection under the microscope, it was found that the woven Teflon tape in contact with the tape was badly damaged, with the majority of fibers displaced, thinned down, or broken. Moreover, a large amount of polymer and carbon fibers were found to be lodged in the fabric. Thus, the ToolTec layer was substituted with a 2 mm thick deformable Teflon strip for all subsequent runs using high compaction loads.

During the compaction trials, it was found that the copper roller pressure distribution was highly sensitive in regard to the positioning of the roller with respect to the mandrel, unlike the other conformable pressure elements. Slight inclinations of the rotational symmetry axis of the copper roller would lead to large gradients in the width-wise pressure distribution seen in the static imprints, as shown in Figure 6.8. Even with calibration done using the prescale pressure films, such pressure gradients could be seen to have an impact on the surface quality of the laminates.

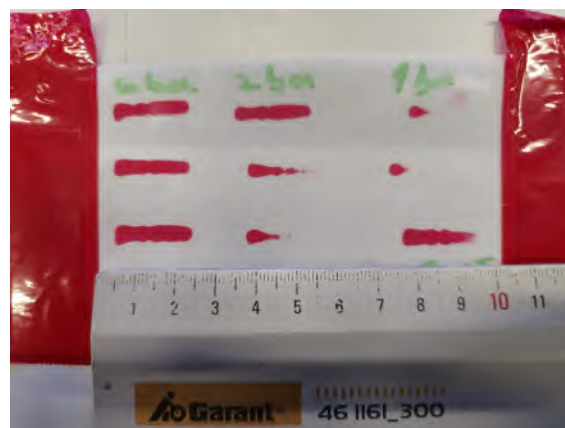
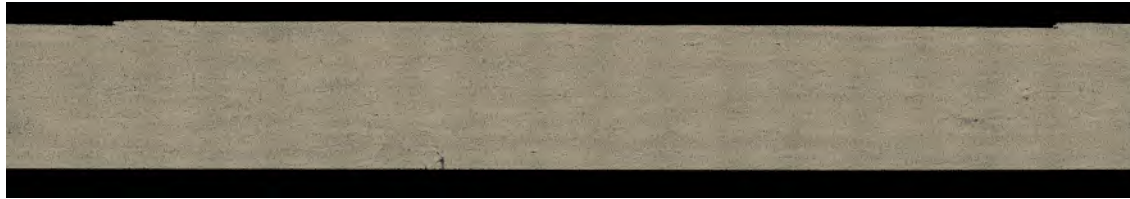
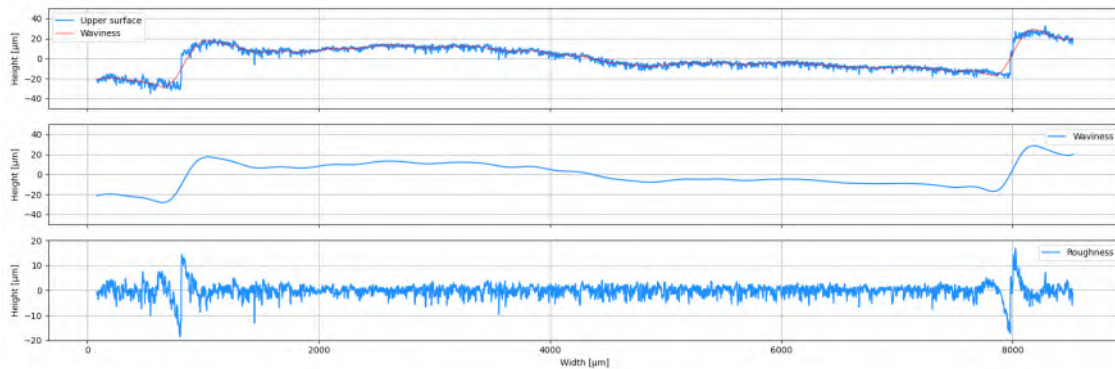


Figure 6.8: Imprints of the copper roller at various actuator pressures, showing the impact of roller misalignment with the mandrel

The gradient in pressure distribution created by the copper roller is believed to have led to the formation of the stepped-like surface profile of preforms consolidated using this pressure element. Each step measures around $7000\text{ }\mu\text{m}$ in width, which would match the width of the melted tape when consolidated under the 4.56 MPa applied average pressure. Thus, it can be assumed that the uneven pressure across the width of the contact zone between the roller and the tape could have led to the imprints seen in Figure 6.9a, as the melted tape would be compressed and displaced under a gradient and, upon cooling, would solidify bearing these marks. Figure 6.9b shows that these imprints account for most of the waviness and roughness of these specimens.



(a) Microscopy image with isolated specimen, taken at 500x magnification



(b) Upper surface profile of specimen, divided into waviness and roughness profiles

Figure 6.9: Run 4, specimen 3, preform laminate showing step-wise indentation in the upper surface, consolidated using a copper roller

6.3. Preform winding

Before delving into the interpretation of the results of preform winding, a brief discussion regarding the heating control used during production is in order. As discussed in Section 4.3, the power provided by the CoRe HeaT unit was changed by hand, layer by layer, during the winding process, based on the temperature readings on the thermal camera, either before or after the nip point. Although the increases in power were consistent from run to run. This was done in order to have a fair basis for comparison between runs. Utilizing the current setup and the resources at hand, no non-invasive method for accurately and reliably measuring the nip point temperature could be implemented. The only reliable indication of the degree of tape heating experienced during the whole winding process can be extracted from the voltage drops actively monitored during production. Large voltage drops from the target value would be evidence for a drop in tape resistance, which would correlate to a drop in provided heat. Yet, since CoRe HeaT is still in its development, no simulation or model is accurate enough to provide actual temperature values based on these voltage drops. These are the main reasons why nip point temperature was not chosen as a controlled variable for this study, even if viscosity plays an important role during consolidation. Nevertheless, through trial and error, the temperature range of the tape around the nip point, visible to the temperature-sensing equipment, was reasonably kept within the processing window specified by the manufacturer.

6.3.1. Void analysis

Multiple specimens were subjected to large delaminations, mostly between the first and second layers, as can be seen in both Figure 5.17 and in Figure 5.20. Most of the delaminations seem to appear toward the ends of the specimens, which could indicate that they were either created or exacerbated by the cutting process. Yet, Run 9 also displays a large delamination positioned far away from the edges of the specimen, which would be more difficult to attribute to cutting or handling. It is thus more probable that for some laminates, such as Run 7, insufficient interlaminar bonding took place between the first two layers. Indeed, by looking at the voltages experienced by two laminates, one with large delaminations, i.e., Run 7, and one without visible delaminations, i.e., Run 8, shown in Figure 6.10, it is possible to correlate the presence of large delaminations with an aggressive drop in voltage in the incipient layers. Run 7 saw a starting voltage of close to 80% and only reached the target voltage in layer 5, while Run 8 started at a voltage close to 90% and reached a voltage neighborhood of 96% to 98% while the second layer was wound. It can be assumed that the low voltage experienced by the first two layers of Run 7 meant that not enough heat was transferred to the tape for sufficient interlaminar bonding to be established under the low average compaction pressure of 0.2 MPa. And even if the first layer of Run 8 also experienced sub-target voltages, the increase in heating in layer two, combined with the increased compaction pressure of 0.6 MPa, may have been enough to avoid the risk of delamination.

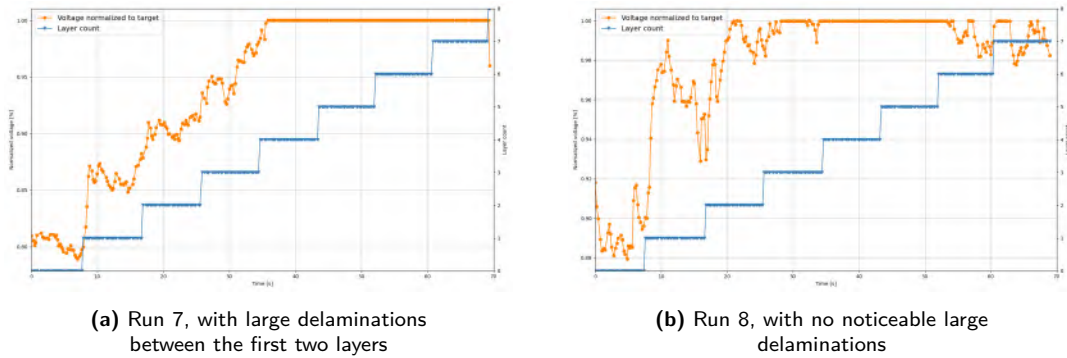


Figure 6.10: Voltage readings during the winding process, normalized to the target voltage, along with the layer count

Figure 6.11 shows the distribution of void sizes through the thickness of Runs 7 and 8, by means of the cumulative distribution of pores. The positions taken along the laminate thickness are taken as the geometric centroids of pores. It can be seen that the delaminations contained by Run 7 account for a large percentage of its void content, as the cumulative void content sharply increases after a single increment in thickness. Besides these large increments, the rate of added porosity seems to be incremental from layer to layer, with the last layers containing more voids as compared to the first few layers. This occurred for all laminates, even though the last layers are more likely to have been under a voltage much closer to the target value than the first layers. This may be attributed to two reasons: the effect of compounded gaps and overlaps, and the impact of repasses from the pressure element.

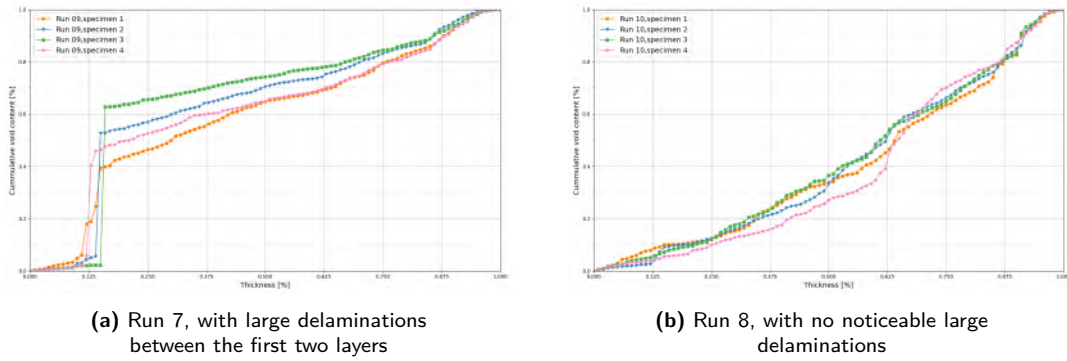


Figure 6.11: Normalized cumulative distribution of voids throughout the thickness of specimens

Omitting the large-scale delaminations from the void distributions allows for evaluating the two aforementioned porosity-influencing mechanisms at the laminate level. Figure 6.12 shows the cumulative distribution of voids for specimens that differ only by one parameter value, with delaminations excluded from the data. The averages of the four specimens for each run are provided as a marked curve, with margins given by their standard deviation. The influence of average pressure can be seen in Figure 6.12a. Although most of the voids are encountered in the last layers for all runs, the rate of porosity increase within the laminas is less steep for specimens consolidated under high pressure. The stepped appearance of the void distribution for the run using the highest level of pressure indicates that a larger percentage of voids are interlaminar as opposed to intralaminar.

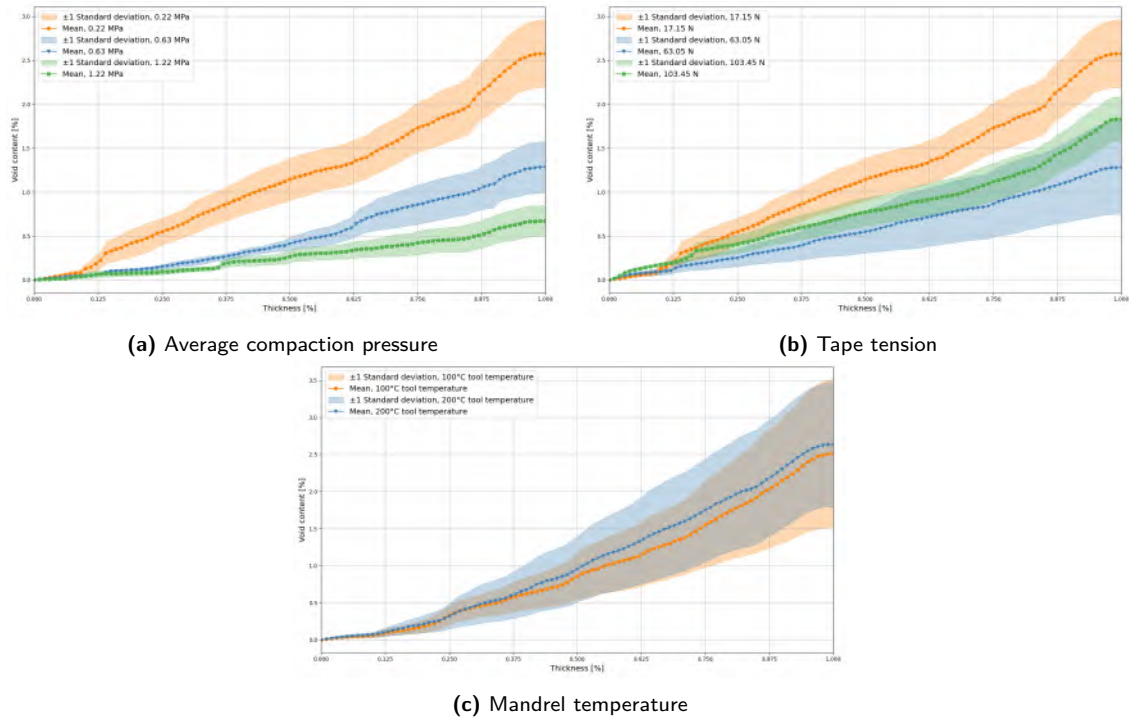


Figure 6.12: Influence of various process parameters on the distribution of voids through laminate thickness, excluding large delaminations

Figure 6.12b shows the influence of tape tension on the buildup of porosity through laminate thickness. Both the 17N and the 103N trials seem to have rapid increases in void buildup rate within their last 2-3 layers, while the 63N has a much more consistent slope, from layer to layer. This may be explained by the compounded effect of gaps and overlaps, which would force upper layers to bend and wrinkle in order to cover the very wavy substrate, and thus lead to both interlaminar and intralaminar pores. It can be seen in Figure 5.20 that all runs have gaps within their last layers, and also have local layer crumbling within interior layers, in places where the deposited tape was forced to occupy the space of gaps in the substrate layer. Thus, it would be expected that laminates wound with higher tape tension, and thus an increased level of applied pressure due to that tension acting on the tape pushing against the substrate, would yield lower porosities. Yet, the laminate wound with the most tape tension shows larger gaps and a higher void accumulation rate layer-by-layer as compared to the laminate wound with the intermediate level of tension. A rough measurement of distinctive tape widths in the last layers of sample 4 of Run 10, loaded by 63 N, and sample 2 of Run 11, loaded at 103 N, shows a difference of approx. $170\text{ }\mu\text{m}$. During deconsolidation trials, a difference of $417\text{ }\mu\text{m}$ in width between tapes loaded at 10 N and 100 N, namely Runs 4 and 7, was observed. It is believed that the narrowing influence of tape tension on deconsolidated tape, as seen in Section 6.1, was a factor in increasing gap width within layers, and thus led to more layer crumbling, which led to a higher amount of voids which could not be closed by the increased constriction load created by the high tape tension. Thus, this effect was compounded, layer by layer, until it was most evident in the outermost lamina, which contains a large amount of visible pores. Examples of such phenomena can be found in Figure 6.13.

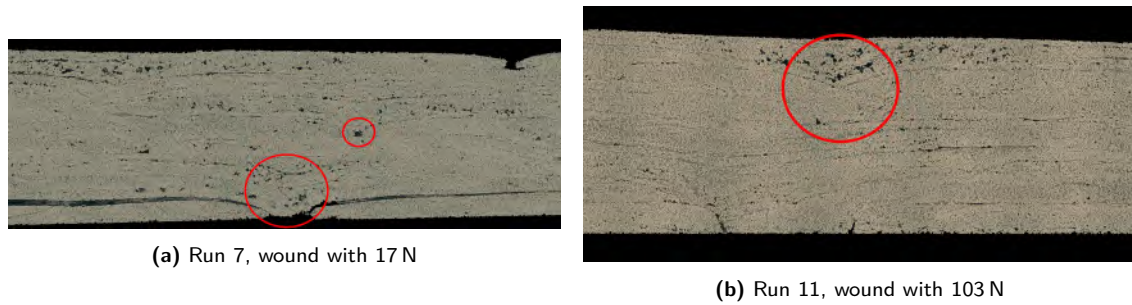


Figure 6.13: Porous zones developed by partial filling of gaps and layer crumbling as caused by the forced filling of gaps

Figure 6.12c shows the cumulative distributions of void content of laminates wound with different tooling temperatures, below T_g and above T_g , respectively. Little difference can be seen between the two curves, which would indicate that tooling temperature did not play a significant role in laminate porosity. This result is quite surprising, based on the contradictory literature discussed in Subsection 2.4.3. The insignificant difference indicates that subsequent passes of the pressure roller have little to no impact on pore closure within substrate layers. If repasses were to be effective, a lower porosity would have been expected in the lower laminas, as they would have been above T_g during subsequent passes of the pressure element, given the lack of a significant heat sink, as in the case of the steel mandrel heated below T_g .

6.3.2. Slider performance

Throughout Runs 1 to 6, the three main compaction elements, namely the hard silicone roller, soft silicone slider, and copper roller, were compared at the same machine settings while increasing winding speed. As seen in Figure 5.15, the best performance was achieved by the copper roller, irrespective of winding speed. Yet, it was found that by increasing the pressure applied to the slider, laminates with less porosity and more consistent void content could be achieved, as seen in Figure 5.18. Thus, it seems that area compactors could be favoured over rollers, if given the right conditions.

Figure 6.14 shows the void content data of Runs 2 through 8 plotted against the time one single point of incoming tape spends under the compaction element. The three datasets represent each pair of runs performed using the same compaction element, with the average compaction pressures provided as taken from the static compaction experiment. The consolidation duration is taken as the measured imprint length divided by the winding speed. Trendlines connecting the means of each run within the set are also provided. Given that only two mean points are available per set, linear trendlines were chosen to fit the data. The linear relationship between consolidation duration and porosity is an assumption that is in accordance with the findings of [Zhao et al.](#), as discussed in Subsection 2.4.3.A striking feature of the trendlines plotted in Figure 6.14 is that they seem to increase proportionally to the applied compaction pressure. By plotting the values of these slopes, it is clear that they follow a linear pattern.

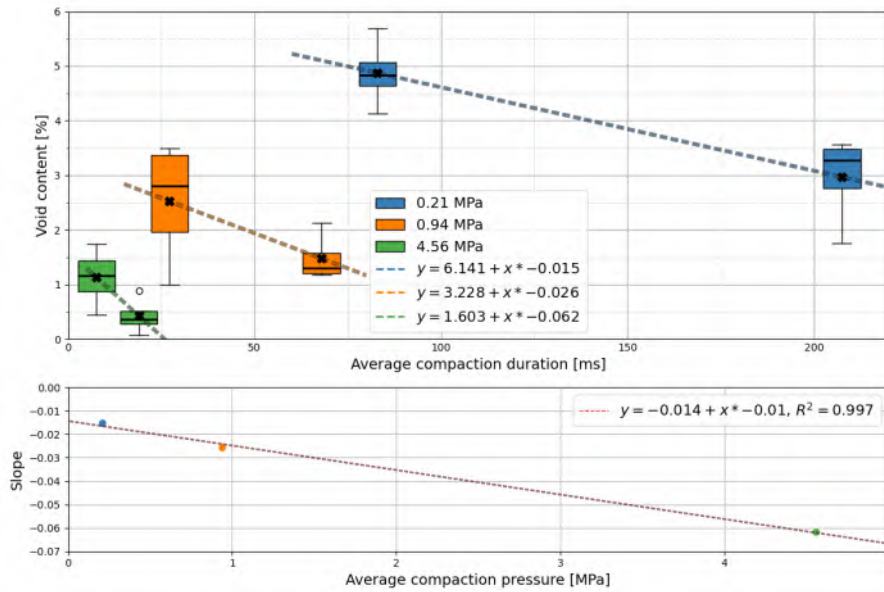
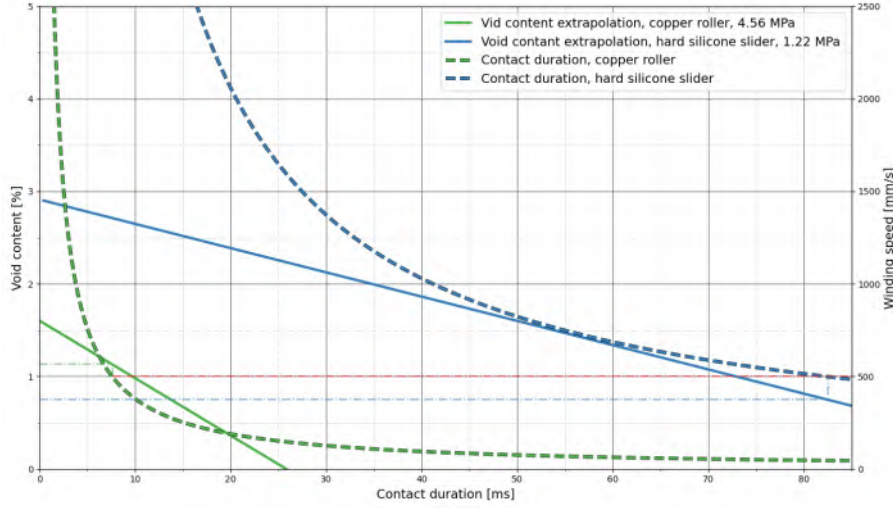


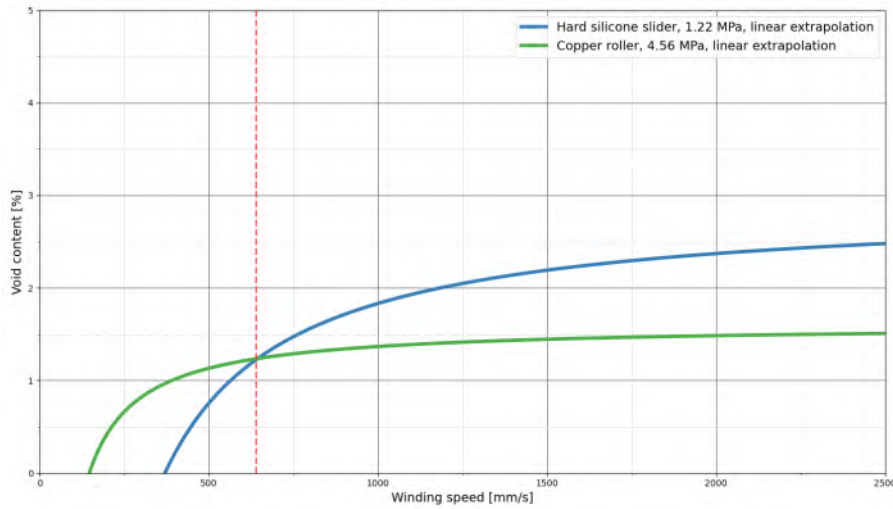
Figure 6.14: Laminate porosity plotted against the consolidation duration for Runs 1 through 6, with increasing average compaction pressure (up), and the slopes of the linear fitting laws, as plotted against their respective average compaction pressures.

By utilizing the rate of change of porosity with an increase in consolidation duration shown in the lower plot within Figure 6.14, and the single data point for the porosity of Run 11, it is possible to compare the expected performance of the slider at higher compaction pressures to that of the copper roller. Additionally, the contact duration can be related to the winding speed, since they are inversely proportional by a known value, namely the length of the imprint of the compaction slier. This comparison is presented in Figure 6.15a. Using this plot, it is possible to obtain the consolidation duration for a given compaction element at a given winding speed, and use that

consolidation duration to obtain the porosity of that compression element, given the specified compaction pressure. The added aid lines show that for a winding speed of 500 mm/s, the slider greatly outperforms the copper roller, while at a winding speed close to 1500 mm/s, the opposite is true. In fact, the copper roller will outperform the slider for any speed above 700 mm/s, as shown in Figure 6.15b.



(a) Expected winding speed-compaction length-porosity relationship for different compaction strategies, given a simplified linear behaviour



(b) Expected porosity-winding speed relationship, given a simplified linear behaviour

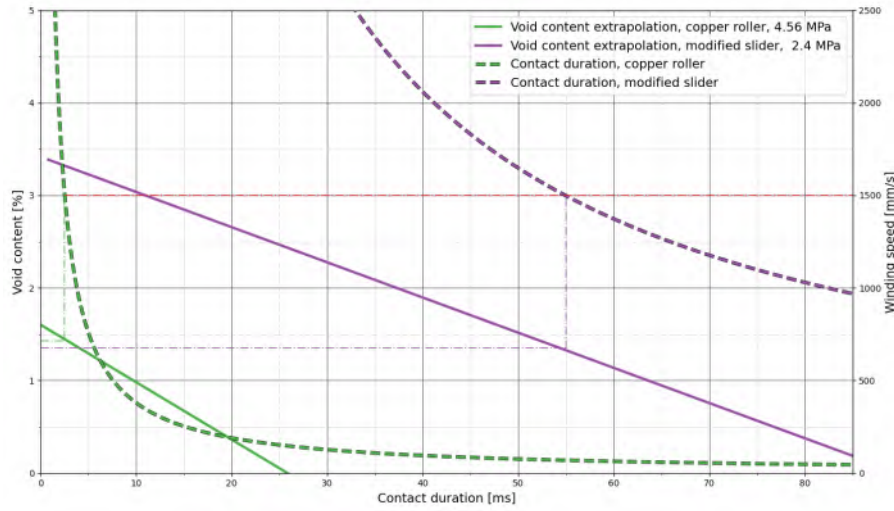
Figure 6.15: Comparison between the expected performance of a slider at 1.22 MPa average compaction pressure to that of the copper roller at 4.56 MPa for various winding speeds, given a simplified linear behaviour

Now, it is clear that performance improvements to the slider can aid in the achievement of competitive laminate porosities at high winding speeds. Two strategies emerge from pursuing this goal. Firstly, the slider compaction pressure can be increased. This has the advantage of lowering the porosity curve of the pressure element, while it also has the disadvantage of increasing its slope. Yet, increased loading could have further disadvantages regarding tape friction. This can be avoided by decreasing the width of the slider. The width used in this study was chosen as

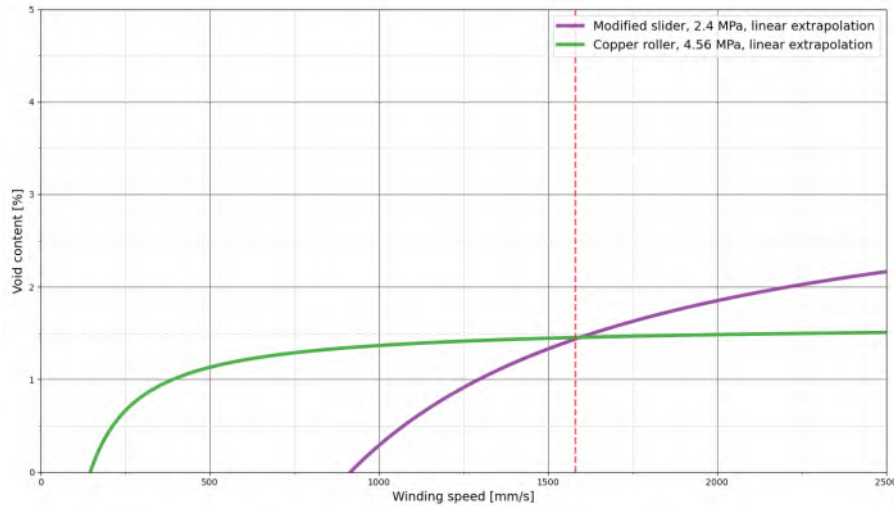
35 mm, but it was observed that the tape does not laterally travel more than half of its width of about 7 mm in either lateral direction. The second option is to modify the relationship between winding speed and consolidation duration, or, in other words, to shift the winding speed curve of the slider further to the right-hand side of the plot. This can be readily achieved by increasing the arclength of the slider.

In Section 5.3, it was established that the impact of compaction pressure on porosity follows a distinct trend. This relationship is shown in Figure 5.18 and illustrates a descending power law behaviour. In other words, at high compaction pressures, a small decrease in porosity would require a huge amount of additional compaction pressure. Thus, in the case of the rigid roller, which already yields 4.56 MPa average pressure at 1 bar of cylinder pressure, additional compaction pressure is not a feasible solution for void reduction, especially if the winding speed is increased, and in turn, the consolidation duration is reduced. Nevertheless, this power law can be utilized further to obtain the porosity provided by the slider at higher compaction pressures.

Figure 6.16 presents the expected performance of a theoretical slider measuring 70 mm arclength, or 80° arcspan, and developing 2.4 MPa of compaction pressure, as compared to the performance of the copper roller at 4.56 MPa. It is expected that such an area compaction element would be able to outperform a copper roller at winding speeds up to 1600 mm/s, and would yield porosities below 2% at speeds close to 1500 mm/s. Yet, increasing the arclength of the slider may increase the heat drain from the tape to the mandrel during compaction through prolonged conduction heat transfer, making the longer compaction length less effective. This may be counteracted by using higher mandrel temperatures far above T_g . More studies are needed to validate this approach of consolidation.



(a) Expected winding speed-compaction length-porosity relationship for different compaction strategies, given a simplified linear behaviour



(b) Expected porosity-winding speed relationship, given a simplified linear behaviour

Figure 6.16: Comparison between the expected performance of a slider at 2.4 MPa average compaction pressure and with an increased arclength of 70 mm to that of the copper roller at 4.56 MPa for various winding speeds, given a simplified linear behaviour

Increasing compaction pressure together with using the slider pressure element may also be beneficial for laminate surface quality. Figure 5.19a and Figure 5.19b show that by reaching compaction pressures of 1.2 MPa, both the mean value and variance in roughness and waviness can be diminished. Furthermore, given that the roughness and waviness achieved by the copper roller at 500 m/s were the lowest and most uniform out of all runs, it is believed that a quick consolidation period, specific to sliders at very high winding speed, would not prove problematic.

It is important to note that this analysis is very limited and is based on assumptions supported by a small data set. Additionally, no other impacts of increasing winding speeds are considered, such as influences on the heating profile of the tape within the heating zone. As the winding speed would increase, the tape would be subjected to a much higher heating gradient between the electrodes that delimitate the heating zone, and the impact of such a change on the porosity

of the laminate is currently unknown. Furthermore, the linear relationship between compaction duration and porosity is only based on the lack of multiple data points. Laminate consolidation during continuous layup is highly complex and involves many non-linear relationships, such as the change in matrix viscosity with temperature, the heat exchange between the melted tape and the steel mandrel, the electrical resistance changes with temperature within CFRP composites, and the squeeze flow of the fiber-matrix phase in melt form. Lastly, it is unknown if the entire compaction length of the presented pressure elements is actively consolidating the laminate, given that the mandrel acts as a significant heat sink and the tape may lose a great amount of heat through conduction as it is compacted. Nevertheless, this analysis can be used to make the case for the further study of area compaction elements, as they show great promise in high-speed tape winding settings.

6.4. Hypotheses evaluation

Now that all relevant findings were presented and interpreted, the initial hypotheses provided in Section 3.4 may be assessed, and their validity be discussed.

Hypothesis 1: The deconsolidation of tapes using CoR HeaT is expected to be highly dependent on moisture content, maximum tape temperature, and heating rate, while only the tape morphology is expected to be impacted by tape tension.

Indeed, moisture was closely correlated with void content within the deconsolidated tapes, with the soaked tape far exceeding the porosity of all deconsolidated samples studied. The oven-conditioned tape showed the lowest amount of void content, followed by the tape kept at ambient conditions. Oven-drying the tape also resulted in a very low variance in porosity among the samples taken at various steps in the heated length. Yet, the large amount of pores within the soaked tape was not found to contribute to lower surface roughness or waviness average values. Oven-drying the tape prior to deconsolidation was also found to result in the roughness distribution along the heating length being much more uniform, comparable to that of the pristine tape. Both heating rate and temperature greatly contributed to the total variance in porosity values. Increases in temperature and heating rate were found to have a negative impact on porosity. Tape tension did not have such a profound impact on porosity. Yet, an increase in tape tension was seen to result in slightly lower tape porosity.

It was found that not tension, but temperature had the largest impact on tape roughness. Tape tension was also found to have a minor, and surprisingly negative, impact on roughness. Yet, due to temperature inconsistencies, it is unclear if tension was the main factor as to why roughness increased. Nevertheless, it is evident that the heating rate did not affect roughness in a meaningful way. On the other hand, tape tension was critical for the waviness and width of the deconsolidated tape. The tape could be seen to wrinkle and reduce in width in the presence of a lack of tension. Heating rate could also be seen to play a role in these large-scale morphology changes, while the maximum reached temperature had little to no impact.

Hypothesis 2: The use of pressure elements with either high consolidation pressure or long consolidation times will have a major impact on preform porosity.

The compaction pressure was found to have a significant impact on preform porosity. Yet, the rate of improvement diminishes at high compaction pressures. Longer compaction lengths were also seen to have a beneficial impact on porosity. Further studies comparing increasing compaction lengths at similar pressures would be needed to estimate the rate of improvement in laminate quality. Yet, if used at low compaction pressures, such consolidation elements could not rival the

efficacy of alternatives with shorter compaction lengths used under high loading. Nevertheless, the best results, from the perspective of preform porosity, as well as surface roughness and surface waviness, were achieved using either long compaction lengths at moderate compaction pressure under a conformable area compactor, or very short compaction lengths at very high compaction pressure under a rigid roller.

Hypothesis 3: Conformable pressure elements with longer contact lengths would prove more effective in void closure than conformable pressure elements with shorter contact lengths and solid rollers, when used at high deposition speed.

The solid roller used in this study was able to outperform the conformable roller in value and consistency in all considered quality indicators, namely porosity, roughness, and waviness, irrespective of winding speed, with the exception of porosity variance at 200 mm/s. Nevertheless, a conformable area compactor was found to either match or outperform the best results obtained using the solid roller at comparable winding speeds. Based on observed trends, it was theorized that by strategically choosing optimal values for slider arclength, slider compaction area, and applied load, new area compacting elements have the potential to outperform solid pressure elements even at winding speeds approaching 1500 mm/s. This analysis does have significant limitations when extrapolating to higher winding speeds, so further experimental studies are needed.

Hypothesis 4: Increased tape tension will have a beneficial effect on lowering interlaminar porosity, as long as the tape is not damaged prior to deposition.

Although tape tension was seen to have a beneficial effect on deconsolidated tape roughness and waviness, its influence on the narrowing of deconsolidated tape could prove problematic if not considered when designing the layup path. Inconsistencies in tape width were shown to be able to cause gaps between tapes within a single layer, leading to voids, crumbling layers, propensity for delamination, and increased surface waviness and thickness variation. These effects could be identified to have caused the unexpected result of having porosity increase while increasing tape tension from 63 N to 103 N, even as compaction would increase as a result of higher tow tension.

Hypothesis 5: High mandrel temperatures are expected to aid in the dissipation of voids within lower laminate layers.

Although high tooling temperatures had a small positive impact on porosity consistency, no significant difference could be seen between the average porosity of runs conducted on different temperature mandrels. Moreover, the distribution of voids along the different laminas was not influenced by the significant increase in tool temperature. In turn, it is safe to assume that rising tooling temperature from 100 N to 200 N did not have a statistically meaningful impact on laminate porosity.

Chapter 7

Conclusion

The objective of this research was twofold. The first aim was to investigate the deconsolidation behaviour of UD CF-reinforced thermoplastic tape using CoRe HeaT and relate it to the laminate preform quality. To study this, static deconsolidation of CF-LMPAEK tapes was performed using resistive heating, while controlling the amount of pre-existing moisture within the tape, the maximum temperature reached during heating, the rate of heating, and the tape tension applied. The second research goal was to assess the influence of consolidation parameters, such as pressure element, applied pressure, consolidation duration, and tow tension, on the laminate quality of quasi-90° preform pipes manufactured using CoRe HeaT tape winding. A purpose-built tape winding machine was constructed in this sense, alongside custom pressure elements varying in geometry (roller and area compactor) and material (copper, hard silicone, and soft silicone). The quality of the deconsolidated tapes and pipe preforms was estimated using cross-sectional microscopy in combination with image processing evaluation methods. This allowed for quantifying volumetric void content, geometrical void distribution, surface roughness and waviness, tape width, and laminate thickness. In this chapter, a summary of key findings and restricting limitations related to each pre-established research question is provided. The chapter is closed with a brief discussion on the relevance of this research on high-speed tape winding using resistive heating methods.

R.Q.1 How does CoRe HeaT influence the deconsolidation behaviour of prepreg thermoplastic tape within the heating zone?

S.Q.1.1 How effective is preconditioning the tape against moisture buildup for achieving low porosity, waviness, and roughness after deconsolidation?

The reference pristine tape, which was not deconsolidated, had an average void content of 0.29%. The deconsolidated tape with the highest moisture content reached an average void content of 8.14%. The tape kept at ambient conditions scored 4.26%, while the oven-dried tape registered an average void content of 2.58%. It is thus clear that moisture content can greatly alter the porosity of deconsolidated tape. Oven pre-conditioning was able to bring a reduction close to 40% in void content as compared to no pre-conditioning. This increment in tape quality is significant and should be valued to lower laminate porosity during manufacturing.

A notable characteristic of the samples with high moisture content was that large pores would concentrate around resin-rich bands spanning portions of the tape width, as seen in Figure 6.1. It

is believed that these resin-rich regions are a direct consequence of the tape manufacturing process and act as regions prone to void nucleation created by the dissolved water molecules contained within the matrix. Similar to the observations made by [Slange et al.](#) and illustrated in Figure 2.4b on preform blanks [20], the buildup of water vapor in these boundary regions leads to localized increased porosity. Although these large pores were most prominent within the water-soaked tape, similar pores, albeit smaller in size, could be found in both the pre-conditioned and ambient-stored tapes. Consequently, it may be the case that improving the distribution of fibers across the prepreg tape and minimizing these matrix-rich bands prone to moisture buildup, in conjunction with oven pre-conditioning, would lead to further improvement in deconsolidated tape porosity.

Regarding surface waviness and roughness, there were no clear improvements brought by oven preconditioning the tape before deconsolidation.

S.Q.1.2. How does tape tension, heating rate, and tape temperature influence tape deconsolidation?

A signal-to-noise ratio analysis was performed in order to establish which of the three deconsolidation parameters was the most critical for the variance of porosity, roughness, waviness, and tape width among all deconsolidated samples. The results were further validated by one-to-one comparisons in which only one parameter was varied.

The most influential parameter on tape void content was maximum temperature, followed closely by the heating rate. A fifteen-fold increase in heating rate was shown to cause an increase of 65% in porosity, while a 20% increase in maximum temperature was correlated with a 45% increase in void content. It is believed that the heating rate increased the magnitude of temperature non-uniformities within the tape, which led to the observed increase in porosity. Tapes heated far above the melting point presented more significantly large pores as compared to the tapes heated to T_m . Tape tension showed a much lower impact on porosity, with a tenfold increase in tension resulting in a reduction of 25% in void content. Nevertheless, tape tension remains a method of reducing deconsolidated tape porosity.

Temperature was also the most influential factor regarding tape roughness. An increment of 20% in maximum average temperature was linked to a 7.5% increase in tape roughness. Although tension was determined as the second most influential factor, temperature differences between the samples made the one-to-one comparison unreliable, showing an increase of 5.7% in roughness for a ten-fold increase in tension. The heating rate was shown to have a negligible effect on tape roughness.

Tape tension was established to be the most influential parameter on large-scale morphological changes for deconsolidated tape. It was observed that a lack of tow tension allowed for global wrinkling of the tape, increasing waviness by 62%. This is thought to be caused by the release of internal stresses within the carbon fibers, introduced during manufacturing. In the presence of tow tension, the fibers would be further restricted in out-of-plane movement, and such large-scale shape changes would be impeded. On the other hand, an increase in tape tension from 10 N to 100 N led to a decrease in tape width by 6.4%. Because of this, it was concluded that high tow tension favors in-plane lateral movement of the fibers within the melted matrix phase, leading to tape narrowing. The heating rate was also found to have an influence on waviness and, to a lesser extent, on tape width, yielding an increase in waviness of 45% when excluding outliers, and an increase of 1.1%. The increase in waviness can be attributed to hot spots leading to localized void expansion and affecting the surface profile, as well as to deep marks caused by pore evacuation. To visualize the difference between the global and local large wavelength morphological changes caused by tape tension and heating rate, respectively, refer to Figure 6.3. Temperature was shown

to have a minor impact on waviness and no significant impact on tape width.

It is essential to specify one important limitation of these findings in regard to tape deconsolidation. For all runs, the tapes were heated statically, utilizing a single electrical pulse. Although the heating principle is the same as for CoRe HeaT during manufacturing, the pulsing profile would differ. Thus, the deconsolidation behaviour during winding will differ from the static deconsolidation response. Nevertheless, the trends in laminate quality are believed to resemble the ones discussed above. Yet, using the data presented here as input to model the dynamic process could prove divergent from the real-life outcomes.

R.Q.2. How can different consolidation strategies affect laminate quality (i.e., porosity, surface quality, fiber distribution) of tape-wound CF-LMPAEK preforms?

S.Q.2.1. How do different pressure elements (i.e. rigid, hard conformable, soft conformable) affect laminate quality?

The impact of compaction elements was categorized based on two indicators. Firstly, on their average compaction pressure, taken as the theoretical force output of the pneumatic actuator divided by their imprint area, evaluated using FujiFilm Prescale pressure-sensitive films. Secondly, the associated compaction duration is quantified as the measured imprint length divided by the winding speed. This allowed for the identification of three different compaction manners. The copper roller delivered 4.56 MPa during a compaction duration range of 7.6 ms to 19 ms, the silicone roller provided 0.94 MPa for in between 27.2 ms to 68 ms, and the silicone slider, essentially an area compactor, performing at 0.21 MPa for in between 83 ms to 207.5 ms. The ranges of compaction durations were taken as the winding speed was increased from 250 mm/s to 500 mm/s, with the latter representing the upper range used for commercial tape winding processes.

It was found that increasing winding speed, and thus decreasing compaction duration, increased the porosity of all laminates, irrespective of the pressure element used. More specifically, rising the winding speed from 250 mm/s to 500 mm/s led to an increase in void content by 64%, 71%, and 163% for the laminates wound using the slider, silicone roller, and copper roller, respectively. Moreover, the rate of porosity increase with a decrease in compaction duration was found to be linearly proportional to the compaction pressure, as illustrated by Figure 6.14. In other words, the relative increase in porosity caused by an increase in winding speed would be more pronounced when using a non-conformable pressure element as compared to a highly-conformable one.

The rigid roller provided the most pore-free laminates at both winding speed settings, with 0.43% and 1.13% void content. It was followed by the silicone roller, with 1.48% and 2.53%, and the slider, with 2.97% and 4.87%. Yet, increasing the compaction pressure of the slider to 1.22 MPa yielded a laminate porosity of 0.75% when winding at 500 mm/s, surpassing the performance of the copper roller. Furthermore, a linear analysis based on the trends seen within this data set estimated that the slider used at 1.22 MPa will outperform the copper roller developing 4.56 MPa for any winding speed lower than 700 mm/s, if the same heating profile is maintained. The outcome of this analysis can be visualized in Figure 6.15. By further extrapolating the performance of a slightly larger slider at 2.4 MPa based on the observed power law trend between laminate porosity and compaction pressure, it was estimated that the copper roller would be further outperformed until a winding speed of 1600 mm/s is reached, as seen in Figure 6.16. Yet, this is based only on extrapolating statistical trends seen in a limited data set and should be validated by further studies. Nevertheless, it shows the potential of using area compactors to achieve low laminate void content at high winding speeds. Nevertheless, the 0.75% porosity reached using the slider at the highest level of compaction pressure exemplifies quality on par with in-situ consolidation in AFP

processes for aerospace applications.

Increasing winding speed could be seen to have a positive influence on both the roughness and waviness of the laminates consolidated using the slider and copper roller, while the opposite was seen in the case of the silicone roller. In fact, major layer crumbling and surface imprinting could be seen when using the silicone roller. The imprinting could be connected to the surface roughness of the roller itself, which is the consequence of the silicone casting mold being 3D printed. This effect was avoided when using the silicone slider by using a smooth Teflon membrane fixed to the surface of the pressure element. Stepwise imprints 7000 μm wide could be identified on the surface of the copper roller consolidated laminate. It is thought of as an artefact of the non-uniformity of the widthwise pressure profile created by the rigid roller, which was validated using the FujiFilm Prescale pressure films. This effect accounted for a large part of the roughness and waviness of these specimens. Nevertheless, the lowest waviness and roughness values were encountered when using the copper roller at 500 mm/s, namely 9.50 μm and 2.27 μm , respectively. Thus, it is believed that a more calibrated construction of the copper roller deposition head would be able to provide an excellent surface finish. Other methods for improving the laminate surface finish for all pressure elements would involve making sure the pressure element surface is extremely smooth and improving the deposition accuracy of the winding machine to minimize gaps that lead to layer crumbling.

S.Q.2.2. What is the relationship between applied consolidation pressure, tape tension, and laminate quality?

The impact of compaction pressure was evaluated using the slider pressure element, since imprint testing showed that their compaction length would not vary by a significant amount when actuator loading is increased, meaning that their consolidating duration could be assumed to remain constant. Three levels of average compaction pressure were considered, namely 0.21 MPa, 0.63 MPa and 1.22 MPa. All laminates were made using 500 mm/s winding speed.

The interaction between laminate porosity and compaction pressure was found to be best described by a power law fitting. The void contents obtained for the aforementioned increasing levels of pressure were 4.74%, 1.29%, and 0.75%. Yet, it was found that a large amount of the porosity, roughly 40%, for the lowest level of pressure came from delaminations caused by a drop in voltage, and in turn, underheating within the first two layers. Nevertheless, the power law fitting is still applicable to the data if all large delaminations are excluded from the porosity data. This would indicate that the rate of porosity reduction would gradually decrease with an increase in applied compaction pressure. And considering the difficulty of increasing machine stiffness in order to maintain deposition accuracy in the case of higher compaction loading, it can be assumed that drastically increasing compaction pressure to lower laminate porosity for high-speed applications can be seen as a consolidating strategy with diminishing returns.

Another positive effect of increased compaction pressure can be seen in the distribution of voids across the thickness of the laminate. It was shown that an increase in pressure lowers the rate of porosity increase with laminate thickness within the laminas themselves. In turn, the increase in void content is influenced more by the interlaminar and less by the intralaminar regions, yielding a more stepped cumulative pore distribution as seen in Figure 6.12a.

Increasing compaction pressure was also shown to decrease both roughness and waviness, as long as gap sizes are maintained to a minimum. Otherwise, layer crumbling can be observed for lower compaction pressures, as is the case for the increase in waviness from 26.00 μm to 33.44 μm for an increase in pressure from 0.22 MPa to 0.63 MPa. Nevertheless, an increase from 0.22 MPa to 1.22 MPa yielded a decrease in roughness by 51% and in waviness by 47%.

It is important to note that the compaction pressures used for this study are determined using the theoretical pneumatic actuator extension load, evaluated based on cylinder cross-sectional area derived from the data sheet of the actuator and applied cylinder pressure. Thus, the friction that may arise within the pneumatic cylinder, which may prove significant if the pneumatic pressure is low, was not taken into account. Furthermore, the compaction pressure was evaluated based on the imprint of the consolidation element directly on the Prescale films. Thus, the amounts of compaction pressures provided are to be taken as orientative and not specifically descriptive of the pressure experienced by the tape. Nevertheless, the compaction conditions were preserved across these experimental trials, so the results of the comparison and emerging trends may be considered apt.

The void content was also seen to decrease, from 4.74% to 1.29%, for an increase in tape tension from 27.50 N to 63.05 N. This was expected, as an increase in tow tension would lead to an increase in the compaction pressure applied by the tape itself on the substrate. Yet, increasing the tape tension further to 103.45 N yielded a slight increase in void content, reaching 2.07%. This unforeseen result was attributed to insufficient gap-filling and compounded layup errors due to layer crumbling. This could be seen in the cumulative pore distribution, as large increments were noticed at interlaminar regions and within the last layer. These effects were further validated by visual inspection of representative samples. The gap distance was also seen to increase within the laminate wound using the highest amount of tow tension. This was related to the narrowing effect of excessive tow tension on deconsolidated tapes.

The laminate roughness was seen to reduce by slight increments with an increase in tape tension, from 4.59 μm , to 4.47 μm and 3.90 μm . On the other hand, the waviness was seen to slightly decrease, from 26.00 μm to 25.78 μm , and then increase to 33.64 μm . This was attributed to layer crumbling and thus exacerbated outer lamina tortuosity. It is thus clear that if not taken into account when designing the layup path, tape narrowing could lead to significant losses in laminate quality, both in porosity and in surface waviness.

R.Q.3. What is the influence of heated tooling on preform quality?

Two trials were conducted to determine the influence of tooling temperature, below the T_g of the LMPAEEK matrix, at roughly 100 °C, and above T_g , at roughly 200 °C. No significant impact could be seen on laminate porosity, which registered 2.53% and 2.64%, respectively. No influence could be seen on the distribution of pores across laminate thickness either. It was then concluded that repasses of the pressure element during the deposition of subsequent layers were not effective, even if the laminate is believed to have been kept at temperatures above T_g , in the absence of a heat sink measuring a subpar temperature. On the other hand, slight improvements in laminate roughness, of 18%, and waviness, of 17%.

The relevancy of the findings presented in this study is demonstrated by their potential to bring further improvements for high-speed tape winding using CoRe HeaT. The deconsolidation data show that heat pre-treatment of CF-LMPAEEK prepreg tape leads to significant improvements in deconsolidated tape porosity, which would further aid the consolidation process in void closure, even more so in the case of high-speed processes, where consolidation duration is limited. The narrowing tendency of the deconsolidated tape based on applied tension would help configure the lay-up path in order to minimize gaps, which would decrease laminate porosity and surface waviness. The deeper understanding of the consolidation process obtained from the preform experiments will aid in the development of better, more effective consolidation strategies and pressure elements. Given the great performance of the silicone area compactor, as well as the trends observed, better optimized sliders may be designed in order to further increase in-situ consolidation quality. These innovative strategies will prove critical in the development of high-speed tape

winding processes, leveraging the capabilities of CoRe HeaT. A better in-situ consolidation would require a shorter post-consolidation, would increase production output, and ultimately would make thermoplastic composites more attractive for producers and designers. And considering that previous production runs required an hour of shrinktape post-treatment to reach a laminate quality comparable to the one achieved in this study within minutes of winding, it is fair to say that the rate of progress shows great promise for this manufacturing technology.

Recommendations

Useful insights on resistive heating tape deconsolidation and on laminate consolidation in high-speed tape winding settings could be extracted from the work presented in this study. Yet, limitations in scope and time leave multiple interesting research avenues open. Furthermore, this study may be used as a foundation for other research aimed at improving high-speed thermoplastic winding processes using CoRe HeaT. In this chapter, some recommendations are provided for further work on the topics tackled in this paper.

Nip point temperature influence

It has been mentioned before in Section 6.3 that nip point tape temperature could not have been accurately controlled or monitored. This is partly a consequence of the novelty and low technology readiness level of CoRe HeaT, and partly caused by spatial limitations in the current iteration of the deposition head and winding machine. Yet, it has been shown in the deconsolidation study and by the literature that nip point temperature is an important parameter that influences porosity and surface finish. Moreover, having capable temperature monitoring and control would aid in the understanding of consolidation mechanisms at play during winding. Hence, it is strongly recommended that further studies develop the CoRe HeaT module and the winding setup further in order to analyze the effect of temperature on laminate quality.

Gap minimization

Increased gap size has been shown to cause layer crumbling and insufficient gap filling across multiple samples covered by this study. In turn, such layup inaccuracies cause porosity and increased surface waviness, negatively affecting laminate performance. It is recommended that further work pay attention to improving machine deposition accuracy in order to further improve laminate quality and isolate the impact of the investigated parameters. This may be achieved by utilizing controlled servo motors for setting deposition winding angle, instead of pneumatic actuation, as well as further investigating the tape narrowing behaviour of deconsolidated tape under tension. Ideally, predicting tape width based on process parameters and improving layup paths by increasing machine accuracy should work synergistically for the achievement of minimizing gaps.

Pressure element optimization

The laminate consolidated using the sliding area compactor element at the highest level of applied pressure was shown to yield the lowest porosity and very low amounts of surface roughness and waviness. The dimensions of the slider were arbitrarily chosen in order to have a wide selection of compaction characteristics across the used pressure elements. Yet, it was hypothesized that strategic choices in slider construction and application could deliver quality competitive laminates even at winding speeds above 500 mm/s. Such choices include increasing slider arclength, decreasing slider width, and increasing compaction load. Furthermore, investigating different adhesives, silicones, supporting materials, and manufacturing methods could have a beneficial influence on slider performance and longevity. Consequently, it is recommended that future studies tackle the optimization of area compactor geometry, construction, materials, and application. It is believed that such optimization efforts are bound to bring significant performance quality improvements.

Process and post-process refinement

One driving force for increasing in-situ consolidation performance was to effectively reduce the required time for post-consolidation, thus decreasing manufacturing time. However, conducting post-consolidation on the enhanced preforms realized in this research was deemed out of the scope of the study due to time restrictions. It is therefore recommended that the required post-consolidation times and parameters be further investigated in processing the preforms produced using the insights derived from this study. Mechanical testing, as well as crystallinity evaluation, are some recommended means of determining the impact of a better in-situ consolidation, and conversely a less extensive post-consolidation, on final product quality. Furthermore, it is advised to investigate the resulting part quality and throughput time for higher winding speeds.

Bibliography

- [1] Blumenfeld, L., *FAST (Flight Airworthiness Support Technology)*, Airbus, 2013. URL https://aircraft.airbus.com/sites/g/files/jlcbta126/files/2022-04/FAST_specialA350.pdf.
- [2] CW editorial team, “Thermoplastic composites gain leading edge on the A380,” , Jan 2006. URL <https://www.compositesworld.com/articles/thermoplastic-composites-gain-leading-edge-on-the-a380>.
- [3] CW editorial team, “Thermoplastic primary aerostructures take another step forward,” , Jun 2019. URL <https://www.compositesworld.com/articles/thermoplastic-primary-aerostructures-take-another-step-forward>.
- [4] Clean Aviation, “Multi functional fuselage demonstrator,” , 2025. URL <https://www.clean-aviation.eu/multi-functional-fuselage-demonstrator>.
- [5] Ozturk, F., Cobanoglu, M., and Ece, R. E., “Recent advancements in thermoplastic composite materials in aerospace industry,” *Journal of Thermoplastic Composite Materials*, Vol. 37, No. 9, 2023, p. 3084–3116. doi:10.1177/08927057231222820.
- [6] van de Schoot, R., de Bruin, J., Schram, R., Zahedi, P., de Boer, J., Weijdem, F., Kramer, B., Huijts, M., Hoogerwerf, M., Ferdinands, G., and et al., “An open source machine learning framework for efficient and transparent systematic reviews,” *Nature Machine Intelligence*, Vol. 3, No. 2, 2021, p. 125–133. doi:10.1038/s42256-020-00287-7.
- [7] Baekeland, L. H., “Method of making insoluble products of phenol and formaldehyde,” , U.S. Patent 383,684, December 1909, month=Dec.
- [8] Mumford, J. K., *The story of Bakelite, by John Kimberly Mumford*, Robert L. Stillson Company, 1924.
- [9] Myhra, D., *The horten brothers and their all-wing aircraft*, Schiffer Publishing, Ltd, 1998.
- [10] Ebnesajjad, S., *Handbook of Adhesives and surface preparation: Technology, applications and manufacturing*, William Andrew/Elsevier, 2011.
- [11] Castan, P., “Process of preparing synthetic resins,” , U.S. Patent 431,157, July 1943.
- [12] Nemessanyi, C., “Brief history of fiber reinforced polymers as structural material,” *Periodica Polytechnica Architecture*, Vol. 54, No. 3, 2023, p. 193–206. doi:10.3311/ppar.23291.

- [13] American Chemical Society, Sep 2003. URL <https://www.acs.org/education/whatischemistry/landmarks/carbonfibers.html#pan-based-carbon-fibers>.
- [14] Chang, C., Geng, H. B., Feng, Y., Han, Z. Y., and Sun, S. Z., “Effect of filament winding process parameters on interlaminar performance for CF/PP Thermoplastic Composite,” *Journal of Physics: Conference Series*, Vol. 2353, No. 1, 2022, p. 012008. doi:10.1088/1742-6596/2353/1/012008.
- [15] Gierulski, M. P., Tomlinson, R., and Troughton, M., “Electrofusion welding and reinforced thermoplastic pipes – a review,” *Journal of Reinforced Plastics and Composites*, Vol. 41, No. 3–4, 2021, p. 147–163. doi:10.1177/07316844211051207.
- [16] Sorrentino, L., Anamateros, E., Bellini, C., Carrino, L., Corcione, G., Leone, A., and Paris, G., “Robotic filament winding: An innovative technology to manufacture complex shape structural parts,” *Composite Structures*, Vol. 220, 2019, p. 699–707. doi:10.1016/j.compstruct.2019.04.055.
- [17] Boon, Y. D., Joshi, S. C., and Bhudolia, S. K., “Review: Filament winding and automated fiber placement with in situ consolidation for fiber reinforced thermoplastic polymer composites,” *Polymers*, Vol. 13, No. 12, 2021, p. 1951. doi:10.3390/polym13121951.
- [18] Morgan, S., “UK’s first open-access, fibre-reinforced, thermoplastic tape capability,” , Jun 2025. URL <https://www.iom3.org/resource/amrc-announces-open-access-fibre-reinforced-thermoplastic-tape-development.html>.
- [19] Çelik, O., Choudhary, A., Peeters, D., Teuwen, J., and Dransfeld, C., “Deconsolidation of thermoplastic prepreg tapes during rapid laser heating,” *Composites Part A: Applied Science and Manufacturing*, Vol. 149, 2021, p. 106575. doi:10.1016/j.compositesa.2021.106575.
- [20] Slange, T., Warnet, L., Grouve, W., and Akkerman, R., “Deconsolidation of C/peek blanks: On the role of prepreg, Blank Manufacturing Method and Conditioning,” *Composites Part A: Applied Science and Manufacturing*, Vol. 113, 2018, p. 189–199. doi:10.1016/j.compositesa.2018.06.034.
- [21] Khan, M. A., Mitschang, P., and Schledjewski, R., “Tracing the void content development and identification of its effecting parameters during in situ consolidation of thermoplastic tape material,” *Polymers and Polymer Composites*, Vol. 18, No. 1, 2010, p. 1–15. doi:10.1177/096739111001800101.
- [22] Çelik, O., Bussink, T., Peeters, D., Teuwen, J., and Dransfeld, C., “The effect of laser-induced deconsolidation on the compaction behavior of thermoplastic composite tapes,” *Composites Part A: Applied Science and Manufacturing*, Vol. 151, 2021, p. 106670. doi:10.1016/j.compositesa.2021.106670.
- [23] Bonmatin, M., Chabert, F., Bernhart, G., and Djilali, T., “Rheological and crystallization behaviors of low processing temperature poly(aryl ether ketone),” *Journal of Applied Polymer Science*, Vol. 138, No. 47, 2021. doi:10.1002/app.51402.
- [24] Gaitanelis, D., Worrall, C., and Kazilas, M., “Detecting, characterising and assessing peek’s and CF-peek’s thermal degradation in rapid high-temperature processing,” *Polymer Degradation and Stability*, Vol. 204, 2022, p. 110096. doi:10.1016/j.polymdegradstab.2022.110096.
- [25] Donough, M. J., Shafaq, St John, N. A., Philips, A. W., and Gangadhara Prusty, B., “Process modelling of in-situ consolidated thermoplastic composite by Automated Fibre Placement – A Review,” *Composites Part A: Applied Science and Manufacturing*, Vol. 163, 2022, p. 107179. doi:10.1016/j.compositesa.2022.107179.

- [26] Dara, P. H., and Loos, A. C., *Thermoplastic matrix composite processing model*, Virginia Polytech Institution and State University: Blacksburg, 1985.
- [27] Lee, W. I., and Springer, G. S., “A model of the manufacturing process of Thermoplastic Matrix Composites,” *Journal of Composite Materials*, Vol. 21, No. 11, 1987, p. 1017–1055. doi:10.1177/002199838702101103.
- [28] Schaefer, P., Guglhoer, T., Sause, M., and Drechsler, K., “Development of intimate contact during processing of carbon fiber reinforced polyamide-6 tapes,” *Journal of Reinforced Plastics and Composites*, Vol. 36, No. 8, 2017, p. 593–607. doi:10.1177/0731684416687041.
- [29] Yang, F., and Pitchumani, R., “A fractal Cantor set based description of Interlaminar contact evolution during thermoplastic composites processing,” *Journal of Materials Science*, Vol. 36, No. 19, 2001, p. 4661–4671. doi:10.1023/a:1017950215945.
- [30] Kirchhoff, J., Ghattas, O., and Tehrani, M., “Resin percolation and intimate contact in fast processing of Thermoplastic Composites,” *Composites Part A: Applied Science and Manufacturing*, Vol. 182, 2024, p. 108145. doi:10.1016/j.compositesa.2024.108145.
- [31] Zhao, D., Liu, W., Chen, J., Yue, G., Song, Q., and Yang, Y., “Interlaminar bonding of high-performance thermoplastic composites during automated fiber placement in-situ consolidation,” *Journal of Composite Materials*, Vol. 58, No. 20, 2024, p. 2247–2261. doi:10.1177/00219983241263808.
- [32] Khan, M. A., “Experimental and simulative description of the thermoplastic tape placement process with online consolidation,” Ph.D. thesis, Kaiserslautern Technical University, 2010.
- [33] Zhao, D., Chen, J., Zhang, H., Liu, W., Yue, G., and Pan, L., “Effects of processing parameters on the performance of carbon fiber reinforced polyphenylene sulfide laminates manufactured by laser-assisted automated fiber placement,” *Journal of Composite Materials*, Vol. 56, No. 3, 2021, p. 427–439. doi:10.1177/00219983211055827.
- [34] Heathman, N., Koirala, P., Yap, T., Emami, A., and Tehrani, M., “In situ consolidation of Carbon Fiber Paek via laser-assisted automated fiber placement,” *Composites Part B: Engineering*, Vol. 249, 2023, p. 110405. doi:10.1016/j.compositesb.2022.110405.
- [35] Lamontia, M., Guber, M., Waibel, B., and Hulcher, A., “Conformable compaction system used in Automated Fiber Placement of large composite aerospace structures,” 2002.
- [36] de Gennes, P. G., “Reptation of a polymer chain in the presence of fixed obstacles,” *Simple Views on Condensed Matter*, 2003, p. 149–157. doi:10.1142/9789812564849_0015.
- [37] Stokes-Griffin, C., and Compston, P., “Investigation of sub-melt temperature bonding of carbon-fibre/peek in an automated laser tape placement process,” *Composites Part A: Applied Science and Manufacturing*, Vol. 84, 2016, p. 17–25. doi:10.1016/j.compositesa.2015.12.019.
- [38] Barnes, J., and Cogswell, F., “Transverse flow processes in continuous fibre-reinforced thermoplastic composites,” *Composites*, Vol. 20, No. 1, 1989, p. 38–42. doi:10.1016/0010-4361(89)90680-0.
- [39] Shuler, S., and Advani, S., “Transverse squeeze flow of concentrated aligned fibers in viscous fluids,” *Journal of Non-Newtonian Fluid Mechanics*, Vol. 65, No. 1, 1996, p. 47–74. doi:10.1016/0377-0257(96)01440-1.
- [40] Kok, T., “On the consolidation quality in laser asisted fiber placement,” Ph.D. thesis, Twente University, 2018.
- [41] Fereidouni, M., and Hoa, S. V., “Transverse squeeze flow of thermoplastic composite tape during in-situ consolidation via Automated Fiber Placement,” *Composites Part A: Applied Science and Manufacturing*, Vol. 188, 2025, p. 108519. doi:10.1016/j.compositesa.2024.108519.

- [42] Heinecke, F., and Willberg, C., “Manufacturing-induced imperfections in composite parts manufactured via automated fiber placement,” *Journal of Composites Science*, Vol. 3, No. 2, 2019, p. 56. doi:10.3390/jcs3020056.
- [43] Sawicki, A., and Minguett, P., “The effect of intraply overlaps and gaps upon the compression strength of composite laminates,” *39th AIAA/ASME/ASCE/AHS/ASC Structures, Structural Dynamics, and Materials Conference and Exhibit*, 1998. doi:10.2514/6.1998-1786.
- [44] Agarwal, S., “Width deformation of thermoplastic prepreg tapes during in-situ Automated Fiber Placement,” Master’s thesis, Delft University of Technology, 2023.
- [45] Nguyen, M. H., Davidson, P., and Waas, A. M., “Experimental and numerical study on the tensile failure behavior of toughened-interlayer composite laminates with automated fiber placement (AFP) induced gap and overlap defects,” *International Journal of Material Forming*, Vol. 14, No. 1, 2020, p. 105–119. doi:10.1007/s12289-020-01581-w.
- [46] Stokes-Griffin, C., and Compston, P., “A combined optical-thermal model for near-infrared laser heating of thermoplastic composites in an automated tape placement process,” *Composites Part A: Applied Science and Manufacturing*, Vol. 75, 2015, p. 104–115. doi:10.1016/j.compositesa.2014.08.006.
- [47] Dong, N., Luan, C., Yao, X., Ding, Z., Ji, Y., Niu, C., Zheng, Y., Xu, Y., and Fu, J., “Influence of process parameters on the interlaminar shear strength of CF/Pek Composites in-situ consolidated by laser-assisted automated fiber placement,” *Composites Science and Technology*, Vol. 258, 2024, p. 110902. doi:10.1016/j.compscitech.2024.110902.
- [48] Shadmehri, F., Hoa, S. V., Fortin-Simpson, J., and Ghayoor, H., “Effect of in situ treatment on the quality of flat thermoplastic composite plates made by automated fiber placement (AFP),” *Advanced Manufacturing: Polymer amp; Composites Science*, Vol. 4, No. 2, 2018, p. 41–47. doi:10.1080/20550340.2018.1444535.
- [49] Grohmann, Y., and Stüve, J., “High speed tape placement with CoRe HeaT,” *5th International Conference and Exhibition on Thermoplastic Composites, Bremen, Germany*, 2020. URL <https://elib.dlr.de/137338/>.
- [50] v. Heusinger, J., Grohmann, Y., and Stefaniak, D., “A study on Automated Fiber Placement of CF-LM-PAEK using Direct Electrical Resistance Heating,” *Proceedings of the 21st European Conference on Composite Materials (ECCM21)*, , No. 21, 2024, pp. 518–523. doi:10.60691/yj56-np80, nanes, France.
- [51] von Heusinger, J., and Grohmann, Y., “Einflüsse der direkten Widerstandserwärmung von Carbonfaser-Halbzeugen auf die mechanischen Kennwerte des Laminats bei Einsatz des Automated-Fiber-Placement-Verfahrens,” Tech. rep., Technische Universität Dresden, November 2022. URL <https://elib.dlr.de/200629/>.
- [52] von Heusinger, J., Grohmann, Y., and Khan, S., “Methods for the post-consolidation of high-speed-wound thermoplastic CFRP tubes,” *21st European Conference on Composite Materials*, Vol. 5, 2024, pp. 698–705. doi:https://doi.org/10.60691/yj56-np80.
- [53] Khan, S., “Analyzing process parameters and their effects on the part quality for the production of thermoplastic CFRP tubes,” Master’s thesis, PFH- Private University of Applied Sciences, 2024.
- [54] International Organization for Standardization, “4287–Geometrical product specifications (GPS)–Surface texture: profile method–terms, definitions and surface texture parameters,” *International Organization for Standardization: Geneva, Switzerland*, 1997.
- [55] Naumann, J., “Robust Detection and Explanation of Cracks in Microscopic Images,” Master’s thesis, Technische Universität Braunschweig, 2024.

-
- [56] Johnson, K. L., *Normal contact of elastic solids - Hertz theory*, Cambridge Univ. Press, 2003, p. 90–104.

Appendix A

Appendix A

This appendix contains the technical data sheet of the used prepreg UD tape, as provided by the manufacturer.

PRODUCT DATA SHEET

DESCRIPTION

Toray Cetex® TC1225 is a high-end thermoplastic composite material, utilizing a semi-crystalline low-melt PAEK resin with excellent mechanical performance. The distinctive value of Toray Cetex® TC1225, over other composites with a PAEK family matrix, is its superior processability, and excellent VBO (Vacuum Bag Only) performance, due to a low-melt viscosity and reduction in processing temperature of up to 60°C (140°F)*. Toray Cetex® TC1225 doesn't only yield a high-quality product used in ATL/AFP processes, it also speeds up cycle times enabling cost-efficient production in all available formats.

Additionally, Toray Cetex® TC1225 is an ideal composite to be overmolded with neat or short fiber reinforced PEEK resin, creating a very strong bond. Overmolding, integrating continuous fiber reinforced composites in an injection molding process, combines the strength of high-end composites with the design freedom and complexity of injection molding parts.

Toray Cetex® TC1225 is available as a UD tape, a fabric prepreg, and as reinforced thermoplastic laminates (RTLs) of varying thicknesses. RTLs can be equipped with lightning strike protection, and carbon reinforced RTLs can be supplied with a thin glass top layer to protect a partly metallic assembly against galvanic corrosion. Glass scrim is also applicable in structures made from UD tape.

*Standard PEEK processes at temperatures up to 400°C (752°F)

FEATURES

- ▶ **Resin rich surface for superior processability and suitability for wide range of thermoplastic product methods: Press Consolidation, Stamp Forming, ATL, AFP, Continuous Compression Molding, Out-of-Autoclave VBO, Autoclave, Welding, and Overmolding**
- ▶ **Excellent VBO performance**
- ▶ **Form freedom—suited for overmolding with neat or short fiber reinforced PEEK**
- ▶ **Relatively low processing temperature enables shorter cycle times and less energy consumption**
- ▶ **Excellent mechanical performance, also at elevated temperatures**
- ▶ **Excellent toughness—demonstrated by high compression after impact strengths and fracture toughness values**
- ▶ **Very low moisture absorption (high hot/wet property retention)**
- ▶ **Outstanding chemical and solvent resistance**
- ▶ **Indefinite shelf life at ambient temperature storage**
- ▶ **Excellent FST performance**
- ▶ **Recyclability**

PRODUCT TYPE

LMPAEK™ (Low-Melt PolyArylEtherKetone)
Thermoplastic Resin System

TYPICAL APPLICATIONS

- ▶ Primary and secondary aircraft structures
- ▶ High-load aircraft interiors applications
- ▶ Access panels, rib stiffeners, brackets
- ▶ Radome
- ▶ Medical
- ▶ Oil and gas

TYPICAL NEAT RESIN PROPERTIES

Density (specific gravity)	1.30 g/cm ³ (81.2 lb/ft ³)
T _g (glass transition)	147°C (297°F)
T _m (melt)	305°C (581°F)
T _c (crystallinity)	263°C (505°F)
T _p (processing)	340–385°C (644–725°F)

SHELF LIFE

Out Life:	Indefinite at ambient temperature storage
Frozen Storage Life:	Not applicable—product does not require freezing



Contact us for more information:

North America/Asia/Pacific

e explore@toraytac-usa.com

t +1 408 465 8500

Europe/Middle East/Africa

e explore@toraytac-europe.com

t +31 (0) 548 633 933

Cetex®

TORAY_CETEX_TC1225_PDS_v8_2025-02-19

Page 1/9

PRODUCT DATA SHEET

PHYSICAL PROPERTIES—CARBON

Property	TC1225 T700GC Standard Modulus Carbon UD Tape	TC1225 T1100GC Intermediate Modulus Carbon UD Tape	5 Harness Satin (T300JB Carbon Woven Prepreg)
Fiber areal weight (FAW)	145 g/m ² (4.28 oz/yd ²)	145 g/m ² (4.28 oz/yd ²)	280 g/m ² (8.29 oz/yd ²)
Prepreg areal weight (PPAW)	221 g/m ² (6.52 oz/yd ²)	221 g/m ² (6.52 oz/yd ²)	479 g/m ² (14.42 oz/yd ²)
Resin content by weight (RC)	34%	34%	42%
Consolidated ply thickness (CPT)	0.14 mm (0.0054 in.)	0.135 mm (0.0053 in.)	0.31 mm (0.0122 in.)
Density	1.59 g/cm ³ (99.3 lb/ft ³)	1.59 g/cm ³ (99.3 lb/ft ³)	1.53 g/cm ³ (95.51 lb/ft ³)

These reinforcements are available as rolls of semi-prep or as RTLs. Lightning-strike protection layers can be incorporated into RTLs. A glass scrim can also be added to the surface of carbon fiber based laminates. This glass scrim is often used to protect against galvanic corrosion in assemblies where carbon fiber composites are in contact with metal components.

PHYSICAL PROPERTIES—GLASS (STRUCTURAL USE)

Property	US Style 7781 8 Harness Satin (EC6 Glass Woven Prepreg)	US Style 6781 8 Harness Satin (S2 C9 Glass Woven Prepreg)
Fiber areal weight (FAW)	296 g/m ² (8.73 oz/yd ²)	298 g/m ² (8.79 oz/yd ²)
Weight per ply (PAW)	448 g/m ² (13.21 oz/yd ²)	452 g/m ² (13.33 oz/yd ²)
Resin content by weight (RC)	34%	34%
Consolidated ply thickness (CPT)	0.24 mm (0.009 in.)	0.24 mm (0.009 in.)
Density	1.92 g/cm ³ (119.8 lbs/ft ³)	1.87 g/cm ³ (116.7 lbs/ft ³)

The reinforcements above are available as rolls of semi-prep or as RTLs. RTLs can consist of glass plies only or can incorporate UD carbon tapes or woven carbon tapes as required.

PHYSICAL PROPERTIES—GLASS SCRIM

Property	US Style 0120 4 Harness Satin (EC5 Glass Woven Prepreg)	US Style 1080 Plain Weave (EC5 Glass Woven Prepreg)
Fiber areal weight (FAW)	105 g/m ² (3.10 oz/yd ²)	48 g/m ² (1.42 oz/yd ²)
Weight per ply (PAW)	210 g/m ² (6.19 oz/yd ²)	120 g/m ² (3.54 oz/yd ²)
Resin content by weight (RC)	50%	60%
Consolidated ply thickness (CPT)	0.12 mm (0.005 in.)	0.08 mm (0.003 in.)
Density	1.71 g/cm ³ (106.8 lbs/ft ³)	1.61 g/cm ³ (100.5 lbs/ft ³)

The reinforcements above are available as rolls of semi-prep or can be added to the surface of RTLs of carbon UD tape or carbon woven fabric to act as a barrier to prevent galvanic corrosion.

PRODUCT DATA SHEET

MECHANICAL PROPERTIES

T700GC Standard Modulus Carbon 145gsm UD Tape 34% RC				
Property	Condition	Test Method	Results	
Tensile Strength 0°	RTA	ASTM D 3039	2410 MPa	350 ksi
Tensile Modulus 0°	RTA	ASTM D 3039	135 GPa	19.5 Msi
Tensile Strength 90°	RTA	ASTM D 3039	86 MPa	12.5 ksi
Tensile Modulus 90°	RTA	ASTM D 3039	10 GPa	1.4 Msi
Compression Strength 0°	RTA	ASTM D 6641	1300 MPa	189 ksi
Compression Modulus 0°	RTA	ASTM D 6641	124 GPa	18 Msi
In-Plane Shear Strength 5% Strain	RTA	ASTM D 3518	65.5 MPa	9.5 ksi
In-Plane Shear Strength 0.2% Offset	RTA	ASTM D 3518	42.0 MPa	6.1 ksi
In-Plane Shear Modulus	RTA	ASTM D 3518	4.3 GPa	0.62 Msi
Flexural Strength 90°	RTA	ASTM D 790	152 MPa	22 ksi
Interlaminar Shear Strength (SBS) 0°/90°	RTA	ASTM D 2344	96.5 MPa	14 ksi
Open-Hole Tensile Strength	RTA	ASTM D 5766	448 MPa	65 ksi
Open-Hole Tensile Strength	CTA	ASTM D 5766	448 MPa	65 ksi
Open-Hole Compression Strength	RTA	ASTM D 6484	310 MPa	45 ksi
Open-Hole Compression Strength	ETA	ASTM D 6484	262 MPa	38 ksi
Compression After Impact Strength 30.5 J (270 in/lb) Impact Energy	RTA	ASTM D 7137	310 MPa	45 ksi
Mode I Interlaminar Fracture Toughness (G _{IC} Strain Energy Release Rate)	RTA	ASTM D 5528	2.1 kJ/m ²	12.0 in-lb/in ²
Mode II Interlaminar Fracture Toughness (G _{IIc} Strain Energy Release Rate)	RTA	ASTM D 7905	2.6 kJ/m ²	15.0 in-lb/in ²
Room Temperature Ambient (RTA) Cold Temperature Ambient (CTA) is -54°C (-65°F) Elevated Temperature Ambient (ETA) is 121°C (250°F)				